UCSF
UC San Francisco Electronic Theses and Dissertations

Title

Mechanisms that Contribute to Retinal Pigment Epithelium Dysfunction in Macular Degenerations

Permalink

https://escholarship.org/uc/item/0rn410jh

Author

Germer, Colin James

Publication Date

2024

Peer reviewed|Thesis/dissertation

eScholarship.org Powered by the California Digital Library
University of California

Mechanisms that contribute to retinal pigment epithelium dysfunction in macular degenerations

by
Colin Germer

DISSERTATION
Submitted in partial satisfaction of the requirements for degree of
DOCTOR OF PHILOSOPHY

in

Pharmaceutical Sciences and Pharmacogenomics

in the

GRADUATE DIVISION
of the
UNIVERSITY OF CALIFORNIA, SAN FRANCISCO

Approved:

DocuSigned by:
Jason Gestwicki
4909848DBB404E5...

Jason Gestwicki
Chair

DocuSigned by:
David Krizaj
DocuSigned by:
Aparna Lakkaraju
A43151E984D44A2...

David Krizaj

Aparna Lakkaraju

Committee Members

Copyright 2024

by

Colin Germer

Dedication

To my dad. I did it.

Acknowledgments

This project could not have been done without the contributions and effort from my advisor, Dr. Lakkaraju. I first began in her lab as a lab research assistant at the University of Wisconsin-Madison working on exosomes from the RPE before joining on as a full-time graduate student at Madison and then moving with her to UCSF. She has been an inspiring mentor, with no question going unexplored. It was her that allowed me to pursue the topic of Piezo1 mechanosensation in the RPE in regards to drusen and ceramide, which got us a funded BrightFocus grant. Her mentorship towards my writing and presentation has been instrumental in helping me become a better scientist and communicator. Under her mentorship, I have been able to mentor a number of undergraduates over time, many of which have gone on to medical and graduate school.

I'd like to especially thank Dr. Li Xuan Tan for being my mentor when it came to technical skill and rigor. She has been an incredibly reliable source of scientific advice for things from techniques to interpersonal communications. It was with her I first learned about electron microscopy and fell in love with it. So too did she teach me three-dimensional confocal microscopy. I cannot count the number of times I have had to rely not only on her advice regarding analysis and experimental setup, but on her during times of crisis like during the COVID-19 pandemic.

My thesis mentoring committee has played a big role in my progress as well. Dr. Jason Gestwicki has been a source of excitement and passion during my thesis committee meetings and has been exceptionally supportive in every instance. So too has Dr. David Krizaj, who supplied me with the very mice, Piezo1-Flox, that I needed to execute this thesis. Without them, I would not be able to complete this doctoral dissertation. Their instruction and help was integral to my success in graduate school!

I'd also like to thank Dr. Dawiyat Massoudi, who was my undergraduate mentor and was my reason for getting into the science of the eye in the first place. Her exceptional rigor in reproducing experiments exactly as written instilled a particularly fierce drive to properly execute experiments. She also was an excellent trainer in mouse handling, breeding, weaning, and surgery. It was her training and drive that allowed me to single-handedly maintain the massive mouse colony that not only I, but the entire lab, relied on. She's been my professional confidant when it comes to any sort of social advice I need as well as someone I can just laugh with whenever life gets either of us down.

I'm grateful to Nilsa La Cunza, who is graduating at the same time as me. She's been a hugely positive social force in my life, constantly connecting me to other people throughout my PhD and encouraging me to get out of the lab. We've celebrated a number of scientific achievements and working experiments. I know you've encouraged me to take time off a number of times, so after this, I'm gonna have a solid month free!

Thank you to my mother, Debbie Germer. She taught me to read, to push farther, and to not get discouraged when life gets me down. She's been an emotional bedrock to me, constantly supporting me when work in the lab gets me down. Thank you so much for buying all those books to help me advance and giving me a space to study. From AP course books to the Illustrated Kingfisher Encyclopedia, I have my mom to thank for my love of science.

Thank you to my sister, Sarah Germer as well. She's been someone I can share both my triumphs and my tribulations in confidence. I've relied so much on her advice and for her listening to my long-winded explanations with patience. She's been the glue that keeps everyone in my family together and took on so many responsibilities while I'm away from Wisconsin. I'm so grateful to both of you for all you've done for me. Love you.

Lastly, thank you so much to all the people of UCSF for all the opportunities to enjoy a glass of wine or three and all the unique experiences I would've never gotten anywhere else. For my cohort to introducing me to Tahoe and kayaking and helping me out greatly with just adapting to life in SF in the nicest way possible. You guys were amazing to hang out with and cook for and I'm going to miss you all.

Contributions Page

This work presented in this dissertation was performed with the supervision, funding, and guidance of my PI Dr. Aparna Lakkaraju. Ideas and other intellectual contributions came from Dr. David Krizaj and Dr. Jason Gestwicki.

Chapter 2 is part of a manuscript with me as the first author. The other authors in the manuscript are, in order after myself: Li Xuan Tan, Nilsa La Cunza, Valencia Fernandes, An Cheng, Aparna Lakkaraju. This manuscript is titled: Therapeutic Targeting of Ceramide Improves Visual Function by Modulating Extracellular Vesicle Secretion in Preclinical Models of Macular Degeneration

Figure 2.6 was work performed by Li Xuan Tan.

Chapter 3 is preliminary work done by me and others and the manuscript currently under preparation:

Figure 3.4 was data generated by Nilsa La Cunza.

Figure 3.6 and 3.7 were contributions from Li Xuan Tan. She also performed analysis of Figure 3.7

Figure 3.8 is a contribution from Valencia Fernandes.

Chapter 4 is a manuscript that is also under preparation with work done by me and others.

Figure 4.3 is credited to Li Xuan Tan

Figure 4.4 is data generated by Yao Tong

Figure 4.5 as well as analysis from Figure 4.6 was generated by Nilsa La Cunza

Mechanisms that Contribute to Retinal Pigment Epithelium Dysfunction in Macular Degenerations

Colin James Germer

Abstract

Macular degenerations (MD) impact millions across the globe, with this number predicted to grow due to lack of effective therapies to combat the disease. The complex etiology of MD makes therapeutic development difficult. This thesis seeks to explore the underlying cellular mechanisms of MD, how they contribute to the disease, and evaluate novel therapeutics that can preserve healthy vision in disease models.

First, I show how ceramide accumulation drives the release of exosomes from the retinal pigment epithelium (RPE). Through ultracentrifugation and further purification methods along with electron microscopy and Nanoparticle Tracking Analysis (NTA), I show that ceramide increases the apical release of exosomes from the RPE. Using mass spectrometry and super-resolution imaging, I demonstrate these exosomes contain pro-inflammatory cargo. Using electron microscopy, I show this disrupts communication in the retina and recruits harmful microglia into the subretinal space. Finally, I show that small molecule therapeutics can prevent the release of these exosomes, which may preserve vision.

Second, I show that the abnormal mechanotransduction in the RPE leads to pathological features of MD. In “drusen-in-a-dish” models, biologically inert silica beads and synthetic agonists of mechanosensitive ion channels such as Piezo1 can drive mitochondrial fragmentation in the RPE. Using electrophysiology, I also show that RPE-specific ablation of Piezo1 can also

negatively impact the health of the retina. Together, these studies identify novel pathological mechanisms in age-related macular degeneration.

Finally, I show that a Food and Drug Administration (FDA)-approved drug for osteoporosis and Paget disease, zoledronic acid, can be repurposed to treat MD. Using high-resolution confocal microscopy, volumetric reconstruction, and electrophysiological techniques, I show that reducing ceramide levels within the RPE protects mitochondrial health, decrease microglial migration, and improves vision in a mouse model of inherited MD.

Taken together, these findings pave the way for a better understanding of the molecular mechanisms at play in driving vison loss in MD in three major aspects: how disrupted communication within the retina can cause deterioration of visual function, how drusen can negatively impact RPE health, and how small molecule therapeutics can restore vision.

Table of Contents

CHAPTER 1: VISION AND THE RETINA 1

Introduction 1

Vision Fundamentals: Transduction, Vitamin A, and Anatomy 1

The RPE and Disease 4

Drusen Overview 6

Models of Macular Degeneration 7

Established Findings in the Lakkaraju Lab 9

Knowledge Gaps 10

CHAPTER 2: EXCESS RPE CERAMIDE DRIVES SECRETION OF PROINFLAMMATORY EXOSOMES THAT INDUCE MICROGLIAL ACTIVATION 14

Introduction 14

Results 17

Ceramide Increases Apical Exosome Release In RPE 17

RPE with Excess Ceramide Release Pro-Inflammatory Exosomes 18

Ceramide-Enriched RPE Exosomes Recruit Microglia into the Subretinal Space 19

Conclusions 21

Figures 23

Methods 31

PRPE Culture 31

ARPE-19 Cultures 32

Mice 32

Desipramine Treatments 32

Transmission Electron Microscopy of Mouse Retinas 32

Exosome Isolation and Purification 34

Transmission Electron Microscopy of Exosomes 35

Immunoblotting 35

Nanoparticle Tracking Analysis 36

Nanoimaging of Exosomes 36

Live Imaging of Exosome Release 37

Mass Spectrometry 37

Electroretinography 38

Immunofluorescence of Mouse Eyes 38

Statistics 39

CHAPTER 3: ALTERED PIEZO1 ACTIVITY IN THE RPE INDUCES MITOCHONDRIAL DEFECTS **40**

Introduction **40**

Results **44**

Piezo1 Expression is Upregulated in the RPE in Disease States 44

RPE Grown on Beads Activate Piezo1 44

Piezo1 Overactivation Causes Mitochondrial Fragmentation 45

Piezo1 is Important for Photoreceptor Function 46

Conclusions 47

Figures 48

Methods 58

Bead Plating 58

Immunofluorescent Staining 58

Treatments 58

Cell Culture 58

Mouse Lines 58

Desipramine Treatments 59

Cryosection Staining 59

Immunofluorescence of Filters 59

Electroretinography 59

CHAPTER 4: ZA AS A POTENTIAL THERAPEUTIC IN MODELS OF RETINAL DEGENERATION 60

Introduction 60

Results 62

ZA Reduces Cholesterol and Ceramide Levels 62

ZA Prevents Complement Activation and Mitochondrial Fragmentation 63

ZA Prevents Migration of Microglia 64

ZA Restores Photoreceptor Function 64

Conclusions 64

Figures 66

Methods 74

Mice 74

Treatment with ZA 74

ZA-647 Injections into Mice 74

Immunostaining of Mouse RPE Flatmounts 74

Electroretinography 75

Complement Attack 75

Statistics 75

REFERENCES 83

Table of Figures

FIGURE 1.1 ANATOMY OF THE EYE 12

FIGURE 1.2 VISUAL CYCLE OF THE RETINA 13

FIGURE 2.1 HYPOTHESIS: CERAMIDE INCREASES EXOSOME RELEASE 23

FIGURE 2.2 RPE WITH CERAMIDE RELEASE MORE EXOSOMES 24

FIGURE 2.3CERAMIDE CAUSES SORTING OF PRO-INFLAMMATORY PROTEIN INTO EXOSOMES 25

FIGURE 2.4 CERAMIDE CAUSES CONNEXIN43 PACKING INTO EXOSOMES 26

FIGURE 2.5 CERAMIDE CAUSES MORE EXOSOME RELEASE EVENTS 27

FIGURE 2.6 CERAMIDE INCREASES ILVS PER MVB IN RPE 28

FIGURE 2.7 MICROGLIA ARE RECRUITED TO THE SUBRETINAL SPACE 29

FIGURE 2.8 DESIPRAMINE CAN PROTECT PHOTORECEPTOR FUNCTION 30

FIGURE 3.1 ILLUSTRATION OF HYPOTHESIS 48

FIGURE 3.2 PROPOSED MECHANISM OF PIEZO1-MEDIATED MITOCHONDRIAL FRAGMENTATION 49

FIGURE 3.3 RPE EXPRESSES PIEZO1 50

FIGURE 3.4 AMD RPE UPREGULATE PIEZO1 EXPRESSION 51

FIGURE 3.5 TRANSWELL SCHEMATIC 52

FIGURE 3.6 PIEZO1 RESPONSE TO MECHANICAL STRESS ON THE RPE 53

FIGURE 3.7 PIEZO1 ACTIVATION INDUCES MITOCHONDRIAL FRAGMENTATION 54

FIGURE 3.8 PIEZO1 ACTIVATION UPREGULATES MITOCHONDRIAL FISSION MACHINERY 55

FIGURE 3.9 DESIPRAMINE PREVENTS H3K9ME3 LOSS IN MOUSE RPE 56

FIGURE 3.10 PIEZO1 LOSS CAUSES PHOTORECEPTOR DEFICITS 57

FIGURE 4.1 ZA MAY BE A "TRIPLE-THREAT THERAPEUTIC 66

FIGURE 4.2 ZA IS DELIVERED TO THE RPE 67

FIGURE 4.3 ZA REDUCES CERAMIDE IN MICE 68

FIGURE 4.4 ZA REDUCES CHOLESTEROL IN MICE 69

FIGURE 4.5 ZA REDUCES MITOCHONDRIAL FRAGMENTATION DURING COMPLEMENT ATTACK 70

FIGURE 4.6 ZA REDUCES MITOCHONDRIAL FRAGMENTATION IN VIVO _____ 71

FIGURE 4.7 ZA REDUCES THE NUMBER OF SUBRETINAL MICROGLIA _____ 72

FIGURE 4.8 ZA PRESERVES VISION IN MOUSE MODELS OF STARGARDT DISEASE _____ 73

List of Tables

List of Reagents Used 75

List of Abbreviations

A2E: N-retinylidene-N-retinylethanolamine

A2PE: Phophatidyl-Pyridinium bisretinoid

ABCA4: ATP-Binding Cassette sub-family A, member 4

AMD: Age-related Macular Degeneration

ASM: Acid Sphingomyelinase

ATP: Adenosine Triphosphate

BMP: Bis-monoacyl glycerolphosphate

DAPI: 4',6-diamidino-2-phenylindole

DRP1: Dynamin Related Protein 1

dSTORM: direct Stochastic Optical Reconstruction microscopy

ERT2: Estrogen Receptor Type 2

ESCRT: Endosome Sorting Complex Required for Transport

FDA: Food and Drug Administration

GA: Geographic Atrophy

GPCR: G-protein Coupled Receptor

GTP: Guanosine triphosphate

HRF: Hyper-Reflective Foci

ILV: Intraluminal Vesicle

iPSC-RPE: Induced Pluripotent Stem Cell Retinal Pigment Epithelium

MAC: Membrane Attack Complex

MD: Macular Degeneration

MFN2: Mitofusin 2

MVB: Multivesicular Body

NHS: Normal Human Serum

NTA: Nanoparticle Tracking Analysis

OPA1: Optic Atrophy 1

PBS: Phosphate Buffered Saline

PFA: Paraformaldehyde

PRPE: Porcine Retinal Pigment Epithelium

RDH8: Retinal dehydrogenase 8

RPE: Retinal Pigment Epithelium

SD: Standard Deviation

SEM: Standard Error of the Mean

TEM: Transmission Electron Microscopy

TRP: Transient Receptor Potential

TRPV4: Transient Receptor Potential Cation Channel V4

VEGF: Vascular Endothelial Growth Factor

ZA: Zoledronic Acid

CHAPTER 1: VISION AND THE RETINA

Introduction

Vision is one of the most treasured of our five senses. So much of our modern age requires us to be able to use information presented to us on a screen. Being robbed of vision causes a massive decrease in quality of life, loss of income, and an increase in injuries [1]. Preserving vision is absolutely vital and yet millions across the globe are afflicted with incurable diseases like inherited and age-related macular degenerations that cause permanent blindness and have limited therapeutic options. This lack of effective interventions stems from a limited understanding of the complexity of these diseases. Here I will discuss how we see, the pathology behind these diseases, why the complex molecular mechanisms underlying them makes therapeutic development a challenge. This will also lay the groundwork for the next chapters of my thesis.

Vision Fundamentals: Transduction, Vitamin A, and Anatomy

One must understand the anatomy of the eye and the fundamentals of vision to understand why these diseases can be so debilitating. To begin with, light enters the transparent protective cornea and passes through the pupil to the lens (Figure 1.1A). The lens focuses this light onto the retina, where it strikes the outer segment disk membranes of the photoreceptor cells (Figure 1.1B). These disk membranes contain rhodopsin, a complex of 11-*cis*-retinal, (vitamin A), linked to opsin, a G protein-coupled receptor (GPCR). Upon absorbing a photon of light, 11-*cis*-retinal is isomerized to all-*trans* retinal and detaches from opsin, which allows opsin to exchange guanosine diphosphate (GDP) to guanosine triphosphate (GTP) on transducin. Transducin is a G protein, whose alpha subunit binds phosphodiesterase upon activation. Phosphodiesterase then degrades

cyclic guanosine monophosphate to guanosine monophosphate. The loss of cyclic guanosine monophosphate causes the closure of gated ion channels, hyperpolarizing the photoreceptor and sending a signal downstream to the bipolar cells. This electrochemical signal then makes it through to the retinal ganglion cells whose axons form the optic nerve. This signal eventually reaches the optic chiasm and interpreted by the brain as a visual signal which we use in our day-to-day life.

While photoreceptors are located throughout the retina, the area of highest visual acuity comes from the macula, a 6-millimeter diameter area of the retina. The macula is densely packed with cone photoreceptors which are the cell responsible for high-acuity vision. This is also an area of high phototoxicity as the light gathered by the pupil is focused onto this region, making for a highly damaging oxidative environment. Given the post-mitotic nature of many of the cells of the retina, they must be highly resilient to oxidative damage and have multiple mechanisms in place to mitigate this stress before permanent damage occurs. To remove damaged and photobleached disks, photoreceptors engage in daily shedding of outer segments. These outer segments are then engulfed by the underlying retinal pigment epithelium (RPE).

The RPE is a post-mitotic monolayer of cells situated between the photoreceptors and the highly fenestrated choriocapillaris, the vasculature of the outer retina. The RPE has a number of functions vital for the upkeep and maintenance of not only the photoreceptors but the retina as a whole. These include the maintenance of the outer-blood-retinal barrier through its tight junctions, which controls the transport of metabolites and nutrients into and out of the retina. The photoreceptors are unique in that they are the only non-cancer cell in the body to be exclusively reliant on glycolysis. As such, the majority of glucose derived from the blood supply is transported by the RPE to the photoreceptors instead of being consumed by the RPE, which relies entirely on oxidative phosphorylation. Photoreceptor waste products from glycolysis, such as lactate and fatty

acids, act as the major source of energy for the RPE. The RPE also removes water from the retina and secretes various growth factors and proteins to maintain the extracellular matrix around the photoreceptor outer segment tips and ensure photoreceptor health. Furthermore, as the name suggests, the RPE contains melanosomes, pigmented organelles, to absorb stray light which assists with keeping vision sharp.

Most important of all is the role RPE plays in vision: The daily phagocytosis of outer segments and the recycling of vitamin A. It is this function that imposes an incredible burden on the RPE as efficient degradation of phagocytosed outer segments is crucial to preventing the buildup of vitamin metabolites called bisretinoids. After a photon of light strikes rhodopsin bound to 11-*cis* retinal within the disk membrane of the outer segment to make an electrochemical signal, 11-*cis* retinal is converted to all-*trans* retinal, a reactive aldehyde (Figure 1.2). All-*trans* retinal must be flipped to the cytosolic side of the disk membrane to enable retinal dehydrogenase 8 (RDH8) to reduce it to all-*trans* retinol before it has a chance to cause oxidative damage. If not, all-*trans* retinal can form Schiff base adducts with phosphatidylethanolamine in the disk membrane along with other vitamin A products to form bisretinoids [2,3]. One such adduct is A2PE, composed of two molecules of vitamin A and one molecule of phosphatidylethanolamine. Once disks containing A2PE are ingested by the RPE, A2PE can then be cleaved to A2E by phospholipase D within RPE lysosomes, where it will reside in the RPE for the life of the cell in the form of lipofuscin granules [4]. Lipofuscin bisretinoids are autofluorescent and can easily be seen during a routine fundus exam.

The RPE and Disease

The focus of this thesis is to glean better insight into the molecular mechanisms underlying two major blinding diseases, Stargardt disease and non-neovascular age-related macular degeneration (dry AMD), and to develop small molecule therapeutics. Both these diseases affect the macula, robbing patients of central vision. In both diseases, the primary site of damage is the RPE.

Stargardt disease, the most prevalent inherited retinal degeneration, is caused by mutations in the *ABCA4* gene and affects ~1:8,000 people across the globe, [5]. The hallmark of the disease is a rapid accumulation of lipofuscin bisretinoids within the retina and hyper-reflective foci (HRF) [6]. Those afflicted with Stargardt disease lose their central vision starting in childhood but may be delayed until early adulthood depending on the specific ABCA4 mutation involved.

In contrast, age-related macular degeneration (AMD) affects those in late adulthood, typically over the age of 50 [7]. The current prevalence of AMD is ~50 million across the world and this is predicted to increase to 288 million by the year 2040 [8]. Unlike Stargardt disease, which is monogenic, over 50 independent genes have been implicated in AMD [9]. This disease also has a strong environmental component with lifestyle factors such as smoking and diet playing a role in susceptibility. The hallmark of dry AMD is the appearance of large cholesterol- and protein-rich deposits termed "drusen" underlying the retina [10]. Like with Stargardt disease, those affected by dry AMD will slowly and inexorably lose central vision. Patients progress from early to intermediate and finally to late-stage AMD. These stages are characterized by soft drusen deposits, RPE atrophy, photoreceptor degeneration, and eventual vision loss.

Early-stage AMD patients have medium-sized drusen (~63-123 μm), minimal RPE changes, and no visual deficits. Intermediate stage AMD patients will usually present with few

large drusen > 123 microns with possible pigmentation changes in the RPE [11]. These patients will suffer mild vision loss, but the degree can vary widely from person to person, with most reporting few problems. Others can report difficulty seeing in low light or blurriness in their vision. The final stage, late AMD, has two different types: Wet or neovascular and dry or non-neovascular geographic atrophy (GA). Patients suffering from either form will report wavy lines, blank or black spots in their central vision, a reduction in color perception, and reduced vision in low light. Neovascular AMD is characterized by the proliferation of choroidal blood vessels into the retina and the loss of vision is typically acute and sudden. Neovascular AMD currently has no cures, but the loss of vision can mitigated over time through the use of anti-vascular endothelial growth factor (VEGF) injections, which prevent growth of new vessels and can stabilize vision [12].

Geographic atrophy or dry AMD develops much more slowly, typically over decades [10,13]. No new blood vessels grow, but instead an area of atrophy forms where RPE cells are lost in patches, leads to a subsequent loss of photoreceptors and blood vessels. These atrophic lesions will slowly spread, destroying central vision. Dry AMD patients currently have two interventions available to them: Syfovre and Izervay, both of which have FDA approval. Syfovre is a monoclonal antibody that binds C3 and prevents its cleavage while Izervay is an RNA aptamer that binds C5. Both of these prevent the early and intermediate steps in the complement pathway, respectively [14]. However, there is debate among clinicians as to whether Syfovre should be used, owing to the fact that pooled Phase 3 data showed significant risk of conversion from dry AMD to wet AMD in patients and many involved in two of the three trials did not complete the study[15]. Izervay also has a similar risk of conversion to wet AMD during treatment, though it is slightly lower. Both of these drugs also have similar risks that come with intravitreal injections: inflammation risk of infection,

and possible retinal detachment. Despite these risks, neither drug can restore vision nor stop progression, they only slow down the growth of the area of atrophy.

Drusen Overview

Drusen is a mixture of lipids and proteins derived from both the retina and systemic circulation [1617]. The protein content is widely varied, but many proteins found are also shared by Alzheimer's disease and atherosclerotic plaques, such as complement proteins, HLA-DR, ApoE, and fibrinogen to name a few [18,19]. The lipid content within drusen is oxidatively modified, which likely contributes to drusen formation and is likely due to the oxidative stress that the retina is under[16]. Druse, singular, range in size and shape within the retina, and these aspects are used in diagnosing AMD stages, with intermediate and large drusen deposits indicating early and intermediate stages of AMD, respectively. Excellent work has been done in the field regarding the protein content of drusen deposits, which consist of apolipoproteins, complement pathway proteins, and various oxidized proteins [20,21].

Both lipofuscin and drusen accumulate as we age in small quantities. As we get older, more will accumulate over time[2223]. However, a rapid accumulation of either presents a challenge for the RPE and can disrupt homeostasis, resulting in impaired RPE function. This impaired RPE function can in turn cause further disruption to the retina and the RPE itself, inducing a feedback loop that can kill the RPE. Without the RPE, photoreceptors die off resulting in the loss of central vision and thus, blindness.

Models of Macular Degeneration

Current models of macular degeneration (MD) are very limited, owing to the highly complex nature of not only the eye itself but the eyes of diurnal vertebrates. As mentioned before, human vision relies on the macula as the area of highest acuity. This limits "true" models of MD to primates, which greatly increases costs, time, and labor. There are dog and rabbit models, but these only have small visual streaks. These visual streaks are areas that are higher acuity but are still not the same level as human or primate vision. Again, these models are still quite expensive or have limited genetic manipulation tools available. Other models with cone-rich domains in the retina such as the 13-lined-ground squirrel have limitations such as hibernation for a portion of the year, making them poor experimental models. Most labs rely on mice and rats, which have a plethora of genetic tools available to them and a relatively limited lifespan, making these studies far shorter. The drawback is that mice are nocturnal and do not have a macula, thus not ideal to study MD. However, a compromise would be to use mouse models to study specific mechanisms of disease, be it immune dysfunction, lipid accumulation, oxidative stress or a mechanism yet to be identified. Mouse models can be used to tease out how that insult can affect the RPE and how this impacts the rest of the retina. Data from mouse models can be corroborated using more relevant models, such as human donor tissue or cell cultures.

Cell culture models are also necessary in vision research, allowing far more manipulations and specific measurements than can be made in an animal. Cell lines are the most abundant and common culture model, with the immortalized human cell line ARPE-19 used for RPE studies. The advantage of these lines is the generation of a huge number of samples and experiments with comparatively little time and effort. The disadvantage is that cell lines often do not recapitulate the features of cells from the retina. ARPE-19 cells in particular lack pigment granules, do not form

tight junctions which results in a leaky monolayer, and, most pertinently, these cells are mitotically active unlike the RPE *in situ*. Recent advances have been made to solve some of these drawbacks, such as culturing the cells with nicotinamide to promote melanin synthesis and a more hexagonal morphology, although the tight junctions are still leaky [24,25].

Other cell culture models include RPE derived from induced pluripotent stem cells (iPSC-RPE) established from reprogramming fibroblasts, blood, or urine from healthy donors and patients [26–28]. The major advantage with this model is that these are of human origin and can tap into a wealth of tools. iPSC-RPE also form tight junctions and typically grow into a polarized monolayer. The disadvantage is that there are currently numerous protocols to culture iPSC-RPE and no standardization. Many iPSC-RPE cultures need further validation to ensure that they express the repertoire of genes expressed by the RPE in situ, which originates from the neuroectoderm and expresses P-cadherin, unlike iPSC-RPE, which express E-cadherin.
Also, these iPSC-RPE have a limitation on the number of passages they can go through before they need to be re-derived [29,30].

The Lakkaraju Lab has pioneered the use of primary porcine RPE cultures, established from freshly harvest pig eyes [31]. This model has several advantages over other culture models. First, the RPE are fully pigmented and polarized, requiring no additional steps as for iPSC-RPE to pick colonies or passage cells. Porcine RPE also readily form polarized monolayers when cultured on collagen-coated Transwell filters with no additional manipulations. These RPE monolayers readily phagocytose and rapidly degrade photoreceptor outer segments, with kinetics similar to those seen in vivo. Given the availability of pigs, new cultures can be made weekly, and usually cheaply, without the need for passaging and the risk of losing the characteristics of the RPE.

Established Findings in the Lakkaraju Lab

The Lakkaraju lab has shown that accumulation of lipofuscin bisretinoids can induce multiple levels of dysfunction within the RPE. To begin with, accumulation of A2E within RPE lysosomes prevents cholesterol efflux leading to a secondary accumulation of cholesterol [32]. Cholesterol in turn abnormally activates the enzyme acid sphingomyelinase (ASM) by sequestering bis-monoacyl glycerophosphate (BMP), the ASM co-factor[33]. This enzyme cleaves sphingomyelin to ceramide within the RPE. Ceramide is a cone-shaped lipid with variable chain lengths, which we discovered that the C16 and C24 species of ceramide interfere with many homeostatic functions of the RPE. These include an increase in acetylated, or static, microtubules, which leads to impaired autophagy. Within the RPE, the rapid transport of autophagosomes occurs on dynamic microtubules that are marked by tyrosination. An increase in acetylated microtubules and a concomitant decrease in tyrosinated microtubules prevents autophagosome transport.

As ceramide has a cone shape due to its wide hydrophobic side chains and small hydrophilic headgroup, it increases negative curvature in the bilayer resulting in inward budding and homotypic fusion of early endosomes. These enlarged early endosomes internalize the complement protein C3 into the RPE, which is cleaved to C3a fragments. C3a activates mTOR which reduces transcription of autophagy-related genes and can induce dedifferentiation of the RPE [34].

Increased levels of ceramide can also cause an impaired response to complement attack. Ceramide can also inhibit recycling of CD59 to the apical membrane. CD59 is an important complement regulator required to inhibit formation of the membrane attack complex (MAC). Furthermore, acetylated microtubules prevent the rapid movement of lysosomes from the perinuclear region to the periphery, and prevent lysosome exocytosis required for the RPE to repair

its plasma membrane after a complement attack [35]. Impairing these responses to complement attack result calcium influx into the RPE via membrane attack complex pores, which cause mitochondrial fragmentation and loss of RPE homeostasis [35].

Knowledge Gaps

This thesis will strive to answer three unaddressed gaps in our current knowledge of how excess ceramide promotes RPE pathology. First, how does ceramide alter intercellular communication in the retina? The RPE is a central player in communication both within the retina and the rest of the body, as it forms the outer blood-retinal-barrier. Any impact on the RPE's ability to communicate would certainly negatively impact the overall functionality within the retina. Chapter 2 will seek to answer how ceramide in the RPE in models of MD alters its communication with the rest of the retina and if this can be modulated via small molecule drugs.

The second question is what effect could drusen and ceramide have on the RPE in a mechanical context? Could drusen exert strain on the RPE that disrupts its homeostasis and ability to carry out duties important for the survival of the photoreceptors and maintenance of the blood-retinal barrier? Would cholesterol or ceramide accumulation alter mechanotransduction in the RPE? Other groups have shown that cholesterol and ceramide can alter mechanosensitive ion channel function in cell lines and other epithelial cell types [36,37]. Within Alzheimer's disease, plaques have been shown to activate mechanosensitive responses in neurons. It stands to reason that ceramide and drusen in and around the RPE may have the same outcomes. Chapter 3 will show how Piezo1, a mechanosensitive ion channel, modulates how the RPE senses its environment and how aberrant Piezo1 activation through lipid or mechanical means can cause RPE dysfunction which may impact the rest of the retina.

The third question is what drugs could be developed to combat ceramide buildup? Our lab has shown that desipramine, a tricyclic antidepressant, acts as a functional ASM inhibitor and can lower ceramide. Are there more powerful drugs that can target ASM and other upstream pathways such as cholesterol? And, if ceramide and cholesterol can be reduced, will visual function be restored or can vision loss be halted? These questions will be addressed in Chapter 4 of this thesis, where I show that a drug approved for osteoporosis has powerful therapeutic effects on the RPE and restores visual function.

Figures

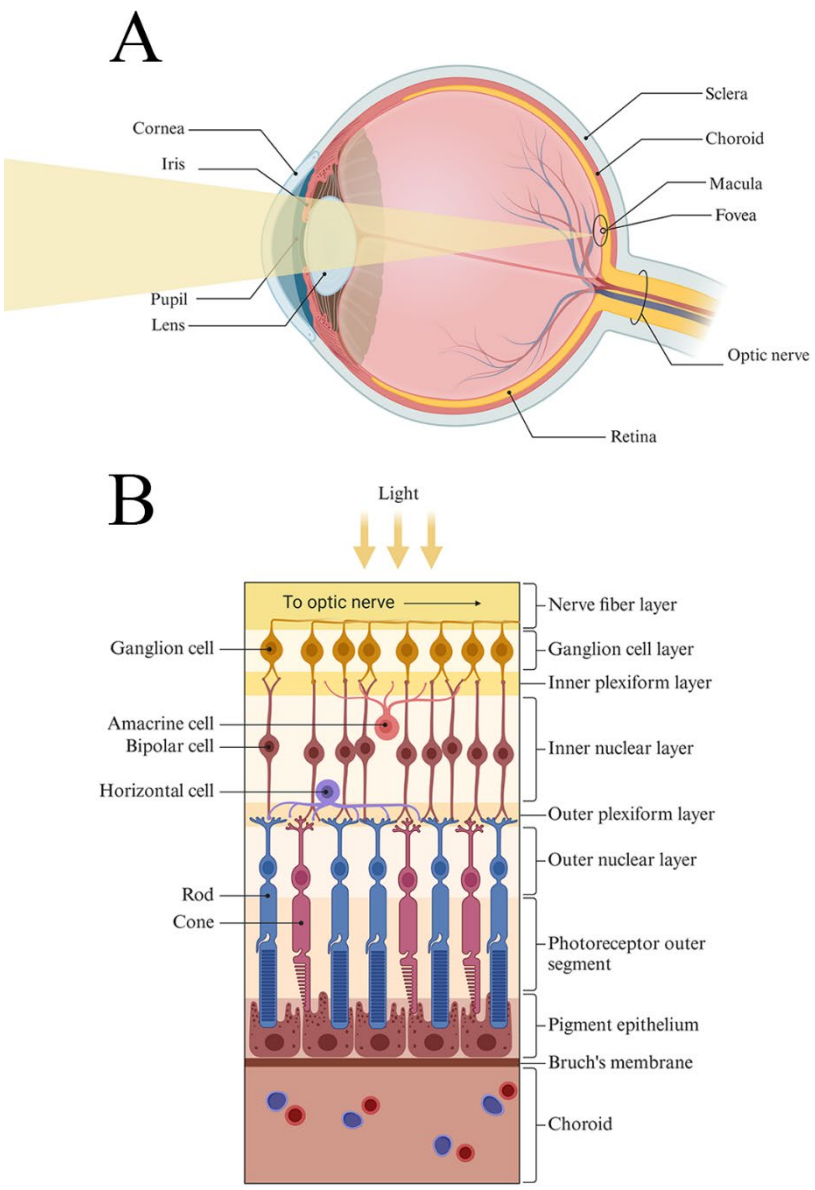


FIGURE 1.1 ANATOMY OF THE EYE

A. Cartoon schematic of the eye with major anatomical features shown. Light enters through the cornea and is focused by the lens onto the retina at the back of the eye where it strikes the retina. B. Cartoon schematic of the layers of the retina. When light strikes the photoreceptors, an electrochemical signal is transmitted from the photoreceptor outer segments into the bipolar cells, into the retinal ganglion cell layer and then into the optic nerve. From there, it is moved into the brain. Created with BioRender.com

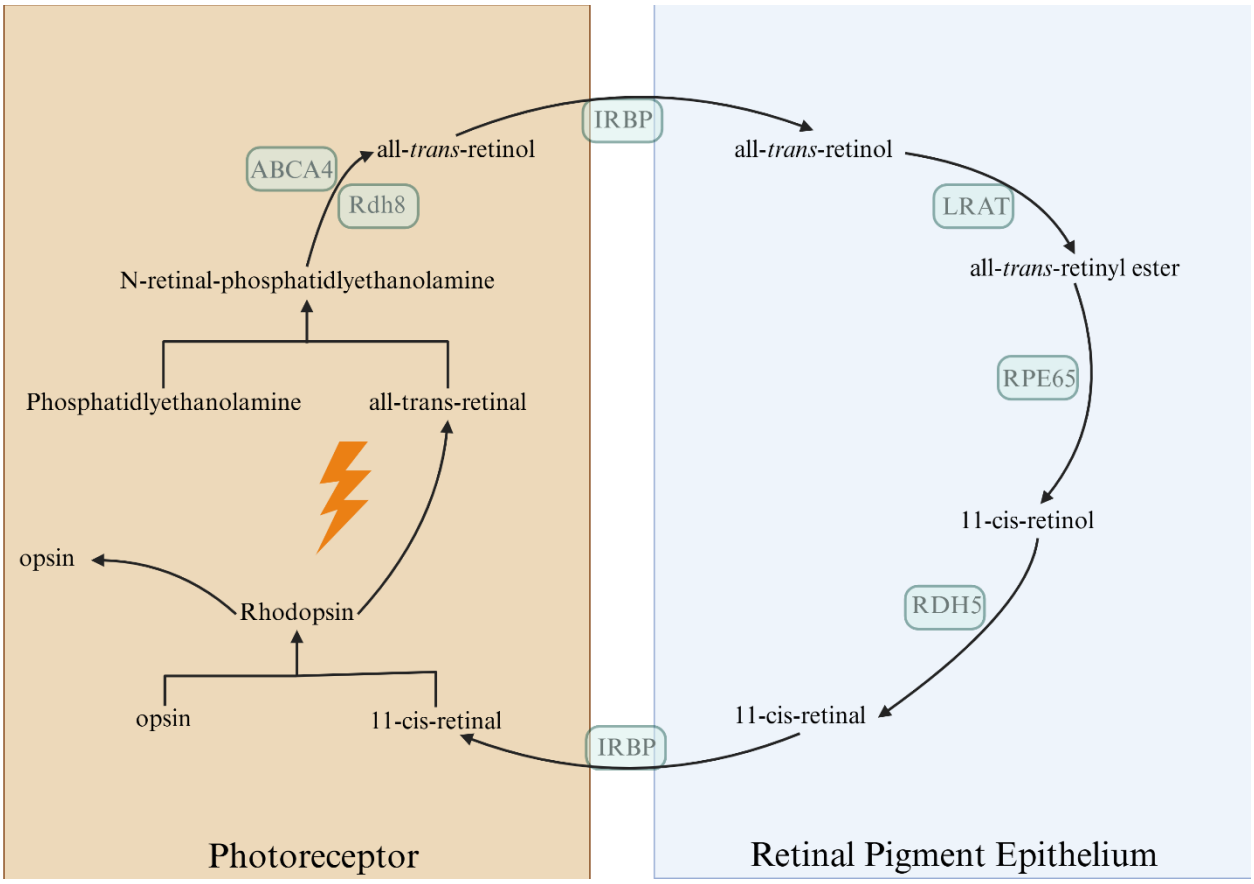


FIGURE 1.2 VISUAL CYCLE OF THE RETINA

Schematic of the visual cycle showing how the retinal pigment epithelium is involved in recycling vitamin A back to the photoreceptors. Vitamin A compounds are in plain text while proteins involved in the movement and processing of the intermediates are in boxes. Created with BioRender.com

CHAPTER 2: EXCESS RPE CERAMIDE DRIVES SECRETION OF PROINFLAMMATORY EXOSOMES THAT INDUCE MICROGLIAL ACTIVATION

Introduction

Exosomes are a class of 30-120nm sized extracellular vesicles derived from the endolysosomal recycling pathway [38]. Exosomes begin as intraluminal vesicles (ILVs) in a multivesicular body (MVB). They form from inward budding into the late endosome and from there they can either be degraded by the lysosome or the MVB can fuse with the plasma membrane and these ILVs are released into the extracellular space in the form of exosomes [39]. Originally thought of as cellular debris, research in the recent decade or so has shown that exosomes play vital roles in cell-cell signaling, extracellular matrix remodeling, and disease [40–43]. From establishment of metastatic tumor niches, to expanding cell protein repertoire, exosomes are not only cell-specific but can carry a wide variety of protein, RNA, and lipid cargo [41]. Exosomes derived from healthy cells may have uses as therapeutic delivery systems if not outright interventions themselves [44,45]. Excellent work regarding exosomes within the retina has demonstrated their role in the eye. Studies have shown their usefulness as a liquid biopsy to evaluate eye health or their role in drusen formation or even cell-cell communication in the retina [46–48]. This work seeks to explore what role exosomes play in models of MD, and if they can be modulated via small molecule therapies.

Isolating pure populations of exosomes is difficult as their sedimentation rate is similar to that of many proteins and many other classes of extracellular vesicles. The first step is generating exosome-depleted media, which can be made by using media without any serum. Serum, usually

sourced from fetal animals, typically pig, sheep, or cow, contains many of the growth factors needed by cells and also contains large numbers of exosomes derived from the host. Most cells do not grow well in serum-free media and so complete media, media with all the components in it necessary for normal cell growth including serum, must be subjected to ultracentrifugation in excess of 100,000xg over the course of 16 hours. After this, a large pellet forms in the bottom of the tube and is discarded. The remaining supernatant can then be filter sterilized and fed to cells.

The next step is harvesting conditioned media, which is media that has been exposed to cells for some time. This media is then cleared of any cells at a low-speed centrifugation in the range of 300xg and can be stored for a limited time, usually a week at 4°C, or frozen. When enough conditioned media has been gathered, isolation can commence. To date, there are a handful of techniques that can isolate exosomes: Differential ultracentrifugation is the most common where samples are spun at increasing *g*-force and the pellet is discarded at every step. However, this technique is typically lossy as many exosomes may not pellet or the pellet may come loose or the exosomes may pellet at earlier stages alongside apoptotic bodies and microvesicles [49].

Another technique is the use of density gradient purification which uses a gradient of different densities to isolate exosomes, which are then directly harvested, typically at 1.15g/mL. These gradients can be made of sucrose, iodixanol, or cesium chloride and can be either self-generated through special rotors or lengthy ultracentrifugation times, or they can be made using a gradient-maker which precisely distributes the gradient with the highest density on the bottom and the lowest at the top. Density gradient ultracentrifugation generates exosome populations that are more pure, but the yield is typically as low as ultracentrifugation and is prone to operator error [50]. The use of size-exclusion chromatography, where conditioned media is concentrated via molecular weight cut-off filters and then run through a column containing beads with small pores in them,

can also be used to isolate exosomes. This column causes exosomes, proteins, and other extracellular vesicles to flow through at different rates and allows the user to collect the precise fraction desired [51].

According to the International Society for Extracellular Vesicles, a society established to standardize exosome isolation and increase the reproducibility of papers on exosomes, mere isolation methodology is not enough. To confirm a population of vesicles is truly exosomal it must also meet additional criteria. They must fit within a narrow band of 30-120nm diameter sizes. This can be confirmed via electron microscopy, as diffraction-limited microscopy cannot resolve these sizes. Under electron microscopy, exosomes will have a "collapsed donut" morphology, a result of the dehydration process during electron microscopy processing along with the extremely high vacuum inside of the column of the electron microscope itself [52]. Exosome size distribution can also be visualized via Nanoparticle Tracking Analysis (NTA). This process involves shining a laser through a special optical flat while the exosomes are suspended in a solution of known viscosity, volume, and temperature. Videos can be taken with a simple upright microscope and camera system that are then analyzed through special software that measures their Brownian motion. That is, the random motion that small particles undergo. If viscosity and temperature are known and the system is free of vibration or any sort of flow or drift, then accurate sizes can be determined based on the random motion of the particles [53].

Finally, exosome populations must be confirmed for known markers. Currently, there is no "one size fits all" to identify exosomes through protein alone. The protein cargo of exosomes changes based on stimulus to the cell secreting them along with the cell type itself [51,54]. Instead, prospective exosome populations are subjected to western blotting and examined for proteins that are typically associated with exosomes. Tetraspanins are typically the major protein to look for

and those such as CD9, CD63, and CD81 are indicators that a given isolation contains exosomes. Other proteins stained for are those from the Endosomal Sorting Complex Required for Transport (ESCRT) pathway, such as TSG101, ALIX, and Hrs [3855,5657]. These proteins are specifically involved in some way in the generation of or sorting of cargo into exosomes via ILV formation. However, not all exosomes are generated via the ESCRT pathway. Some, as mentioned, are generated through ESCRT-independent pathways such as ceramide [58]. So other proteins can also be examined such as Hsp70, a heat-shock protein associated with exosomes. Lastly, a preparation must be evaluated to ensure it contains low or no levels of secreted proteins. This is done by confirming the absence of proteins from the endoplasmic reticulum and Golgi, such as calnexin or Giantin, respectively.

Results

Ceramide Increases Apical Exosome Release In RPE

Work from other labs has shown that ceramide can promote inward budding into the late endosome, to form ILVs that are released as exosomes (Figure 2.1) [58 59]. Previous work from our lab has shown that ceramide causes a myriad of RPE dysfunctions including inward budding at the plasma membrane to form abnormal early endosomes (discussed in Chapter 1) [34]. Based on these studies, we hypothesized that inward budding into MVBs would increase ILV formation and exosome secretion. We first sought to quantify the number of exosomes secreted by healthy RPE cultures or RPE with the bisretinoid A2E, which increases ceramide accumulation [32,33]. We harvested media and purified exosomes from the apical and basolateral chambers of polarized RPE cultures with or without A2E. Purified exosomes were then analyzed by immunoblotting. We observed a significant increase in CD63, a tetraspanin that is a canonical marker for exosomes, in

exosomes released by RPE with A2E. Other exosome markers such as a Hsp70 and flotillin-2 were also increased. An absence of calnexin indicated the purity of our exosome isolations (Figure 2.2A). To ensure the criteria for exosomes were met, these exosomes were imaged by transmission electron microscopy (TEM). We observed the typical "collapsed donut" shape seen with negative stain methods (Figure 2.2B). As immunoblotting cannot discern if the number of exosomes is increased or the amount of protein is merely higher, and counting through electron microscopy is highly labor intensive and relies on uniform adsorption of all exosomes onto the grid, we used NTA to quantify the size distributions and numbers of exosomes. Increased ceramide did not alter the number of exosomes released towards the basolateral chamber by the RPE. However, there was a two-fold increase in exosome counts per cell from A2E-treated RPE, indicating an increase in apical secretion in RPE with high levels of ceramide (Figure 2.2C).

RPE with Excess Ceramide Release Pro-Inflammatory Exosomes

To analyze the protein repertoire of these exosomes, we generated ultra-pure exosome populations by self-generating iodixanol gradient and subjected them to mass spectrometry analysis. As mass spectrometry requires a large quantity of protein for accurate assessment, porcine RPE cultures could not be used as they were available in limited quantities. Instead, ARPE-19 cells were grown and treated with U1866A, a compound that induces cholesterol accumulation in cells. This activates ASM, leading to ceramide accumulation. Exosomes released by U18-treated cells had an increase in pro-inflammatory proteins (e.g., HLA-DR, Connexin 43, S100A8) and a decrease in anti-inflammatory proteins (lactoferrin) (Figure 2.3). This indicates that ceramide alters the protein cargo of exosomes, which could promote inflammation in the retina.

To validate our mass spectrometry data, we purified exosomes released by porcine RPE monolayers and analyzed them by Nanoimaging. This relatively new technology allows super-resolution imaging (dSTORM microscopy) of individual exosomes labeled with antibodies to exosome or other proteins. We labeled exosomes with antibodies to canonical exosome markers (CD9, CD63, CD81), ceramide, and Connexin 43. Nanoimaging analysis showed that exosomes derived from RPE treated with A2E had an increased amount of Connexin 43 compared to exosomes released by healthy RPE (Figure 2.4A, B). Connexin 43 is a gap junction protein, which is vital for cell-cell communication. It is especially important in the RPE, where it mediates electrical properties of the RPE and overall barrier function[60,61]. Pertinently, its secretion also functions as a pro-inflammatory factor, and has been shown to recruit immune cells [62].

To explore if exosome secretion could be ameliorated via small molecule therapies and further confirm the role of ceramide in driving RPE pathology, we performed live cell imaging of exosome release from porcine RPE cultures. These RPE were transfected with CD63-pHluorin which is quenched in the acidic compartment of the MVB. Upon the fusion of the MVB with the plasma membrane and the release of ILVs into the neutral extracellular space, the pHluorin probe is unquenched and will fluoresce. These fluorescence "bursts" are counted as exosome release events. In RPE treated with A2E, we observed more exosome release events compared to healthy cells (Figure 2.5A). Treatment with desipramine, which inhibits ASM and decreases ceramide production, significantly reduced the number of release events in RPE with A2E (Figure 2.5B).

Ceramide-Enriched RPE Exosomes Recruit Microglia into the Subretinal Space

To ensure that these findings were not an artifact of cell culture, we analyzed MVBs and ILVs in pigmented *Abca4*$^{-/-}$ mice, the well-characterized model for Stargardt disease [63–65].

Exosome purification from the subretinal space is not possible with currently available technologies; instead, we performed TEM on flatmounted whole retinas that were high-pressure frozen (Figure 2.6A). We found similar numbers of MVBs in *Abca4*$^{-/-}$ mouse RPE compared to age-matched wildtype counterparts (Figure 2.6B). There was also an increased relocalization of MVBs near the apical surface of the RPE, in agreement with the increased apical secretion of exosomes seen in our primary RPE cultures (Figure 2.6C). There was no increase in the numbers of total ILVs (Figure 2.6D). To ascertain if exosome biogenesis can be modulated *in vivo* by treatment with ASM inhibitors, *Abca4*$^{-/-}$ and WT mice were administered desipramine (10 mg/kg, three times/week for 4 weeks). This significantly reduced the numbers of ILVs per MVB in *Abca4*$^{-/-}$ RPE back to wild-type levels, indicating that ceramide is the major driving force in exosome biogenesis in the RPE *in vivo* (Figure 2.6E).

As these exosomes contain pro-inflammatory cargo such as Connexin 43, which can induce migration of immune cells, we asked whether this would cause migration of microglia from the outer and inner plexiform layers to the subretinal space. We stained mouse RPE flatmounts with Iba1, a marker for microglia. We found that the number of microglia were significantly increased in the subretinal space of aged *Abca4*$^{-/-}$ mice when compared to age-matched wild-type mice (Figure 2.7A, B). This is a strong indicator for exosomal secretion playing a role in the recruitment of microglia into the subretinal space.

Microglial infiltration into the subretinal space is a sign seen in many retinal degenerations, including AMD and Stargardt disease [66–68]. While there is still debate as to whether these microglia are protective or detrimental in these diseases, they only accumulate in the subretinal space during degenerations. As such, to evaluate whether these mice would also lose vision and if that vision could be preserved or restored by desipramine treatment, we performed electroretinography

(ERGs) on vehicle-treated wild-type, vehicle-treated *Abca4*$^{-/-}$, and *Abca4*$^{-/-}$ mice treated with desipramine for 8 weeks. This longer treatment was deemed necessary due to the more advanced age of the cohort at 16 months and thus higher ceramide accumulation and a greater progression of the disease. ERG measurements showed that the a-wave, the signifier of photoreceptor health in the retina, was better preserved in *Abca4*$^{-/-}$ mice treated with desipramine than with vehicle alone (Figure 2.8). Although desipramine did not restore vision to that of age-matched wild-types, this represents a promising therapeutic avenue.

Conclusions

This chapter has shown that excess levels of ceramide within the RPE, both in cell culture and in mice, can cause aberrant secretion of exosomes towards the apical surface. These exosomes contain proinflammatory cargo that is released towards the retina, which may in turn recruit microglia into the subretinal space. By employing inhibitors of ASM, ceramide levels can be decreased and this, in turn, reduces the number of exosomes generated by the RPE. This may be a promising therapeutic intervention in treating MD. However, more work needs to be done in order to understand the exact roles these exosomes may play within the retina. It has been thought that excess exosome secretion may contribute to drusen formation. This study now demonstrates that exosome secretion from stressed RPE could also recruit microglia into the subretinal space [69]. Exosome secretion from stressed RPE could also mediate epithelial-to-mesenchymal transition in the RPE, which would harm the retina overall. It has also been shown that exosomes secreted by the RPE under oxidative stress can promote angiogenesis, an important step in proliferation of blood vessels and development towards neovascular AMD [46,70].

This chapter has also demonstrated that the use of ASM inhibitors can prevent the recruitment of microglia to the subretinal space. Desipramine is a well-tolerated tricyclic antidepressant with a wide therapeutic index and typically minor side effects. The dosages employed for this study are well below what is necessary to obtain the anti-depressant effects, indicating a promising avenue for drug repurposing for both AMD and Stargardt patients. These patients typically have a high incidence of depression, and future studies should consider progression of either of the diseases while the patient was under a desipramine regimen.

Although the nature of these microglia was not ascertained through the course of this thesis, the fact they were outside of their normal niche, which is both the inner and outer plexiform layers, indicates they were being recruited to the subretinal space as a result of dysfunction in the retina. More work is needed with this mouse model in particular to unveil the protective or detrimental nature of these microglia.

Figures

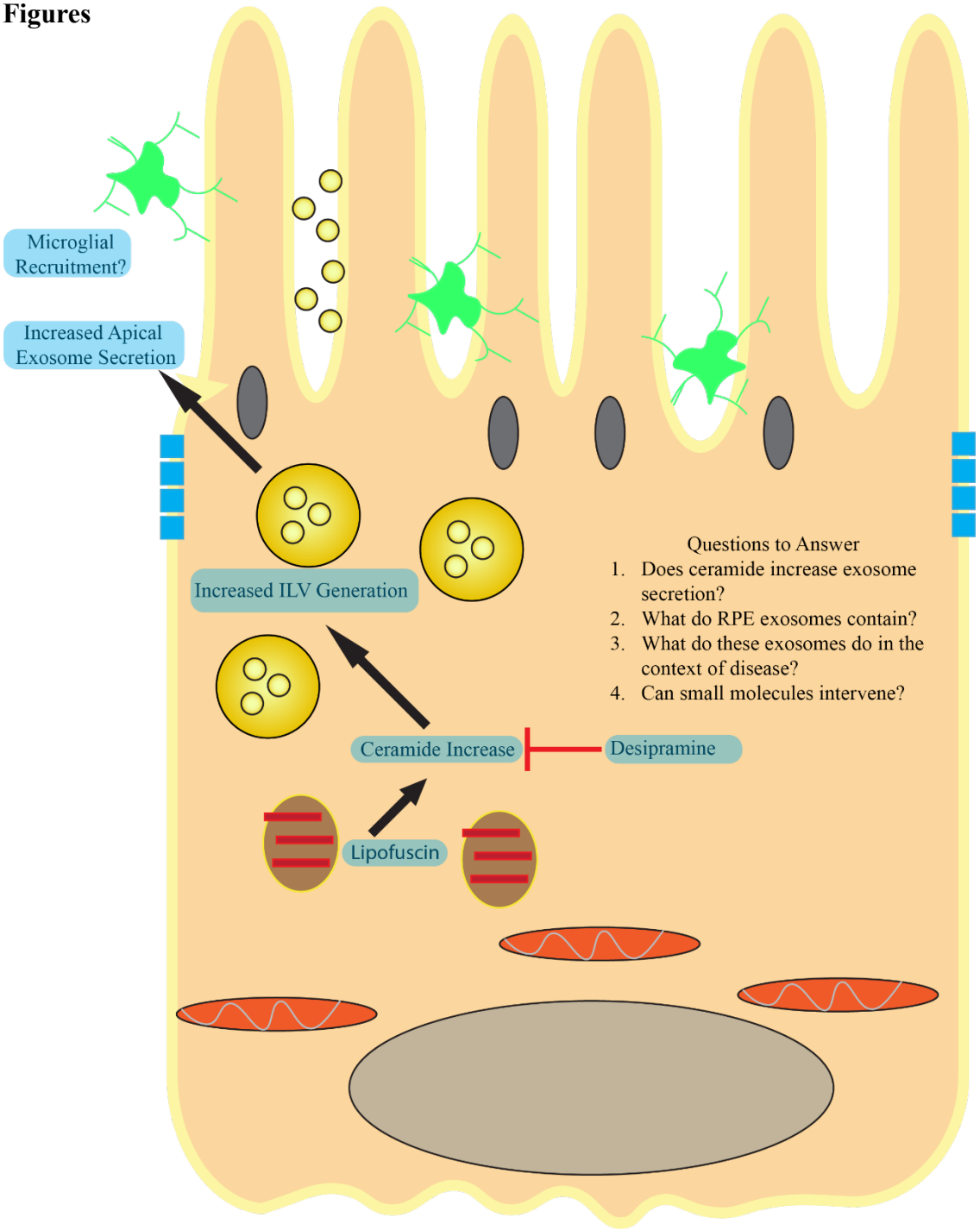


FIGURE 2.1 HYPOTHESIS: CERAMIDE INCREASES EXOSOME RELEASE

Cartoon schematic showing how ceramide causes inward budding into multivesicular bodies and their resultant fusion with the plasma membrane causes the release of intraluminal vesicles as exosomes

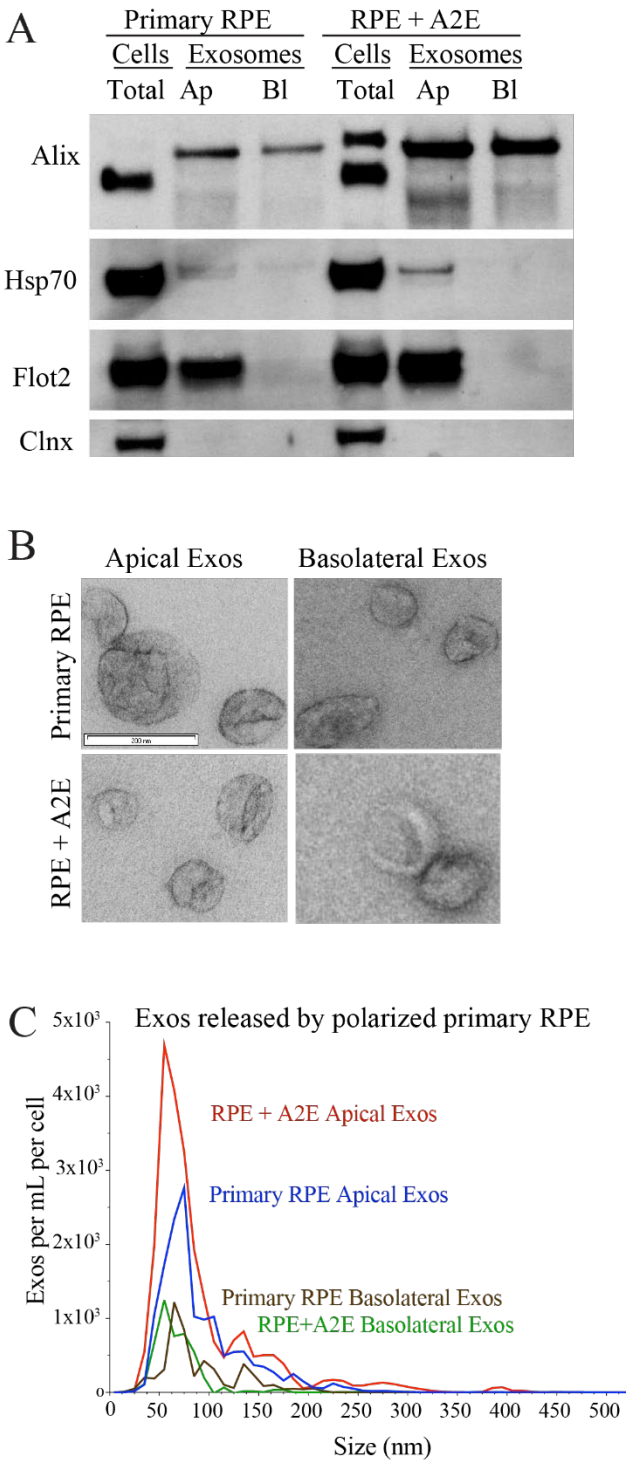


FIGURE 2.2 RPE WITH CERAMIDE RELEASE MORE EXOSOMES

A. Western blot showing exosomal markers such as Alix, flotillin2 (Flot2), Hsp70, and the endoplasmic reticulum marker Calnexin.
B. Representative electron micrographs of exosomes
C. NTA of exosomes derived from control or A2E-treated RPE. Note the increased apical secretion in A2E-treated RPE.

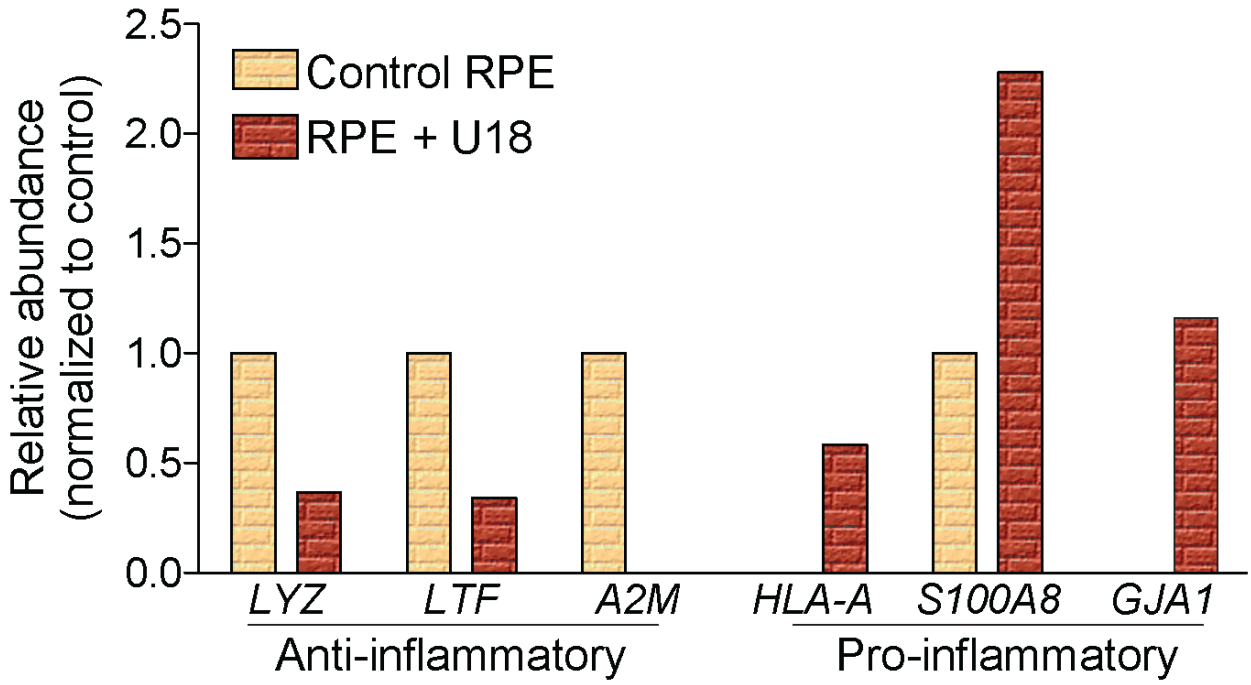


FIGURE 2.3 CERAMIDE CAUSES SORTING OF PRO-INFLAMMATORY PROTEIN INTO EXOSOMES

Bar graph of relative abundances of various proteins identified in exosomes derived from RPE via mass spectrometry.

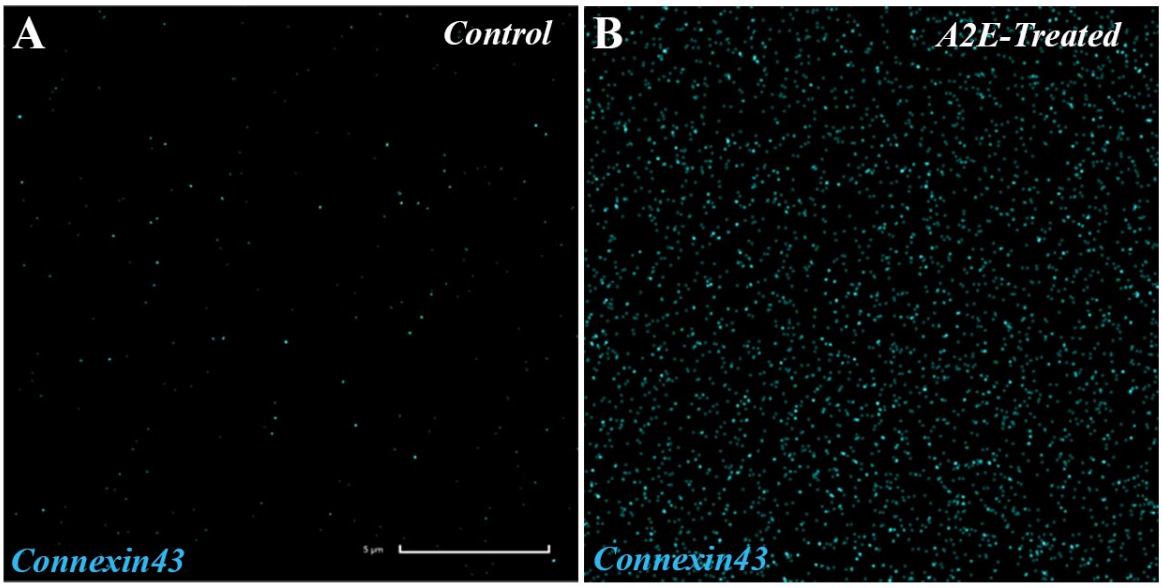


FIGURE 2.4 CERAMIDE CAUSES CONNEXIN43 PACKING INTO EXOSOMES

Representative images from exosomes derived from RPE treated with or without A2E stained for Connexin43.

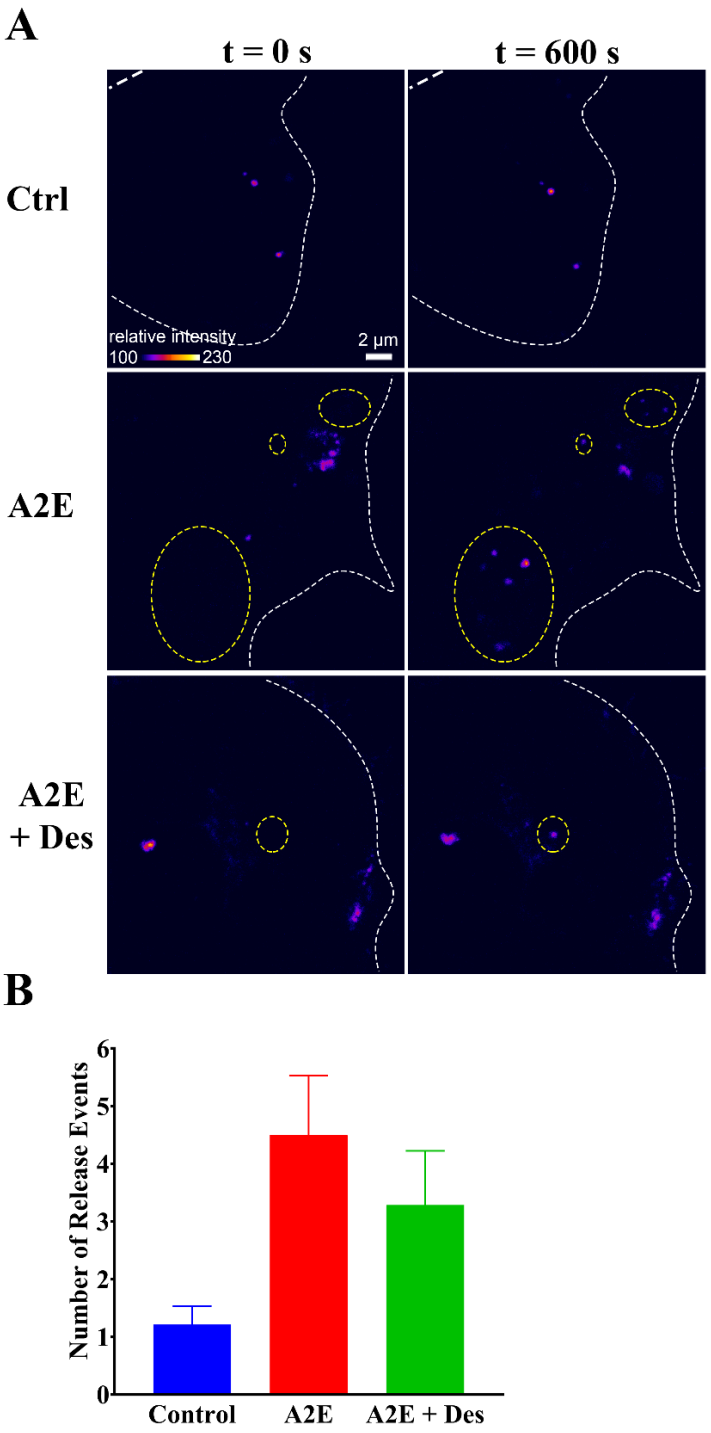


FIGURE 2.5 CERAMIDE CAUSES MORE EXOSOME RELEASE EVENTS

A. Stills from live-imaging of cells transfected with CD63-pHluorin. White dotted line is cell boundary, yellow dotted line highlights release events.
B. Quantification of A. Mean±SEM.

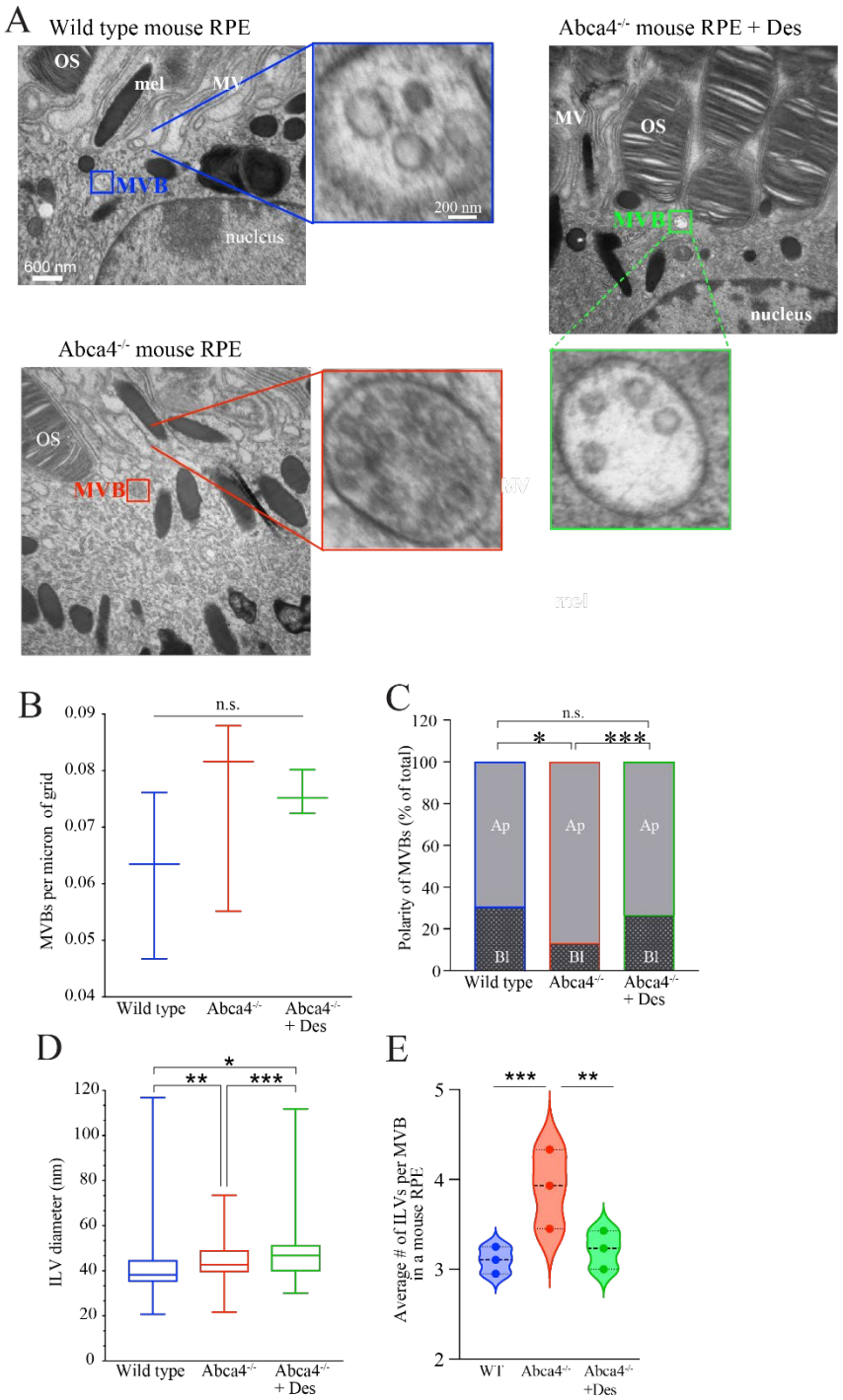


FIGURE 2.6 CERAMIDE INCREASES ILVS PER MVB IN RPE

A. Representative images of ILVs and MVBs from mouse RPE.
B. Quantification of MVBs per micron of grid. Mean±SD. Student's t-test.
C. Polarity of MVBs in the RPE. Student's t-test
D. Diameter of ILVs as box-and-whisker plot. Student's t-test.
E. Number of ILVs per MVB. Mean±SD Student's t-test with Welch's correction * $p < 0.05$, ** $p < 0.01$, *** $p < 0.0001$.

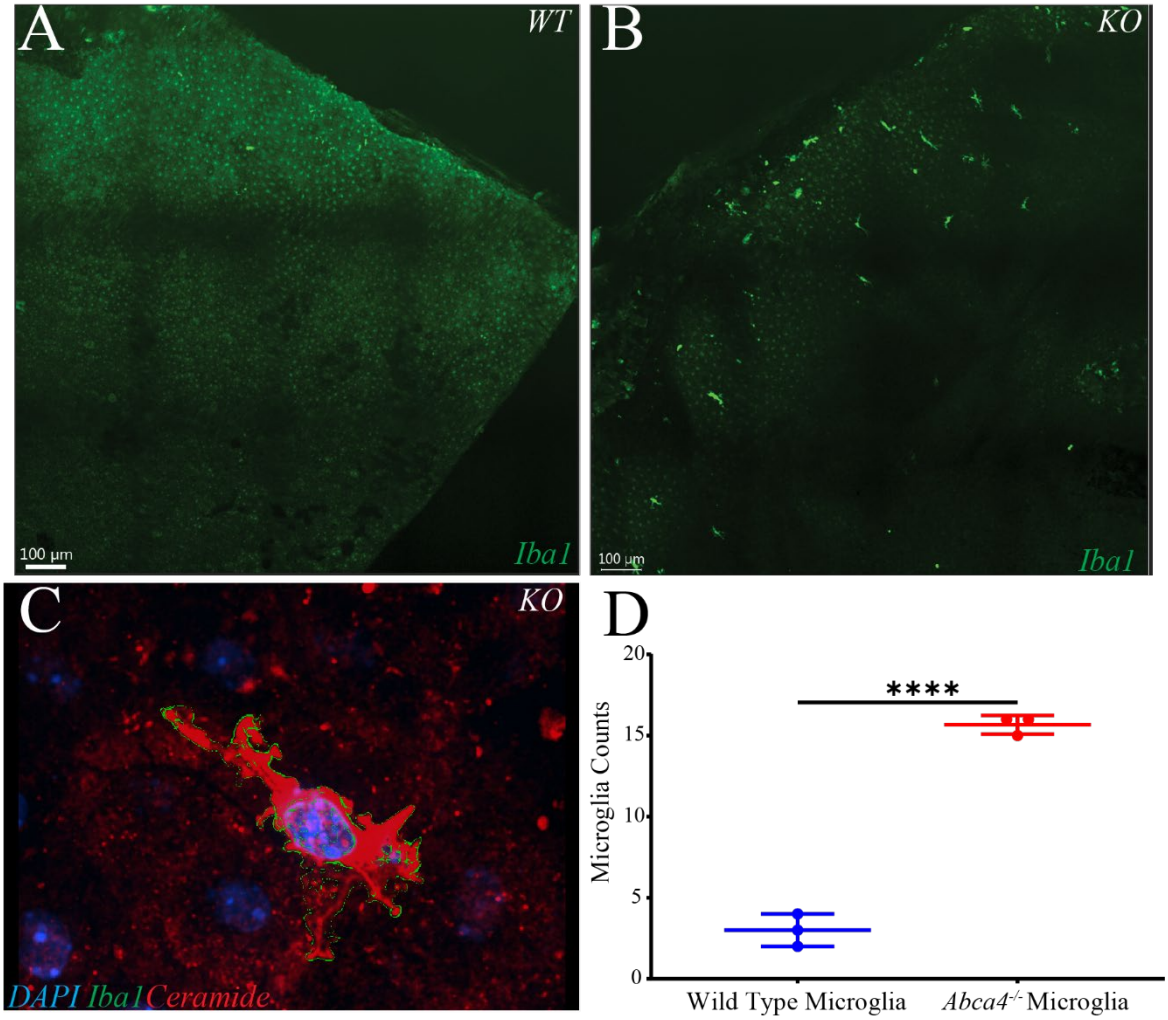


FIGURE 2.7 MICROGLIA ARE RECRUITED TO THE SUBRETINAL SPACE

A. Stitched confocal images from a wild-type mouse RPE flatmount stained for Iba1.
B. Same as A, but for an *Abca4*$^{-/-}$ mouse.
C. 3D reconstruction showing that ceramide is in subretinal microglia.
D. Quantification of A and B. Mean±SD. **** $p < 0.001$ Student's t-test.

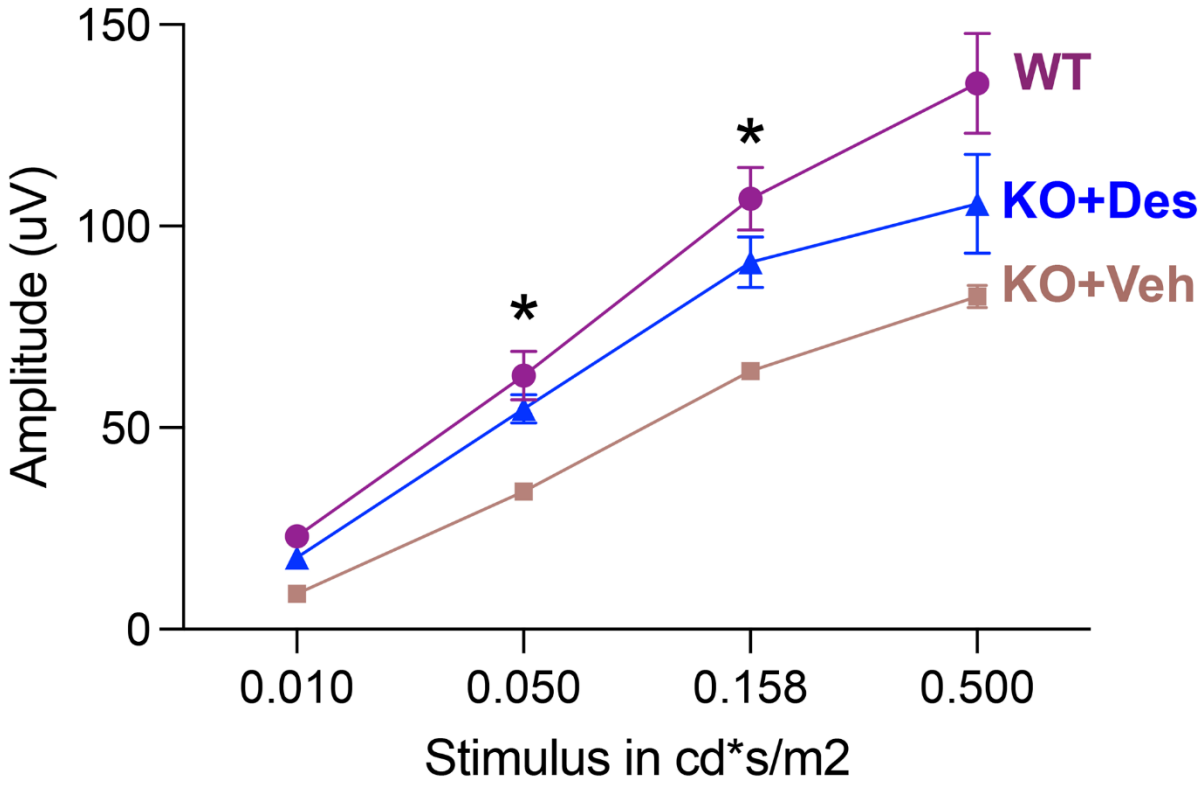


FIGURE 2.8 DESIPRAMINE CAN PROTECT PHOTORECEPTOR FUNCTION

Average of a-wave amplitudes over stimuli from 18-month-old mice. Mean±SD. * $p < 0.05$ Student's t-test.

Methods

PRPE Culture

Primary RPE were isolated from porcine eyes using established protocols [31]. Briefly, extraocular tissues were removed from the eyes, and the eyes were incubated in 20% iodine solution (1 part povidone-iodine diluted in 4 parts autoclaved distilled water) (10 minutes, 4°C) followed by incubation in 1000 U/mL Penicillin-Streptomycin solution (5 minutes, 4°C). The anterior portion of the eyes, the lens, and the vitreous were removed in a biosafety hood, and the eyecups were placed in a 12-well plate. Each eyecup was incubated in 2 mL of PBS with 1 mM EDTA (30 minutes, 37°C). Retinas were gently detached from the eyecup with blunt forceps and removed by clipping at the optic nerve head. Upon removal of retinas, each eyecup was incubated in 1 mL of 0.5% trypsin with 5.3 mM EDTA in Hank's balanced salt solution without calcium and magnesium (30 minutes, 37°C). RPE were dissociated from the eyecups by resuspension and collected into conical tubes containing 8 mL neutralizing media (DMEM with 4.5 g/L glucose, 10% heat-inactivated fetal bovine serum, 1% non-essential amino acids, 1% penicillin/streptomycin, 10 µg/mL ciprofloxacin). Cell suspension from 2 eyecups were pooled into a tube. Each eyecup was subjected to brief rinses with 1 mL 0.5% trypsin solution to collect any remaining dissociated RPE. Cell suspensions were pooled and centrifuged at 300xg for 4 minutes at room temperature. RPE pellets from 6 eyes were pooled and plated onto T25 flasks in growth medium (DMEM with 4.5 g/L glucose, 10% heat-inactivated fetal bovine serum, 1% non-essential amino acids, 1% penicillin/streptomycin, 10 µg/mL ciprofloxacin). Flasks were fed every 2-3 days. After 1 week in culture, 10% FBS growth media was replaced with 1% FBS media and cultured for another week before plating on collagen-coated Transwell filters.

ARPE-19 Cultures

ARPE-19 cells were purchased from ATCC and passaged onto tissue culture treated 10cm plates at 37°C. ARPE-19 cells were grown in medium made up of DMEM with 4.5g/L glucose, 3% heat-inactivated fetal bovine serum, 1% non-essential amino acids, 1% penicillin/streptomycin, and 1% antimycotic/antibiotic. Cells were fed exosome-depleted media after reaching 80% confluence and medium was allowed to condition overnight.

Mice

Wild-type and *Abca4*$^{-/-}$ mice were housed under 12-hour light-dark conditions with a minimum intra-cage lux value of 20 to ensure adequate generation of lipofuscin within the RPE. Mice were allowed water and PicoLab 5053 diet ad libitum. Mice were sacrificed 3 hours after light onset when they reached 6 months of age.

Desipramine Treatments

Desipramine HCl was dissolved into phosphate buffered saline and administered via intraperitoneal injection at 10mg/kg 3 times per week for 4-8 weeks.

Transmission Electron Microscopy of Mouse Retinas

Whole mouse globes were enucleated, cleaned of excess tissue, then fixed in an excess of 4% paraformaldehyde and 5% glutaraldehyde in 0.1M sodium cacodylate pH 7.4 for 1 hour at room temperature. The anterior portion was then removed (cornea, lens, iris) and relaxing cuts were made to flatten the eyes, with the retina remaining attached. Eyes were then rinsed in 0.1M sodium cacodylate pH 7.4 three times before being moved into 1-hexadecene. Five 2 millimeter punches were taken from each eye with a biopsy punch. These punches were then moved into 0.3 mm type B freezing hats coated in 1-hexadecene. Excess 1-hexadecene was applied to remove air before being capped with another type B freezing hat for a total space of 0.6 millimeters total

These were subjected to high pressure freezing in a Balzers HPM-010. Hats were separated under liquid nitrogen and placed in frozen freeze substitution media (0.1% methanolic uranyl acetate and 4% osmium tetroxide). The freeze substitution media was placed into a Leica AFS set to -70˚C for 72 hours before ramping up to 4˚C over the course of 24 hours. Excess freeze substitution media was removed by three rinses in pure acetone. Hats were removed and samples were incubated with mixtures of 50:50 and 75:25 complete Embed-812 Hard formulation/acetone for 16 hours each with rotation. Following this, three changes of pure resin were conducted over the course of eight hours before being held under vacuum overnight. Samples were removed and put into fresh resin in coffin molds with labels. Sections were cut using an ultramicrotome (Reichart) at 70 nm thickness and placed onto 1 millimeter copper slot grids with formvar. Grids were stained using 4% uranyl acetate in a Hiroka staining chamber, rinsed with deionized water and stained with lead citrate in a CO_2 depleted environment created by sodium hydroxide pellets. Grids were dried and imaged on a Philips CM120 at an accelerating voltage of 80 kV and 2 µm spot size using a BioSprint 12 camera (Advanced Microscopy Techniques) at a one second exposure and two-frame average. The entire grid was imaged. Images were analyzed using the AMT plugin for FIJI to calibrate pixel sizes. ILVs were identified based on the presence of a complete membrane surrounding the vesicle and a clear doughnut morphology. For an organelle to be counted as a MVB required at least 2 ILVs. Diameters of ILVs and MVBs were measured using the Line tool. To classify MVBs as apical or basolateral, low magnification shots of the RPE were taken to encompass basal infoldings and microvilli. Distances were measured from the bottom of the basal infoldings to the base of the microvilli. Determination of polarity was determined based on whether the MVB was within the apical or basolateral domain of the RPE. To calculate MVBs per micron, a “burn” was performed on the grid by increasing the beam intensity to make a mark at the start of

each imaging session and at the end. The lowest mag possible on the scope was then using to image the entire grid. The Segment tool in FIJI with the AMT plugin was used to trace along the basolateral infoldings of the RPE from each burn. This total distance was used to calculate MVBs per micron.

Exosome Isolation and Purification

Cells were cultured in EV-depleted media. Briefly, complete media was centrifuged in an SW28 rotor at 100,000xg for 16 hours at 4 ˚C. The media was harvested and the pellet was discarded. Cells were fed this media along with A2E or any other agents. Apical and basolateral media from 17 12mm Transwell filters per condition were harvested twice, with each harvest occurring every 48 hours and pooled. EVs were isolated via differential ultracentrifugation, density gradient ultracentrifugation, or size exclusion chromatography according to established protocols [71]. For differential ultracentrifugation, apical and basal media were centrifuged at 300x*g* for 10 minutes to remove cellular contaminants at 4˚C in an Eppendorf 5240 centrifuge. Pellets were discarded and supernatants centrifuged in fresh tubes at 2,000x*g* for 10 minutes at 4˚C in an Eppendorf 5240 centrifuge. Supernatants were transferred into polyallomer tubes and centrifuged at 10,000xg for 30 minutes at 4˚C in a Beckman L8-80M preparative ultracentrifuge with a SW28 rotor to remove apoptotic particles. Supernatants were centrifuged at 100,000xg for 3 hours at to isolate purified EVs. Pellets were rinsed in sterile PBS and centrifuged in an SW44Ti rotor for 100 minutes at 4˚C at 100,00xg to remove any external proteins and debris.

For iodixanol gradient, a mix of PBS and OptiPrep was used to form a discontinuous gradient with 40, 20, 10, 5% layers. Exosomes isolated via differential ultracentrifugation were overlaid on top and spun at 100,000xg for 16 hours. Fractions were harvested in 200 microliter increments and subjected to absorbance spectroscopy at 244 nanometers. The fractions with an

absorbance value of 0.477, corresponding to a density of 1.15 g/mL, consistent with published literature, were pooled together and wash step was performed to remove iodixanol and concentrate exosomes [72].

For size exclusion chromatography, Izon columns were used according to manufacturer's instructions. Briefly, exosome-depleted cell-conditioned media derived from 3 flasks per condition, either A2E or control, harvested 7 times, once every 48 hours, was concentrated using pre-rinsed Centricon 100kDa filters. This concentrated media was then centrifuged to remove aggregates at 10,000x*g* for 10 minutes at 4˚C. Pellets, if any, were discarded. Supernatants were applied to Izon columns and fractions 6-9 were collected as pure EVs. These EVs were then spun at 10,000xg to remove any aggregates and used in downstream preparations.

Transmission Electron Microscopy of Exosomes

Transmission electron microscopy of EVs was performed as described in literature [71]. Briefly, purified exosomes were fixed in 4% PFA for 20 minutes before being adsorbed onto a 200-mesh copper slot grid with a carbon-formvar coating. Grids were fixed with 2% glutaraldehyde, rinsed in deionized water, and stained with 4% aqueous uranyl acetate and uranyl oxalate. Grids were imaged using same microscope and camera as described for MVB analysis of eyes.

Immunoblotting

Exosomes or cells were lysed in 1X HNTG lysis buffer (50 mM HEPES, 150 mM NaCl, 10% glycerol, 1.5 mM $MgCl_2$, 1% Triton X-100) supplemented with a protease inhibitor cocktail. Protein concentrations were measured by the DC Protein Assay. NuPAGE LDS sample buffer was added to the lysates, and samples were heated to 85°C for 10 minutes. Samples were resolved on a NuPAGE 4-12% Bis-Tris gel at 150 volts for 1 hour at room temperature. Gels were transferred onto nitrocellulose membranes using the iBlot transfer device for 7 minutes using the preset

program 3. Membranes were blocked in Intercept PBS Protein-Free Blocking Buffer for 1 hour at room temperature with gentle shaking and incubated with indicated primary antibodies diluted in blocking buffer supplemented with 0.1% Tween20. Membranes were then incubated with IRDye secondary antibodies for 1 hour at room temperature and scanned using LI-COR Odyssey CLx. Band intensities were quantified using Image Studio.

Nanoparticle Tracking Analysis

Purified EVs were resuspended in PBS that was pre-filtered through a 20-nanometer pore size fiberglass filter. This suspension was measured by an LM10 NanoSight (Malvern) with temperature recording. Five 30-second videos were acquired per sample, and each sample was measured in triplicate. Camera setting of 13 with a sensitivity threshold of 3 was used for both acquisition and analysis. Between each measurement, the optical flat and instrument was thoroughly cleaned with pure ethanol and deionized water. A background video was taken of the filtered water to subtract contaminating particles.

Nanoimaging of Exosomes

To evaluate exosome cargo, purified exosomes were processed as per EV Application kit instructions (Oxford Nano Imaging). Briefly, exosomes isolated by size exclusion chromatography were stained with the exosomes kit and conjugated antibodies using Mix-n-Stain kits overnight before being fixed onto the ONI Chip. The IgM linker was used to conjugate the 647 dye to the ceramide antibody. To conjugate Cx43, the 561 linker was used. EVs were imaged using ONI's B^3 buffer, acquiring 1,500 frames at a 30˚ angle with a laser power of 15%. The standard imaging protocol was applied along with CODI drift correction. Images were further quantified using Imaris 10 with intensity-based colocalization and background subtraction and Gaussian filtering.

Live Imaging of Exosome Release

Primary porcine RPE transfected with CD63-pHluorin (5 μg/1.5x10^6 cells) were treated with A2E (10 μM for 6 hours followed by a 48 hour chase in fresh culture medium [33,73]. Some cultures were treated with desipramine (10 μM) immediately before imaging [33,34,74]. Cells were imaged in recording medium (1 x HBSS, 4.5 g/L glucose, 0.01 M HEPES) supplemented with 1% FBS and 1% NEAA as described previously. Imaging was performed at 37°C in an Okolab humidified microenvironmental chamber on the Nikon spinning disk confocal microscope using a CFI60 Apochromat TIRF 100X oil immersion objective (1.49 NA). The system is equipped with: Yokogawa CSU-X1 confocal spinning disk head, Nikon Eclipse Ti2-E inverted microscope, Live-SR super-resolution module, Andor iXon Ultra 888 EMCCD camera, Ti2-S-SE-E motorized stage with piezo-Z for rapid Z-stack acquisition, and a laser combiner with four solid-state lasers at 405, 488, 561, and 640 nm and the corresponding band-pass emission filter sets (Chroma) loaded on a FLI high speed filter wheel. Identical laser power, exposure and gain settings were applied for all conditions within a set of experiments. To capture apical exocytosis, a plane with pre-docked CD63-pHluorin puncta near the apical membrane was determined and time-lapse movie was acquired at 30 second intervals for 10 minutes (50 millisecond exposure). Surface reconstructions were performed with the "Surfaces" module with tracking enabled on Imaris. The appearance of new surfaces absent in the preceding time frame were quantified as exocytic events.

Mass Spectrometry

ARPE-19 cells treated with or without 2.5 μM U18666A were cultured in exosome-depleted medium overnight. EVs were purified from the media by differential ultracentrifugation as described above. The resultant pellet was resuspended in PBS and purified using a self-generating continuous iodixanol gradient. The gradient was then harvested in 200 μL increments

and absorption spectra were matched to determine the ideal percentage iodixanol for EV harvesting. Upon isolation of the correct density, samples were processed by the Mass Spectrometry Core at the University of Wisconsin-Madison.

Electroretinography

Mice were dark-adapted overnight to evaluate scotopic response. All mice were anesthetized using a mixture of ketamine and xylazine until deep anesthesia was reached. Whiskers were trimmed and a mydriatic solution of 1% tropicamide and 5% phenylephrine was applied. Liberal amounts of GenTeal Severe were used to keep eyes moist and maintain contact with electrodes. The Celeris in Active/Reference/Ground configuration was used. The ground electrode was placed in the skin near the base of the tail. The reference electrode was placed in the cheek of the animal. 9 steps with luminances ranging from 0.01 $cd \cdot s/m^2$ to 50 $cd \cdot s/m^2$ were used with a two minute recovery period between each step. A recording epoch of 4 seconds was used to capture a, b, and c waves and ten sweeps were averaged for each step. Each sweep had a 20 second pause to avoid light adaptation. Wave peaks from both eyes were averaged together. After measurement, atipamezole was administered and mice were left in a warm clean cage to recover before being put back into housing.

Immunofluorescence of Mouse Eyes

Enucleated mouse eyes were dissected to remove the anterior portion of the eyes including the lens. Four relaxing cuts were made on the eye cups prior to fixation in 4% PFA for 1 hour at room temperature. The retinas were clipped and removed. Each RPE flatmount was blocked for 1 hour at room temperature in 300 μL of 2% BSA in PBS supplemented with 0.1% Triton-X. After blocking, flatmounts were incubated in primary antibodies diluted in 1% BSA in PBS at 4°C for 16 hours, followed by incubation in AlexaFluor secondary antibodies and phalloidin diluted in 1%

BSA for 2 hours at room temperature. After secondary staining, flatmounts were rinsed as above and stained with DAPI. After three rinses, flatmounts from mice older than 6 months were incubated with TrueBlack for 30 seconds to quench RPE lipofuscin autofluorescence. After rinsing, flatmounts were mounted and sealed on clean slides with PBS and Vectashield Vibrance. Images were taken using the Nikon spinning disk microscope.

Statistics

Graphpad Prism 10 was used and statistical testing was performed as described in the figure.

CHAPTER 3: ALTERED PIEZO1 ACTIVITY IN THE RPE INDUCES MITOCHONDRIAL DEFECTS

Introduction

Mechanical forces are a fundamental aspect of life. Cells and tissues have mechanosensitive ion channels that allow them to not only sense, but make use of mechanical forces [75]. Mechanosensation has typically focused on touch and hearing, but it is now well-appreciated that mechanosensation is an important player in tissue homeostasis [76]. Normal brain development relies on neurons being able to sense different stiffnesses in order to properly find and enervate the right organs[77]. The stomach and intestines are reliant on mechanosensation in order to sense satiety or the feeling of fullness, the loss of which can induce obesity in mice [78]. Surprisingly, even bones are regulated by mechanical stress, with an increase in stress causing an increase of bone mass and a loss causing a drop in bone density [79]. The eye is also subjected to numerous mechanical stresses, from choroidal and inner retinal vascular beds that perfuse the retina to the thousands of saccades, or rapid minor eye movements, that constitute vision. Excellent work has been done on the mechanobiology of eye in regards to glaucoma [80,81]. However, little is currently understood about the importance of mechanotransduction in the retina or RPE.

Among the channels that can transduce mechanosensation, the Piezo channels (Piezo1 and Piezo2) have been the focus of intense research interest in recent decades. Piezo channels, with 26-40 transmembrane helices and over 2,500 amino acid residues [82] have been shown to have numerous functions, from neuronal pathfinding and vasculature development to iron metabolism and more [83,84]. Piezo channels have been found to play a number of roles in both organismal development and the progression of diseases [85] [86]. They control the spread and growth of epithelial cells, planar cell polarity, as well as overall organismal growth [87] [88]. Within epithelia, Piezo

channels can prevent or induce extrusion from the monolayer and thus prevent overcrowding. Loss of Piezo channels is embryonic lethal as many organisms fail to develop the lung and vasculature structures sufficient to sustain life [89,90].

Piezo channels have extremely rapid activation and inactivation kinetics, on the order of a few hundred milliseconds. Perhaps most fascinatingly, to date, no endogenously-expressed ligands have been identified for either Piezo1 or Piezo2 [91]. These channels can only be activated by mechanical deformation, unlike many other mechanosensitive ion channels such as the transient receptor potential (TRP) channels [92]. In fact, the Piezo1 channel shares very little homology with other known mechanosensors. Mechanical stimuli that activate the Piezos include shock, osmotic stress, shear stress, pulling, and pushing forces. These can derive from external forces affecting the lipid bilayer or intrinsic forces, such as cell swelling or alterations in the composition of the bilayer itself [93,94].

This chapter of the thesis focuses on understanding the role of Piezo1 in the RPE. Piezo1 is a 900-kDa homotrimeric cation channel. It is composed of a cap and a trio of three "blades" that are composed of an arm and a beam each. When fully assembled, Piezo1 has a central pore formed by the C-terminus that allows for selective conductance of predominantly calcium ions [95]. When force is applied to the channel, these blades flatten and expand, causing tilting and lateral movement that allows the central pore to open and allow ions through [96].

The Piezo1 synthetic ligand Yoda1 activates Piezo1 by binding to a pocket at the base of the arm, close to the central pore and lowering the channel's activation threshold[89,90]. While there are no specific inhibitors of Piezo1, non-specific inhibitors of mechanosensitive channels such as GsMTx4 have been shown to inhibit Piezo1. GsMTx4 is a component of Chilean spider toxin venom and works to reduce the transmission of force by acting as a cushion through intercalating

into the lipid bilayer. Through this mechanism, it can inhibit not only Piezo1 activation but nearly all mechanosensitive ion channels [97,98].

Piezo1 has been shown to be activated by beta-amyloid plaques found in Alzheimer's disease and extracellular matrix stiffening like those found around gliomas [85,99]. These studies suggest that large lipid-protein aggregates such as drusen could induce mechanical stress on the RPE and drive Piezo1 activation and signaling. Another trigger for Piezo1 activation could be the Bruch's membrane, a 2-4 micron matrix that sits between the RPE and the choroid. It is composed of the basement membrane of the RPE, two collagenous layers, an elastin layer, and the basement membrane of the choriocapillaris, [100]. With age, thickening of the Bruch's membrane prevents or slows diffusion of macromolecules. Crosslinking of collagen and calcification of elastin lead to stiffening and thickening of the Bruch's membrane [101,102]. This could transmit more force to the RPE and activate Piezo1 as seen with the extracellular matrix around solid tumors.

Ceramide and cholesterol have also been shown to be coupled to Piezo1 function [103]. Cholesterol alters rigidity in cell membranes, with more cholesterol causing stiffening of the bilayer. This can allow for mechanical force to be more readily transmitted from one location in the bilayer to another. As previously discussed, A2E accumulation drives cholesterol increases within the RPE. It may be that excess cholesterol can increase the force transmitted to the Piezo1 channel. Ceramide, as previously discussed, is a cone-shaped lipid which can alter membrane topology. Published studies suggest that an increase in membrane ceramide can slow the inactivation kinetics in Piezo1, resulting in longer channel opening times which would allow more calcium influx into the cell [36,94]. Taken together, these studies suggest that cholesterol and ceramide accumulation in the RPE could not only cause the Piezo1 channel to open more readily in response to mechanical stimuli, but also stay open for longer periods, increasing intracellular calcium ion

concentrations. This is particularly important as excess levels of calcium can cause mitochondrial damage and depolarization, inducing fission and mitophagy as protective responses to preserve cell health (Figure 3.1A,B). Since autophagy is defective in *Abca4*$^{-/-}$ Stargardt disease mouse RPE and in RPE with A2E, as the Lakkaraju lab has shown, this would lead to an accumulation of damaged mitochondria that would further compromise RPE functionality and health [33].

Piezo1 signaling has been reported to activate feedback loops that increase its expression [10485]. Piezo1 activation also remodels the nuclear envelope and heterochromatin as a response to prevent DNA and maintain genome integrity[105]. In post-mitotic cells, epigenetic silencing is particularly important to maintaining differentiated states. The loss of certain histone markers, such as H3K9Me3 is associated with a loss of ability to repair DNA damage and an increased expression in pluripotency genes [106]. Within the context of RPE and disease, epithelial-to-mesenchymal transitions are thought to play a role in RPE atrophy in AMD and in proliferative vitreoretinopathies. It may be that altered Piezo1 activation can be causing a shift in RPE from post-mitotic to pluripotent, and this loss of polarity would compromise the ability of the RPE to perform its essential functions to maintain the health of the retina.

Taken together, Piezo1 activation, either due alterations in the lipid composition of the membrane or via drusen causing mechanical stress on the RPE, could disrupt RPE homeostasis and function. This could cause retinal dysfunction and result in loss of vision. This chapter will seek to explore this possibility (Figure 3.2).

Results

Piezo1 Expression is Upregulated in the RPE in Disease States

Piezo1 is ubiquitously expressed in many tissues, however little is known about Piezo1 in the RPE. Wildtype and *Abca4*$^{-/-}$ mouse RPE flatmounts were stained with a Piezo1 antibody, which revealed that the RPE does indeed express high levels of Piezo1 (Figure 3.3). Staining human donor cryosections showed that while both healthy and AMD RPE expressed Piezo1 (Figure 3.4A), AMD donors expressed more Piezo1, in agreement with reports showing that Piezo1 activation can promote its own expression (Figure 3.4B).

RPE Grown on Beads Activate Piezo1

Currently, there are no mouse models that generate drusen deposits as seen in humans. While there are cell culture models that secrete drusen-like deposits, these usually require several months of culture before they can be used[107]. Our goal was to identify how drusen induced mechanical stress on the RPE. To model drusen in a dish, we cultured polarized PRPE on silica beads of varying size in a matrix of collagen to simulate sub-RPE drusen (Figure 3.5). These beads are biologically inert cannot be phagocytosed by the RPE. This prevents any frustrated phagocytosis and allows only the mechanical forces they transmit to be the sole effector on the RPE. These beads ranged in size from 0.166 μm in diameter to well over several hundred microns and were deposited at a density of 40 beads/cm^2 in a 10 μg/cm^2 collagen matrix on 6.5 mm Transwell filter. Primary porcine RPE cells grew formed a polarized monolayer within 2 weeks and had normal transepithelial electrical resistance values. This indicated that the beads were not detrimental in allowing the RPE to grow on the Transwell filters.

Live imaging of the cell-permeable Ca^{2+} probe Fluo4NW was performed to assess calcium influx as a measure of Piezo1 activation in healthy RPE monolayers and RPE grown on beads. A short treatment with Yoda1, which was used as a positive control, increased Fluo4NW signal within the cell compared to healthy RPE (Figure 3.6A). This increase was even more pronounced on RPE cultured on silica beads. GsMtX4 treatment decreased calcium influx to control levels, indicating that Piezo1 likely increases Ca^{2+} influx into the RPE (Figure 3.6B).

Piezo1 Overactivation Causes Mitochondrial Fragmentation

High levels of calcium can induce mitochondrial fragmentation and our lab has reported that RPE from AMD donors and *Abca4*$^{-/-}$ mice have fragmented mitochondria [35,108]. To examine if Piezo1 may be at play in mediating calcium-induced mitochondrial fragmentation, we immunostained healthy RPE, RPE grown on beads, or RPE treated with Yoda1 with an antibody to TOM20, a mitochondrial outer membrane protein. RPE on beads and those treated with Yoda1 exhibited significant fragmentation of the mitochondrial network (Figure 3.7). The RPE is highly reliant on intact mitochondria for oxidative phosphorylation. This is important to reserve the majority of glucose derived from the choriocapillaris for the overlying photoreceptors which are exclusively reliant on glycolysis.

Fragmented mitochondria indicate a problem with RPE homeostasis and may negatively impact the retinal health overall. We further checked for alterations in the expression of proteins involved in mitochondrial fusion and fission as these would indicate altered machinery (Figure 3.8A,B). We found that in RPE treated with Yoda1, there was a significant increase in the short forms of optic atrophy 1 (OPA1) which promote fission (Figure 3.8C). Yoda1 also increased the pro-fission phosphorylation of dynamin-related protein 1 (DRP1) and decreased the expression of

pro-fusion protein mitofusin 2 (MFN2). This strongly implies that abnormal Piezo1 activation induces mitochondrial fission in the RPE.

Mechanical stress induces nuclear remodeling and alters H3K9Me3 chromatin marks [105]. H3K9Me3 is a histone marker for methylation modifications, which silence gene expression and may help cells stay differentiated. As the RPE is a post-mitotic cell, keeping its differentiated status is paramount to its function. To evaluate the impact mechanical deformation could have on the RPE nucleus, we stained for H3K9Me3 in RPE grown on beads. Our data show a striking loss of the H3K9Me3 in the nuclei of cells grown on beads. The loss of H3K9Me was also evident in *Abca4*$^{-/-}$ mice when we compared them with their age-matched wildtype littermates. Upon treatment with desipramine, which has been shown by the lab in previous papers to reduce ceramide levels in the RPE, H3K9Me3 was restored in the nuclei of mouse RPE (Figure 3.9). This may indicate a role for ceramide functioning in Piezo1 activation and causing nuclear remodeling.

Piezo1 is Important for Photoreceptor Function

How Piezo1 acts within the retina is not well-established. We generated an inducible RPE-specific knockout of Piezo1 by crossing Cre-ERT2 mice with Piezo1-floxed [109]. We injected mice that were positive for Cre with tamoxifen to induce recombination and delete PIEZO1 from the RPE. As tamoxifen has been shown to cause RPE stress and injury, we also injected littermates that were negative for Cre with tamoxifen as a control [110111]. ERG measurements revealed that Piezo1 loss in the RPE caused decrease in a-wave amplitudes, indicating impaired photoreceptor function. These mice also had defects in their c-waves, indicating a negative impact on RPE health (Figure 3.10).

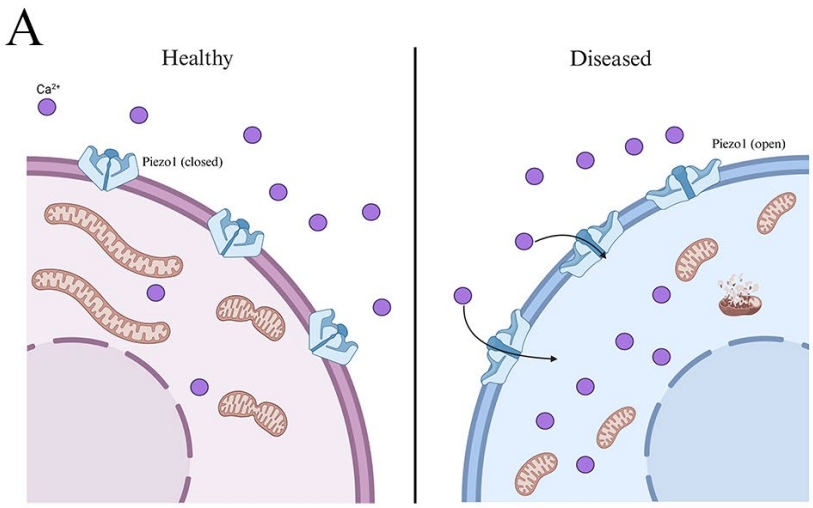
Conclusions

This chapter shows that aberrant activation of Piezo1 can induce mitochondrial fragmentation in RPE via excessive calcium influx into the cytoplasm. These can be either through mechanical stress via beads, which models drusen, or via excess amounts of ceramide, which can prolong Piezo1 activation times. Decreasing ceramide with desipramine or inhibiting mechanosensitive ion channels prevents the fragmentation of mitochondria. Piezo1 activation could remodel the nucleus and drive H3K9Me3 loss, which could alter RPE epigenetics and promote dedifferentiation. Further transcriptomic studies are necessary to fully evaluate the impact of Piezo1 activation or loss on the RPE.

Piezo1 may not be the only culprit behind calcium influx and mitochondrial fragmentation. As alluded to previously, other mechanosensitive ion channels such as TRPV4 can be activated by Piezo1 and these channels have a much greater current than Piezo1, which may allow for a greater calcium wave and intensify mitochondrial fragmentation. Ongoing studies in the lab are evaluating other mechanosensitive ion channels expressed by the RPE such as TRPV4 and TRPML1. Future work will evaluate if these channels are modulated by Piezo1 or have another role to play, which could be promising therapeutic targets for retinal degenerations.

While Piezo1 activation appears to be a major culprit in loss of RPE homeostasis, outright inhibition is also not the solution as evidenced by the phenotype of mice with RPE-specific deletion of Piezo1. Loss of Piezo1 appears to cause photoreceptor and RPE deficits, indicating that some amount of Piezo1 functionality is necessary for the health of the retina. Therefore, a more nuanced approach is required when developing therapies targeting diseases such as AMD and Stargardt disease.

Figures



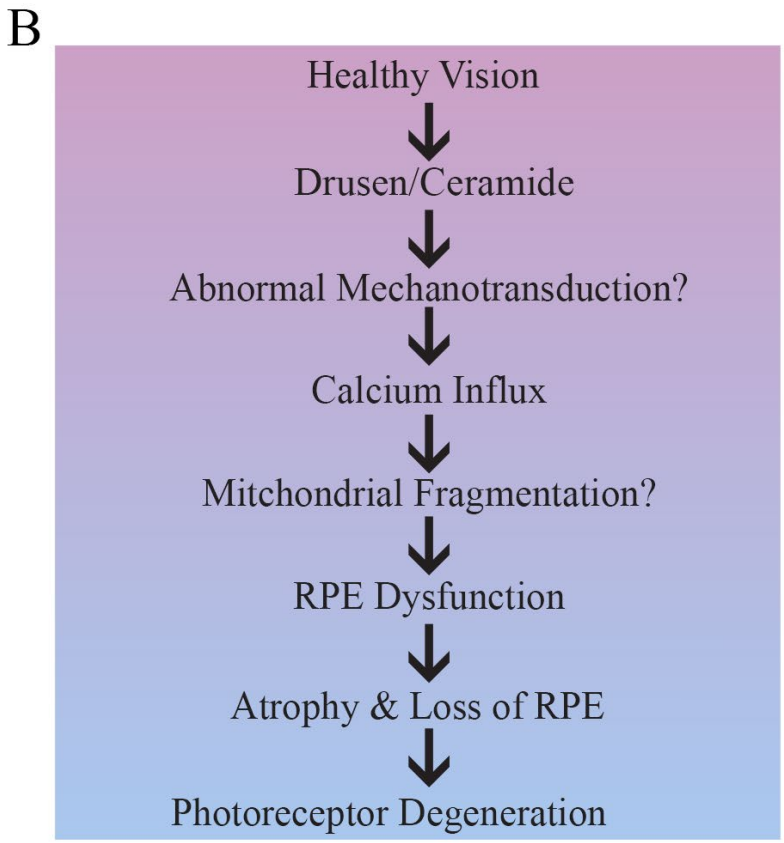


FIGURE 3.1 ILLUSTRATION OF HYPOTHESIS

A. Schematic showing healthy versus diseased states and how Piezo1 channel opening can cause mitochondrial fragmentation via calcium ion influx.
B. Schematic showing the process through which drusen/ceramide can induce abnormal mechanotransduction and RPE injury.

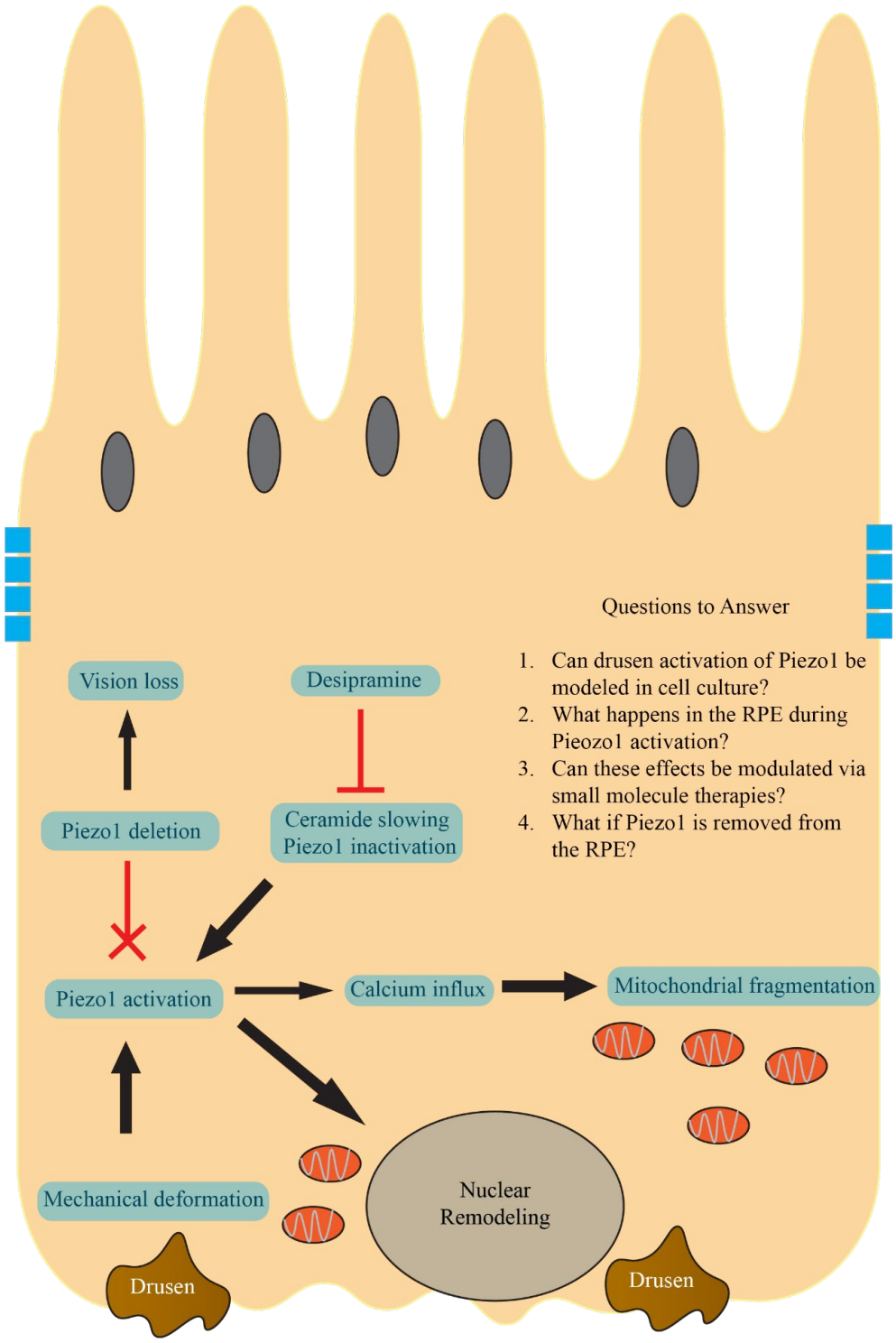


FIGURE 3.2 PROPOSED MECHANISM OF PIEZO1-MEDIATED MITOCHONDRIAL FRAGMENTATION

Schematic showing how Piezo1 activation, either by ceramide or drusen, may cause mitochondrial fragmentation and a possible intervention.

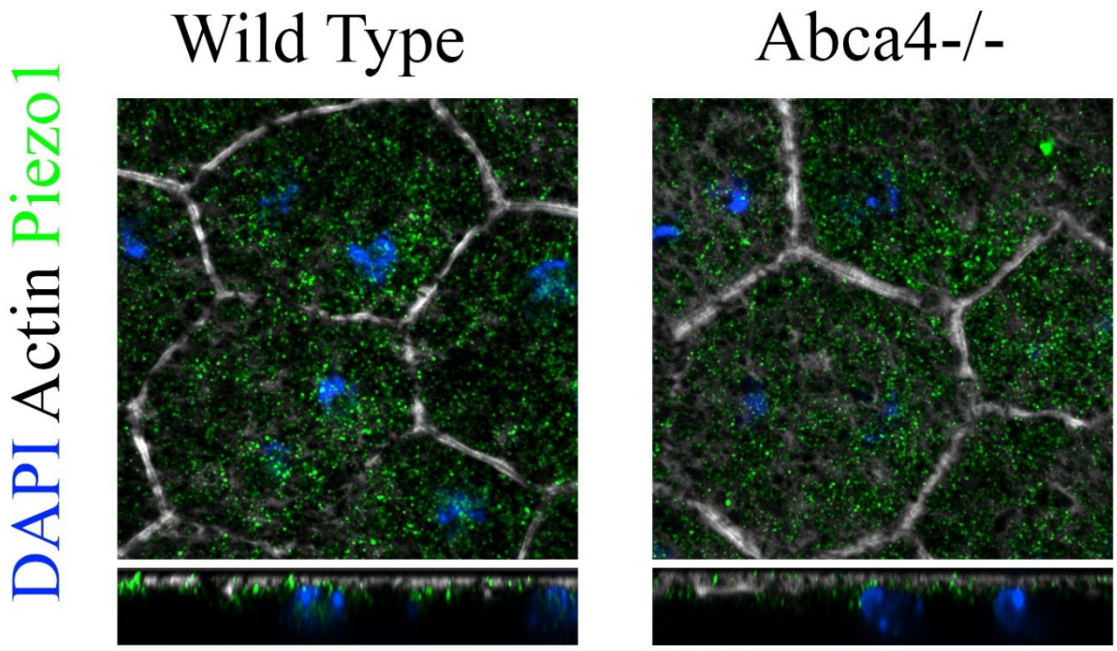


FIGURE 3.3 RPE EXPRESSES PIEZO1

Slice view with an xz view below showing RPE flatmounts of both wild-type and *Abca4*$^{-/-}$ mice. Piezo1 is in green with nucleus stained in blue and actin in white.

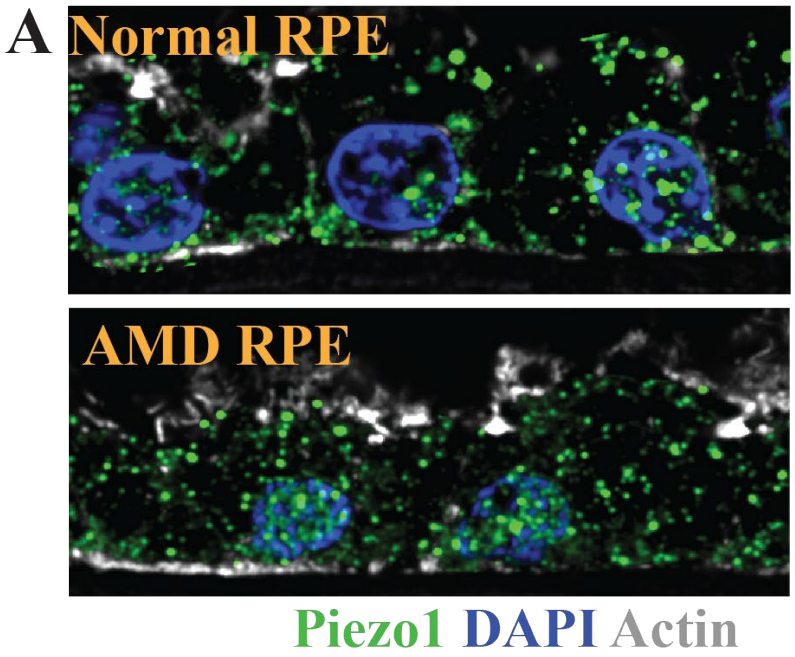


FIGURE 3.4 AMD RPE UPREGULATE PIEZO1 EXPRESSION

A. Cryosections from both healthy and AMD donor eyes showing RPE stained for Piezo1 in green and the nucleus in blue.
B. Quantification of A ±SD. *** $p < 0.001$ Student's t-test.

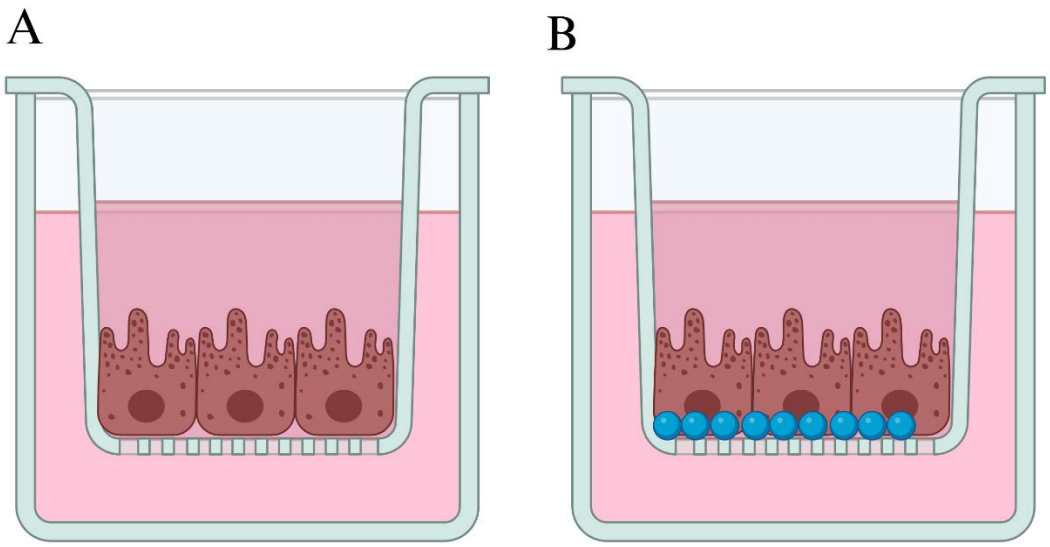


FIGURE 3.5 TRANSWELL SCHEMATIC

Schematic showing how PRPE cells are cultured. A. PRPE grown on Transwell without beads. B. PRPE grown on Transwell with beads. Note that beads are not to scale.

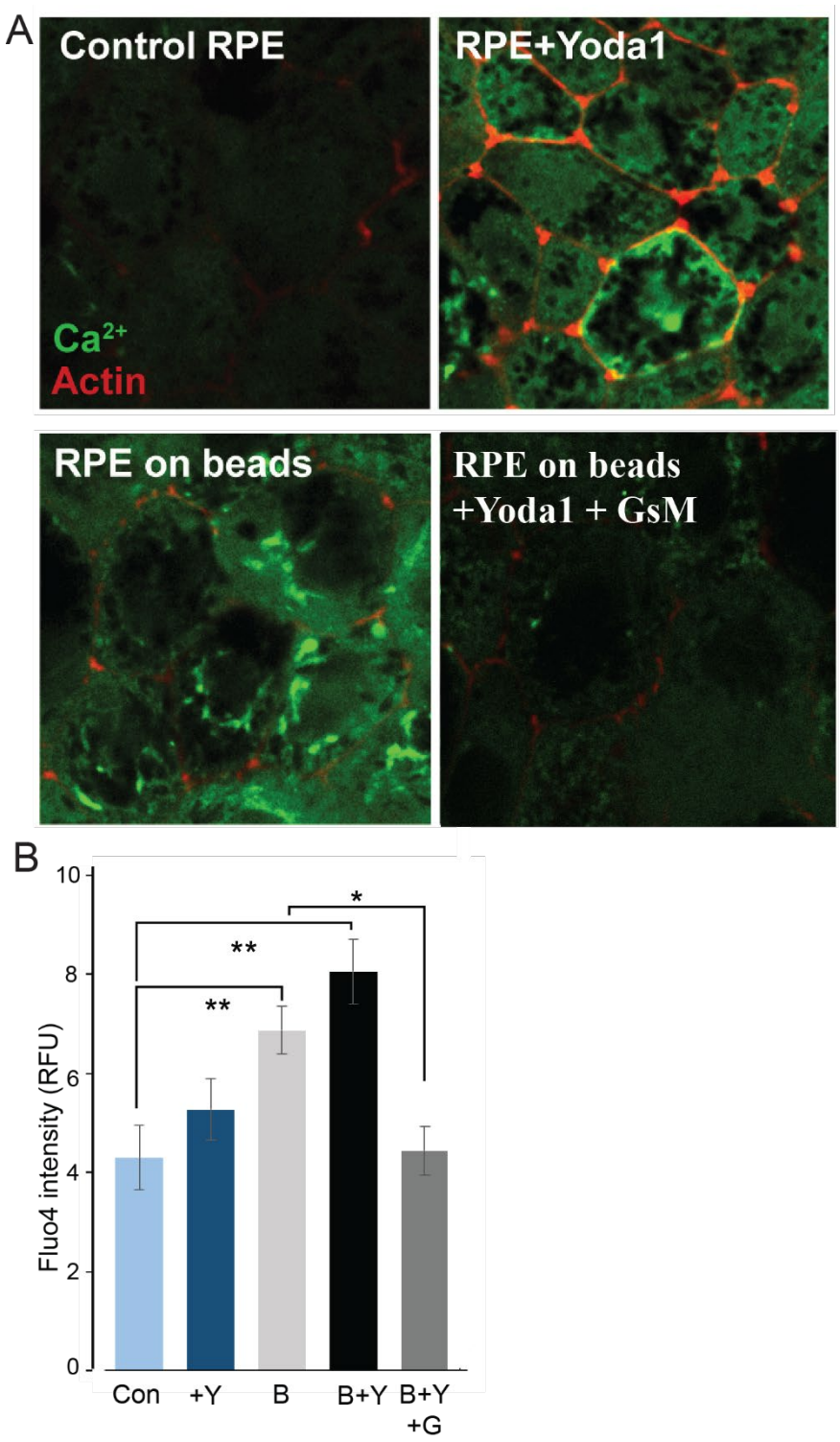


FIGURE 3.6 PIEZO1 RESPONSE TO MECHANICAL STRESS ON THE RPE

A. Stills from live imaging of polarized PRPE loaded with Fluo4NW and SiR Actin. 4
B. Quantification of A. Mean±SD. * $p < 0.05$, ** $p < 0.01$, *** $p < 0.001$ Student's t-test.

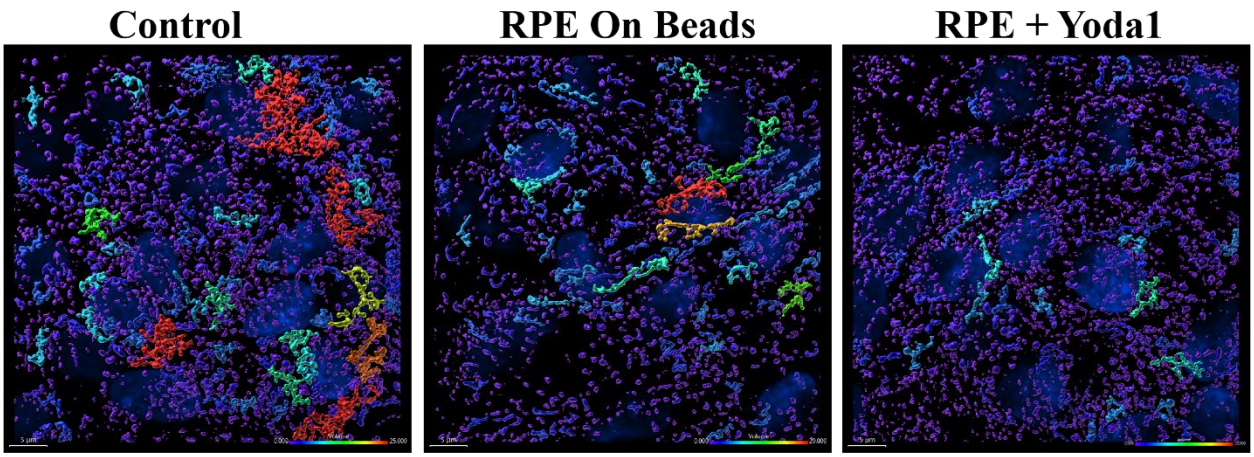


FIGURE 3.7 PIEZO1 ACTIVATION INDUCES MITOCHONDRIAL FRAGMENTATION

3D reconstruction of polarized RPE stained for TOM20. Warmer colors indicate healthy mitochondrial networks while cooler colors indicate fragmented mitochondria.

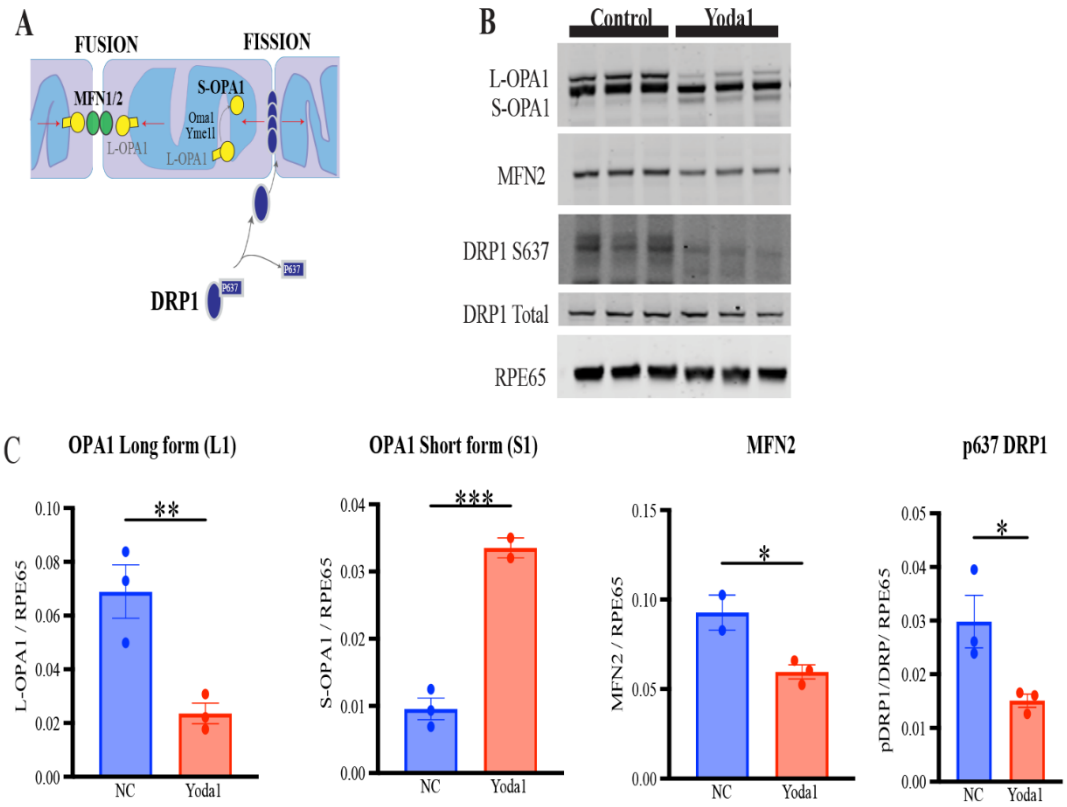


FIGURE 3.8 PIEZO1 ACTIVATION UPREGULATES MITOCHONDRIAL FISSION MACHINERY

A. Schematic of proposed mechanism at work in driving mitochondrial fission.
B. Western blot of RPE lysates treated with or without Yoda1.
C. Quantification of B. Mean±SEM. * $p < 0.05$, ** $p < 0.01$, *** $p < 0.001$ Student's t-test.

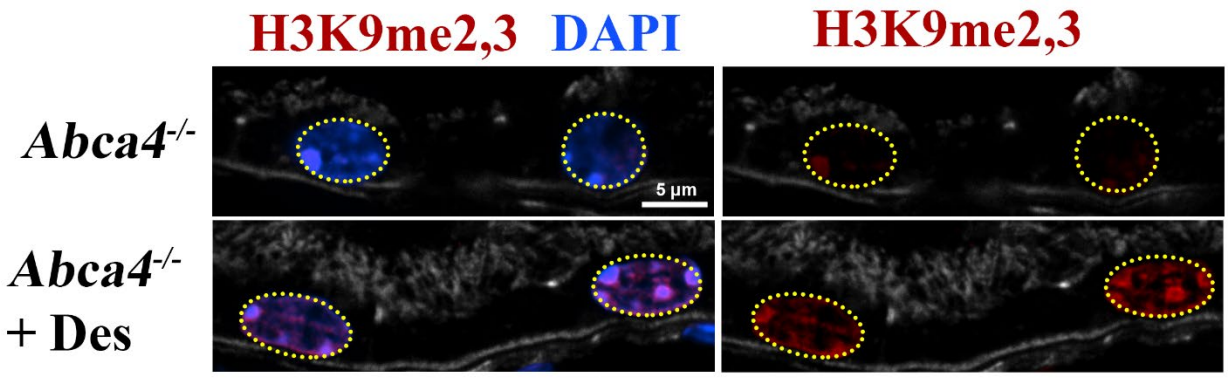


FIGURE 3.9 DESIPRAMINE PREVENTS H3K9ME3 LOSS IN MOUSE RPE

Cryosections of age-matched Abca4$^{-/-}$ mice treated with vehicle or desipramine. These sections were stained for DAPI and H3K9me2,3.

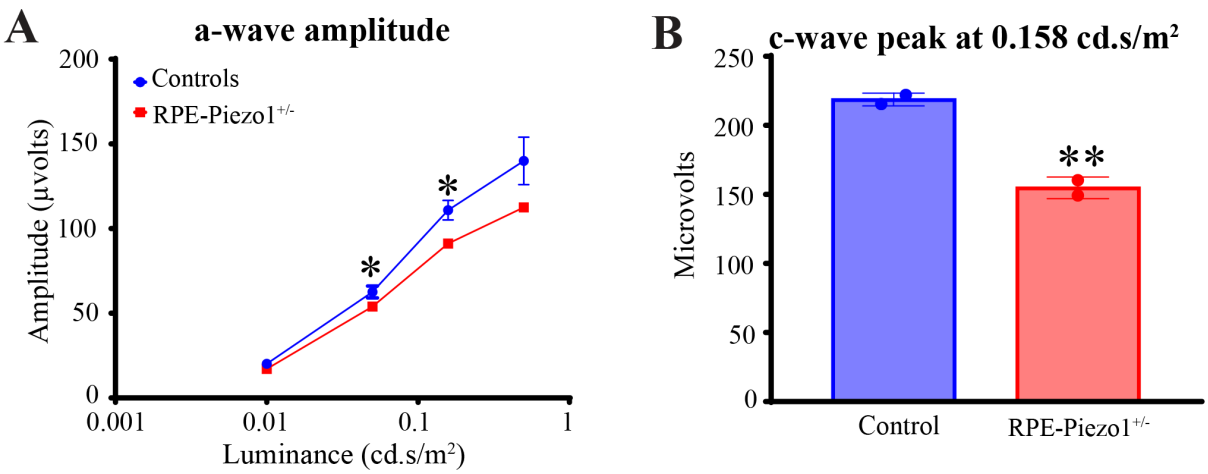


FIGURE 3.10 PIEZO1 LOSS CAUSES PHOTORECEPTOR DEFICITS

A. Trace of stimulus plotted against amplitude of a-wave peaks of mice expressing RPE-Cre or not. Mean±SEM. * $p < 0.05$ Student's t-test.
B. Peak of c-wave at 0.158 cd·s/m^2. Mean±SEM. ** $p < 0.01$ Student's t-test.

Methods

Bead Plating

Beads were immersed in isopropyl alcohol to sterilize them. They were then diluted in sterile Type 1 water and plated at the necessary density during the collagen coating process such that the beads were embedded in the collagen. This prevents them from moving around during the plating process.

Immunofluorescent Staining

RPE were stained as previously described.

Treatments

Yoda1 was used at 10uM for 6 hours in both the apical and basolateral chambers of the Transwell. GsMTx4 was used for 6 hours at a concentration of 500nM.

Cell Culture

Primary RPE were cultured as described in Chapter 2.

Mouse Lines

Abca4$^{-/-}$ mice and 129SvlmJ mice were used and treated as described in Chapter 2. Two different additional mouse lines were employed for this. The C57B6/J mouse and the Piezo1 floxed Cre mouse were employed for this. The Cre mouse was created by crossing the Piezo1-flox mouse with a mouse with a Cre-ERT2 under control of an RPE65 promoter to establish an inducible RPE-specific Piezo1 Cre mouse. This mouse was left hemizygous to evaluate the strength of Piezo1 knockout on the RPE initially. At 3 months of age, these mice were then injected with 75mg/kg tamoxifen dissolved in corn oil 5 times in one week to induce Cre recombination and remove the floxed piezo1 from the RPE. ERGs were performed and then euthanized at 8 months of age.

Desipramine Treatments

Mice were treated as described in Chapter 2.

Cryosection Staining

Whole mouses eyes were enucleated and fixed in 4% PFA in PBS for 1 hour at room temperature. After fixation, eyes were rinsed in PBS and placed into 30% sucrose at 4˚C overnight. Eyes were cleaned of excess tissue before the anterior portion of the eye, including cornea and lens was removed. Eyes were placed into cryomolds containing O.C.T. compound and frozen at -80˚C. Once ready, blocks were placed into Cryostat (Leica) and 14um thick sections were cut. Sections were allowed to dry before being stored at -80˚C until use. Staining was performed by rehydrating the sections in PBS for 10 minutes before blocking in 1% BSA in PBS for 2.5 hours and then staining for 48 hours at 4˚C in primary antibody in 4% BSA in PBS. Sections were rinsed and then stained for 2 hours at room temperature with secondary antibody before being treated with TrueBlack and mounted in VectaShield Vibrance. Imaging was performed on the Nikon Ti2 spinning disk microscope.

Immunofluorescence of Filters

Filters were fixed in 2% PFA in PBS before being excised and blocked for 30 minutes in 1% BSA in PBS with $MgCl_2$ and $CaCl_2$. Filters were probed with primary antibody with 1% BSA in PBS with $MgCl_2$ and $CaCl_2$ with 0.1% saponin for 1 hour. Filters were rinsed and stained with the appropriate secondary in the dark for 30 minutes before being mounted in VectaShield. Filters were imaged on the Nikon Ti2 spinning disk microscope.

Electroretinography

Electroretinography was performed as described in Chapter 2.

CHAPTER 4: ZA AS A POTENTIAL THERAPEUTIC IN MODELS OF RETINAL DEGENERATION

Introduction

Zoledronic acid (ZA) is used to treat osteoporosis, multiple myeloma, Paget disease, and functions to some extent as an anti-cancer drug when the cancer has metastasized to bone [112,113114]. It is sold under the brand names Reclast or Zometa, which cost around $1,000 per 5mg infusion, though generic varieties are available at lower prices. ZA is a nitrogen-containing bisphosphonate which binds to hydroxyapatite in bone where it is then taken up by osteoclasts during bone remodeling, causing them to subsequently detach from the bone and preventing bone resorption [115]. This prevents bone loss in patients and reduces fracture risk, which is a particular issue in older patients who may also be prone to falls. This reduction in bone remodeling also prevents hypercalcemia, where serum blood concentrations of calcium are elevated and can pose additional complications such as renal stones, arrhythmias, pancreatitis, gastric ulcers, and even leading up to coma and even death [116].

ZA has an exceptionally long half-life owing to this absorption in bone, requiring only intravenous once-yearly doses in humans. This intravenous dosage is required as ZA has low absorption through the intestine and frequently causes patient gastrointestinal discomfort when taken orally. It is excreted via the kidneys unchanged, with no action on the liver to alter the drug. ZA is also a potent inhibitor and selective inhibitor of ASM with an IC50 of 5μM [117]. It also acts as an inhibitor in the mevalonate pathway, preventing cholesterol biosynthesis [118,119]. More specifically, ZA acts on the farnesyl pyrophosphate synthase, which prevents both isopentenyl pyrophosphate conversion into geranyl pyrophosphate and geranyl pyrophosphate from converting into farnesyl pyrophosphate [120,121]. This makes it a potential “triple-threat” therapeutic drug.

The Lakkaraju lab has demonstrated that the use of functional inhibitors of ASM, such as desipramine, can reduce ceramide levels in the RPE, even when injected systemically in animals. The dose of desipramine required to reduce ceramide in the RPE is much lower than what is required for central anti-depressant effects: we employed a dose of 10 mg/kg three times per week to be effective at ceramide reduction in the RPE versus 100 mg per day every day to be effective at treating depression. Thus far, this thesis has shown that inhibition of ASM is enough to prevent exosome biogenesis and the subsequent recruitment of microglia to the subretinal space. While not enough to preserve vision to the levels seen in wild-type mice, desipramine is enough to improve a-wave amplitudes in *Abca4*$^{-/-}$ mice when compared to their age-matched vehicle-treated counterparts.

There are no approved treatments for Stargardt disease. Currently approved complement inhibitors to treat dry AMD require intravitreal injections into patients' eyes, an expensive monthly regimen with poor patient compliance. These injections also come with their own risks, including inflammation, fibrosis and scarring, and increased intraocular pressure [122]. Even so, these treatments only decrease RPE atrophy and do not prevent or slow the trajectory of vision loss. This is due to the nature of late-stage AMD because once postmitotic photoreceptors and RPE are lost, they cannot be renewed. Thus, a treatment that halts the disease at the intermediate or even early stages would be a significant boon to patient quality of life and outcomes.

This section will strive to answer if a more potent structural inhibitor of ASM, ZA, is effective in ameliorating the defects seen in mouse models of inherited retinal degenerations. Functional ASM inhibitors are small molecules that are also weak bases which enter the lysosome and cause ASM to fall off of the lysosome membrane, which subsequently gets degraded by the enzymes within [123]. In contrast, a structural inhibitor such as ZA binds directly to ASM, preventing

it from degrading ceramide [124]. Furthermore, because ZA binds directly to ASM and is selective, it has a low chance to induce the degradation of other enzymes such as acid ceramidase, which also resides in the lysosome and cleaves ceramide into sphingosine [125126]. This would not only reduce the production of ceramide through inhibition of ASM, but possibly also allow for ceramide to be degraded by the cell at a higher rate with desipramine treatment. Lastly, as this drug also has been shown to inhibit cholesterol synthesis, it stands to reason that it will be even more effective than other ASM inhibitors [127,128].

Results

ZA Reduces Cholesterol and Ceramide Levels

The first question we sought to answer was if ZA would be taken up by the RPE as ZA has very low solubility and doesn't easily cross the plasma membrane due to its high polarity. Mice were intraperitoneally injected with fluorescently-labeled ZA at a dose of 50 µg/kg for one week. RPE flatmounts were imaged by confocal microscopy. We observed significant ZA fluorescence in the RPE (Figure 4.2), suggesting that ZA is delivered to the RPE after systemic administration.

To determine the therapeutic efficacy of ZA, we administered vehicle or ZA (10 µg/kg intraperitoneally for 1 month to wildtype and *Abca4*$^{-/-}$ mice. Immunostaining of flatmounts for ceramide showed that ZA decreased ceramide to wildtype levels in the RPE when compared with vehicle-treated mice (Figure 4.3A, B).

ZA has been shown to target the mevalonate pathway which would reduce overall levels of cholesterol[119]. Our previous papers have shown that the RPE of *Abca4*$^{-/-}$ mice are enriched in cholesterol, as exhibited by filipin staining. As cholesterol is a major actor in the activation of ASM in the RPE, we measured cholesterol by staining for filipin, which labels free cholesterol

(Figure 4.4A). In agreement with our hypothesis, ZA significantly decreased filipin staining in the RPE (Figure 4.4B).

ZA Prevents Complement Activation and Mitochondrial Fragmentation

As discussed earlier, the RPE limits complement activation by preventing formation of membrane attack complexes by trafficking CD59 to the cell surface and, should that fail, repair MAC pores by lysosome exocytosis [35]. In cells with excess ceramide, these responses are blunted leading to mitochondrial fragmentation. Fragmented mitochondria reduce RPE oxidative phosphorylation and increase reactive oxygen species production. They are also more prone to utilize glycolysis as their primary means of generating ATP, which in turn, robs photoreceptors of glucose.

Complement exposure in primary RPE cultures decreased mitochondrial volumes measured by live cell imaging, indicating fragmentation of the network (Figure 4.5A). A short 3-hour treatment with ZA after complement exposure prevented mitochondrial fragmentation (Figure 4.5B). We further corroborated this evidence using our Stargardt disease mouse model and stained RPE flatmounts for TOM20 (Figure 4.6A). We observed an increase in RPE mitochondrial volumes of *Abca4*$^{-/-}$ mice treated with ZA compared to vehicle-treated *Abca4*$^{-/-}$ mice, indicating that ZA prevents mitochondrial fragmentation (Figure 4.6B). This preservation of mitochondrial integrity will preserve RPE health, reduce reactive oxygen species, and possibly protect the overlying photoreceptors from further damage by preserving glucose for them.

ZA Prevents Migration of Microglia

As demonstrated in Chapter 2, ceramide increases apical secretion of pro-inflammatory exosomes which recruit microglia into the subretinal space. As ZA readily decreases ceramide levels in the RPE of *Abca4*$^{-/-}$ mice, we next sought to answer if ZA could effectively prevent microglia migration. We found a significant decrease in the number of subretinal microglia stained for Iba1 (Figure 4.7A) in 18-month-old *Abca4*$^{-/-}$ mice treated with ZA compared to those treated with vehicle (Figure 4.7B).

ZA Restores Photoreceptor Function

Because ZA is effective at a 1,000-fold lower dose than desipramine in decreasing RPE ceramide, protecting mitochondria, and preventing microglial activation, we next asked if there was any functional recovery of vision in *Abca4*$^{-/-}$ mice treated with ZA. We dark-adapted mice and performed full-field electroretinography on age-matched 16-month-old mice before treatment was initiated. After two months of treatment with either ZA (3 times a week at 10 μg/kg) or vehicle, we repeated the ERG measurements. Our data show that 18-month old *Abca4*$^{-/-}$ mice lose significant function in their a and c-waves, and that ZA can prevent this loss and preserve photoreceptor function at levels comparable to wildtype mice (Figure 4.8A, B, C, D).

Conclusions

Here we have demonstrated that very low doses of ZA are delivered to the RPE perhaps via ZA binding a protein that is then transported to the RPE, perhaps retinal binding protein 4. We are currently investigating the precise mechanisms involved in ZA delivery to the RPE.

We also demonstrate that ZA reduces not only ceramide levels but also cholesterol, and protects mitochondria within the RPE, making it a potent “triple-threat” therapeutic. Cholesterol accumulation increases ceramide by activating ASM. By targeting two enzymes in this pathogenic cascade, RPE homeostasis can be much more effectively preserved. This may explain why ZA is so effective at preserving function vision as evidenced by the recovery of a and c wave amplitudes. This could also be due to altering the microenvironment around the photoreceptors and the RPE. As ceramide accumulation impacts multiple functions in the RPE, such as exosome secretion and aberrant Piezo1 activation, it is likely that lowering cholesterol and ceramide targets many of these pathways, preserving RPE health, resulting in healthier photoreceptors.

Figures

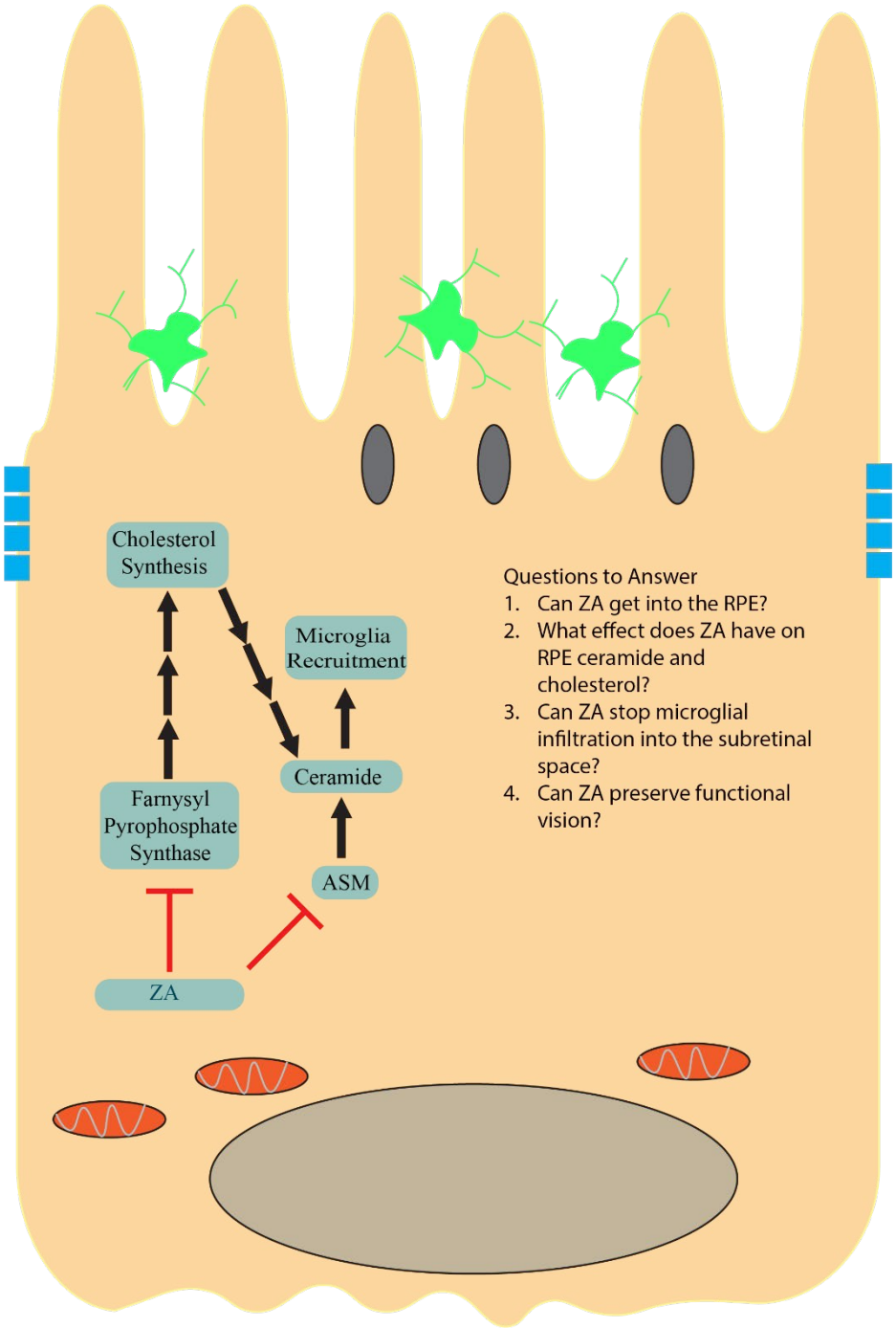


FIGURE 4.1 ZA MAY BE A "TRIPLE-THREAT" THERAPEUTIC

Cartoon showing that ZA may function to prevent ceramide accumulation through inhibition of both ceramide and cholesterol synthesis, which has been shown to cause ceramide accumulation.

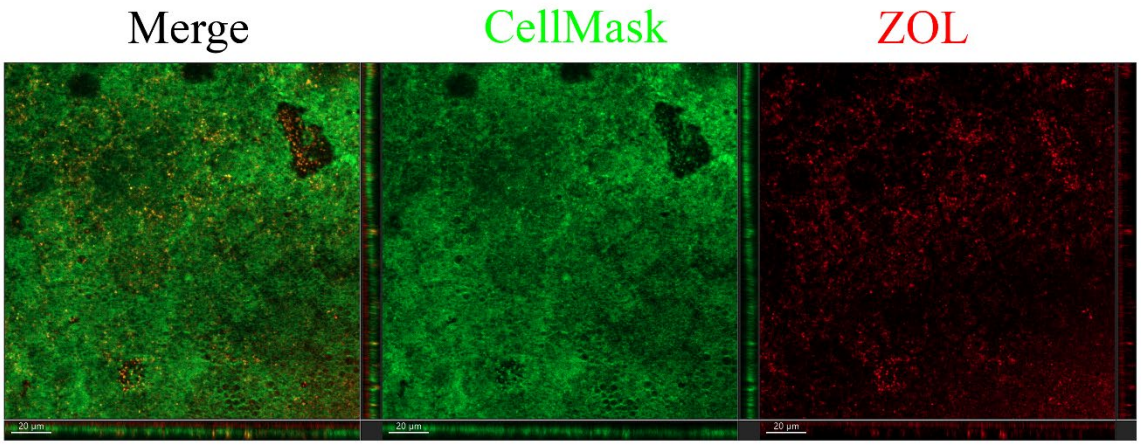


FIGURE 4.2 ZA IS DELIVERED TO THE RPE

Confocal images from an ex vivo mouse RPE flatmount. Green is CellMask and red is fluorescently-tagged zoledronic acid.

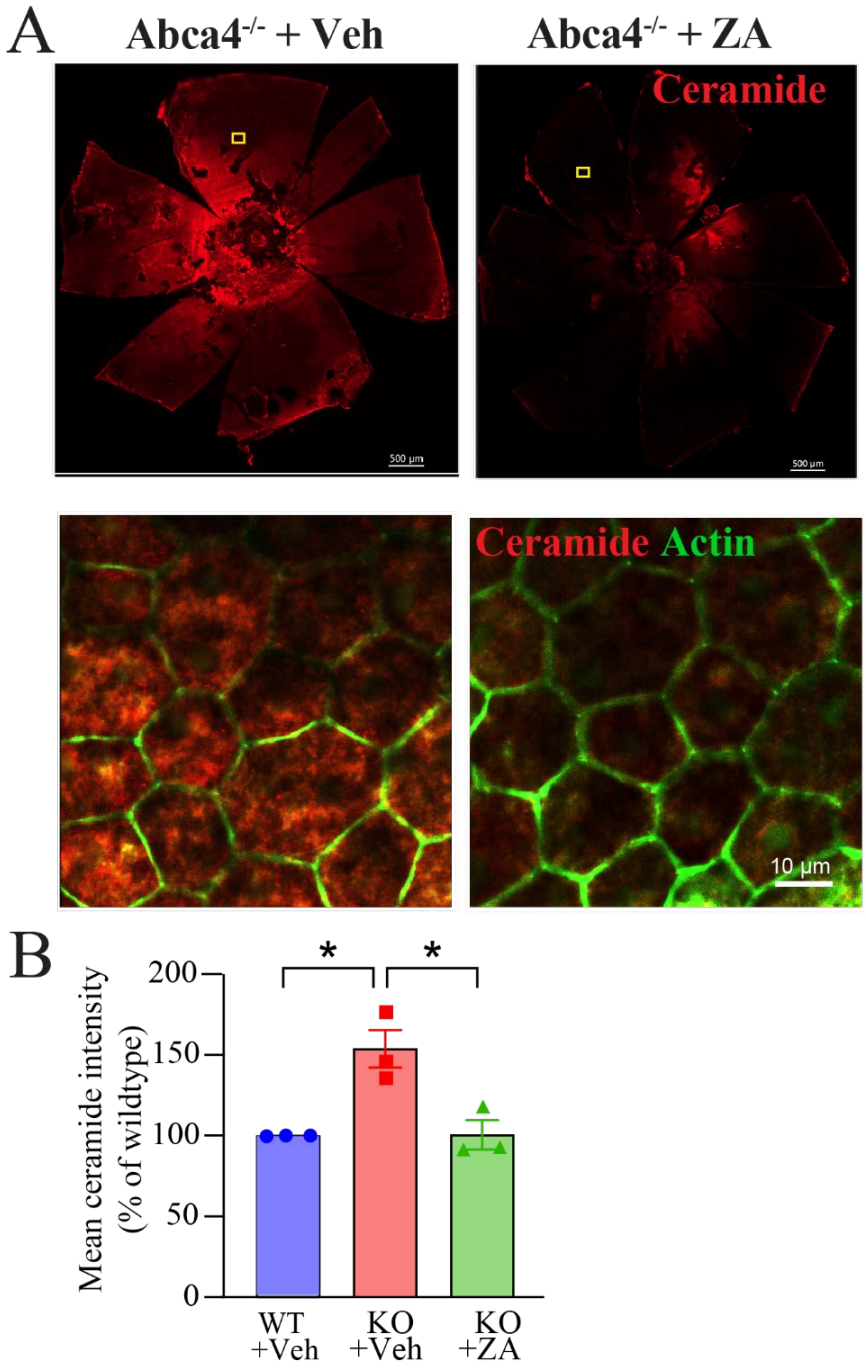


FIGURE 4.3 ZA REDUCES CERAMIDE IN MICE

A. *Abca4*$^{-/-}$ mouse RPE flatmount with ceramide stained in red. Green is actin staining. Yellow box denotes higher magnification area.
B. Quantification of ceramide shown in A. Mean±SEM. * $p < 0.05$ Student's t-test.

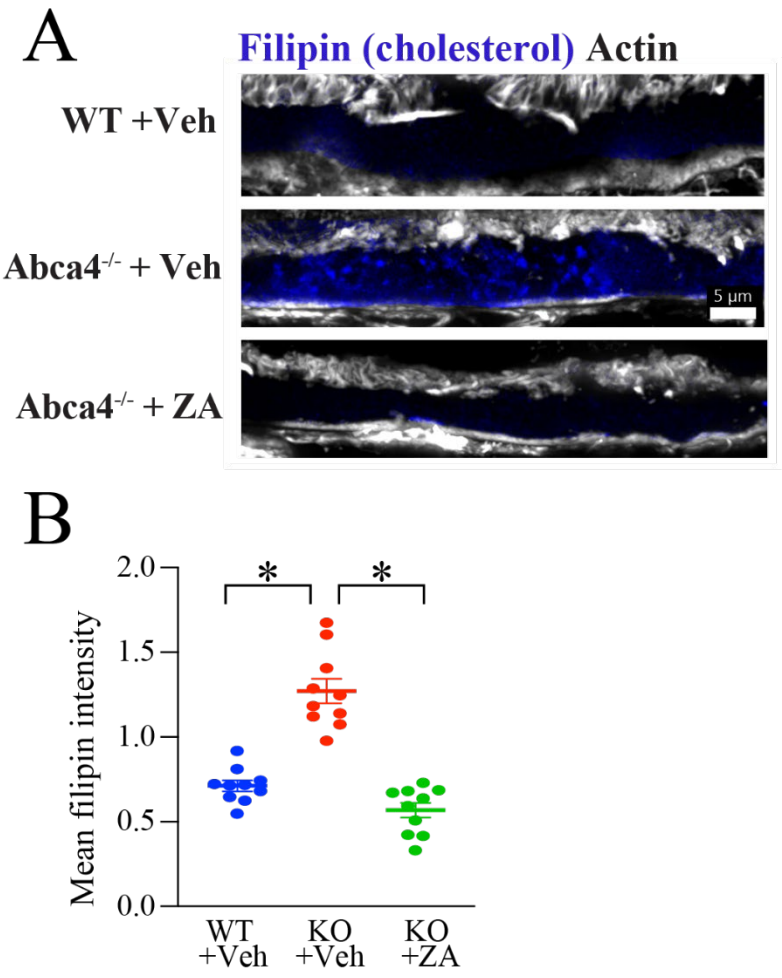


FIGURE 4.4 ZA REDUCES CHOLESTEROL IN MICE

A. Cryosections from mice treated with ZA. Blue is filipin which stains cholesterol, white is actin.
B. Quantification of filipin intensity in A. Mean±SEM. * $p < 0.05$ Student's t-test.

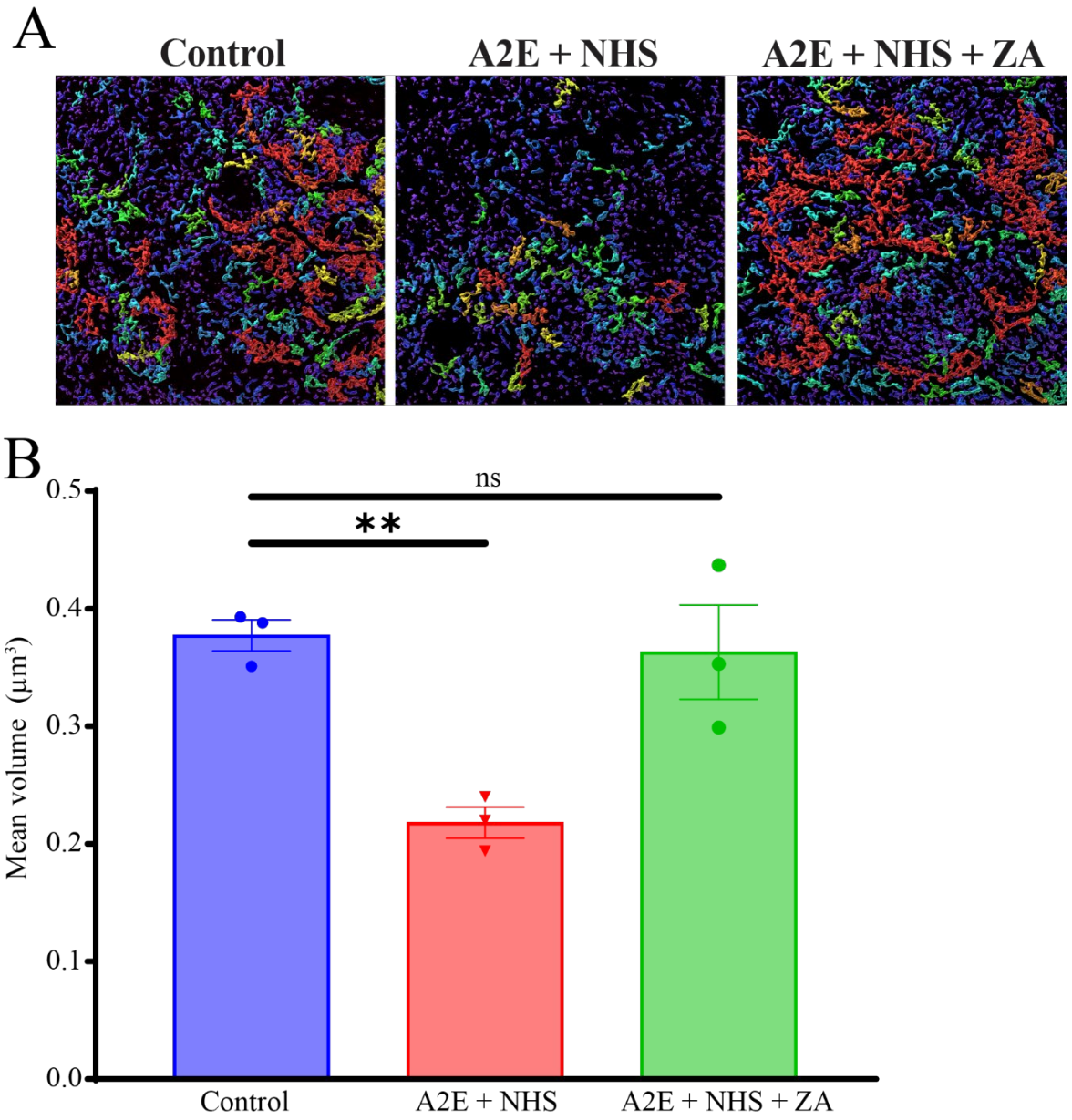


FIGURE 4.5 ZA REDUCES MITOCHONDRIAL FRAGMENTATION DURING COMPLEMENT ATTACK

A. 3D reconstruction of PRPE stained with TOM20. Warmer colors indicate larger mitochondrial volumes. Cooler colors indicate smaller mitochondrial volumes.
B. Quantification of A. Mean±SEM n.s. Not Significant. ** $p < 0.01$ Student's t-test.

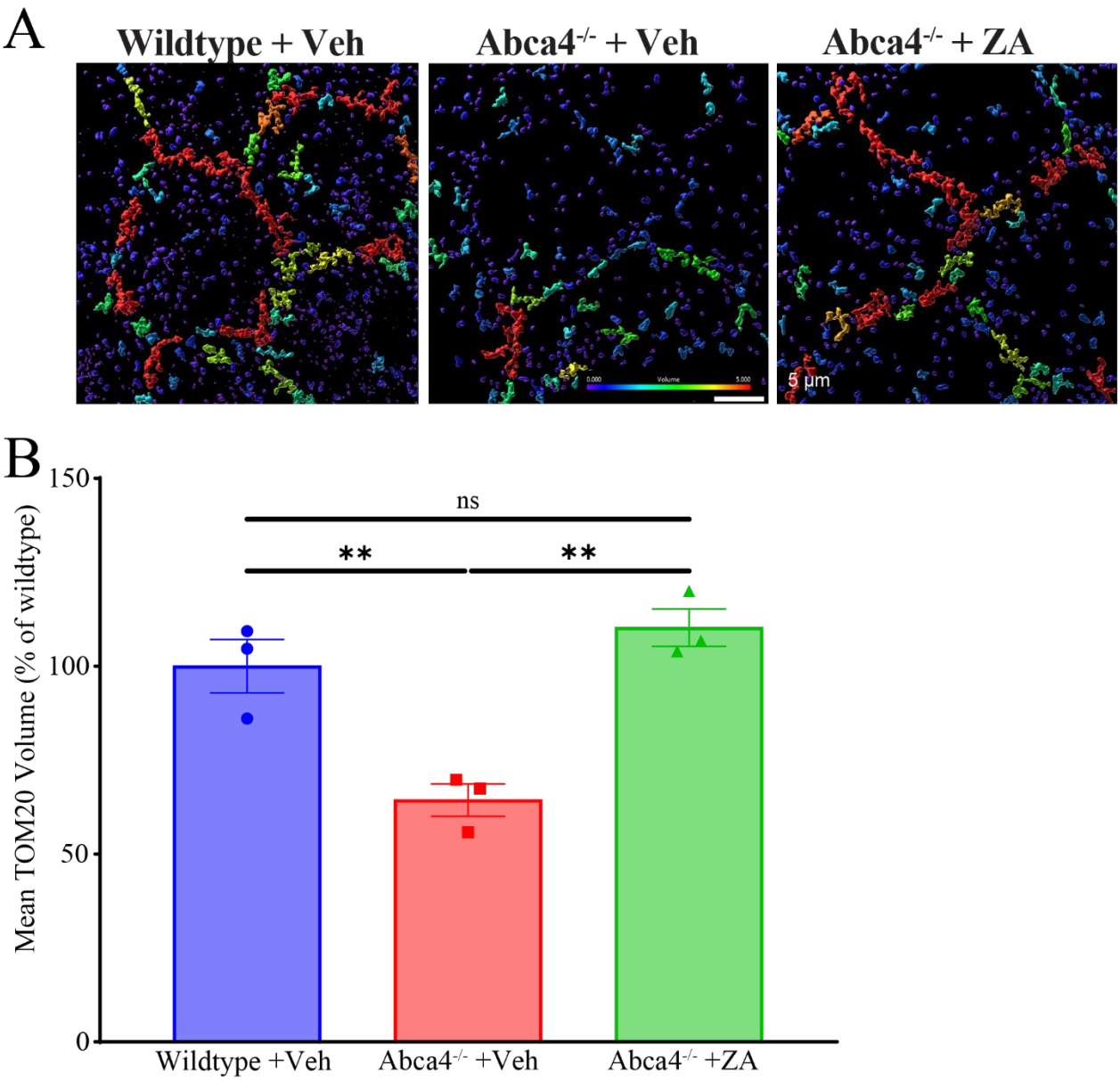


FIGURE 4.6 ZA REDUCES MITOCHONDRIAL FRAGMENTATION IN VIVO

A. 3D reconstruction of mouse RPE flatmounts stained with TOM20. Warmer colors indicate larger mitochondrial volumes. Cooler colors indicate smaller mitochondrial volumes.
B. Quantification of A. Mean±SEM. n.s. Not Significant.** $p < 0.01$ Student's t-test.

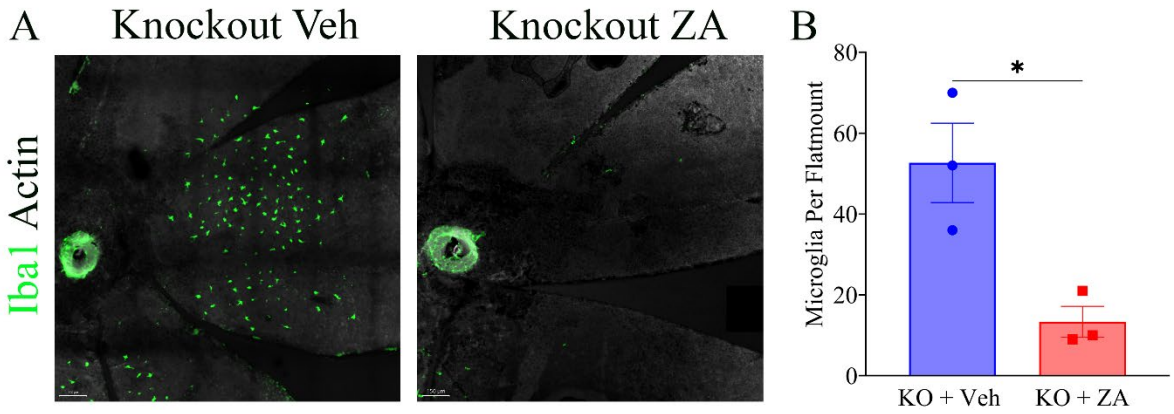


FIGURE 4.7 ZA REDUCES NUMBER OF SUBRETINAL MICROGLIA

A. Confocal stitched images of Abca4-/- vehicle or ZA-treated mouse RPE flatmount stained with actin and Iba1.
B. Quantification of A. Mean±SEM. * $p < 0.05$ Student's t-test.

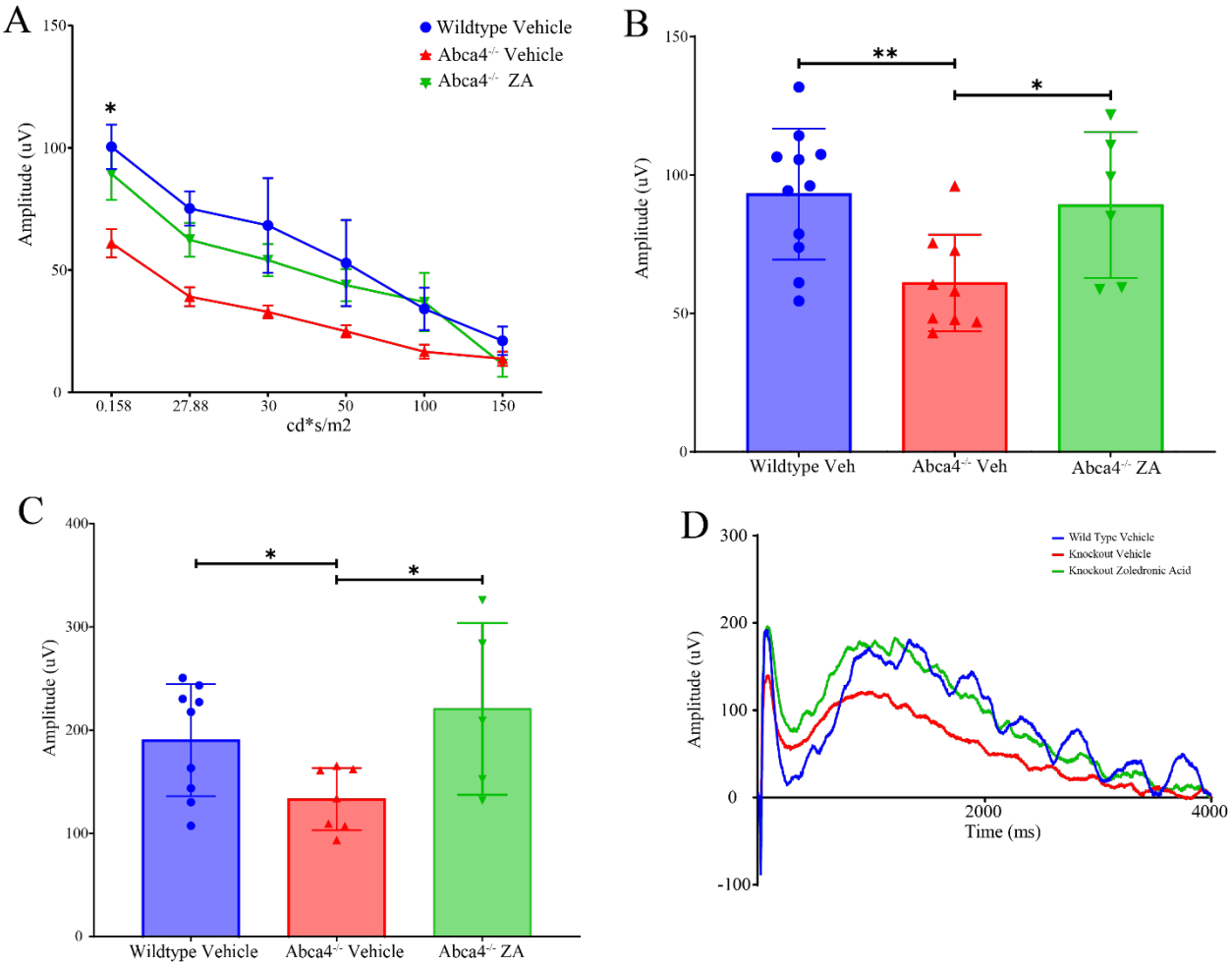


FIGURE 4.8 ZA PRESERVES VISION IN MOUSE MODELS OF STARGARDT DISEASE

A. ERG of a-waves over stimulus. Mean ±SEM.
B. Bar graph of a-wave amplitude at 0.158 cd·s/m^2. Mean ±SEM. * $p < 0.05$, ** $p < 0.01$ Student's t-test.
C. Bar graph of c-wave amplitude at 0.158 cd·s/m^2. Mean±SEM.. *$p< 0.05$ Student's t-test.
D. Example of ERG trace of mice.

Methods

Mice

16-18 month-old wild-type 129S1/SvlmJ and *Abca4*$^{-/-}$ Abca4tm1Ght/J were used. Housing and feed was as described in Chapter 2.

Treatment with ZA

ZA disodium salt tetrahydrate was dissolved in sterile Type 1 water and injected into via intraperitoneal route using a 30G needle. Each mouse was given 10ug/kg of zoledronic acid disodium salt tetrahydrate or vehicle three times per week for two months.

ZA-647 Injections into Mice

ZA labeled with AlexaFluor-647 was purchased from Biovinc as powder. This was dissolved in Type 1 water and frozen until needed. 129SvlmJ mice were injected with this substance at a dosage of 50ug/kg for 3 times a week for 1.5 weeks to ensure high exposure to the drug and increase odds of detection via fluorescence microscopy. Mice were then euthanized and eyes enucleated. One eye was fixed in 4% PFA before the neural retina was removed and the RPE were flatmounted. The RPE was then stained for DAPI and ActiStain 488 before being imaged on a spinning disk confocal microscope after treating with TrueBlack. The other eye was flatmounted without fixation, stained with CellMask Green, and imaged using recording media in a Warner chamber on an LSM900 from Zeiss.

Immunostaining of Mouse RPE Flatmounts

Conducted as described in chapter 2.

Electroretinography

Electroretinography was conducted as described in Chapter 2, but with the following changes. The number of steps for the mice was 7 from 0.01cd·s/m^2 to 25cd·s/m^2 and the mice were measured before and after ZA treatment.

Complement Attack

RPE cells that were either untreated, loaded with A2E, or A2E+ZA were exposed to 10% normal human serum as described previously [35]. Briefly, cells are exposed to growth media containing 10% human serum followed by a washout period and then exposed again for another 10 minutes. Samples were then stained with MitoTracker Green, which is a fixable mitochondrial stain that binds based on the polarization state of the mitochondria.

Statistics

Graphpad Prism 10 was used and statistical testing was performed as described in the figure.

Table 1.1 List of Reagents

Reagent Name	Manufacturer	Catalog Number	Dilution Used (if applicable)
Ketaset (Ketamine HCl)	Zoetis, Girona, Spain		100mg/kg
AnaSed LA (Xylazine)	Llyod, Shenandoah, IA		10mg/kg
Antisedan (atipamezole HCl)	Orion Corporation, Espoo, Finland		5mg/kg
8% Paraformaldehyde	Electron Microscopy, Sciences, Hatfield, PA	157-8	
Bovine Serum Albumin	Rockland Immunochemicals, Pottstown, PA	BSA-50	
DAPI	Sigma-Aldrich, St. Louis, MO	D9542	1:200
Isoflurane	Attane, Bethlehem, PA		
Tropicamide	ThermoFisher Scientific, Waltham, MA	J61132.03	
Phenylephrine	ThermoFisher Scientific, Waltham, MA	207240100	
Eye Spears	Hurricane Medical, Bradenton, FL		
Phosphate Buffered Saline	ThermoFisher Scientific, Waltham, MA	BP665-1	
TrueBlack	Biotium, Fremont, CA	23007	
Sodium Chloride	SigmaAldrich, St. Louis, MO	S5886-1KG	
GenTeal Severe Tears	Alcon	NA	
NuPAGE Bis-Tris 4-12% 1.5mm gel	Invitrogen, Waltham, MA	NP0336BOX	
4x NuPAGE LDS sample buffer	Invitrogen, Waltham, MA	NP0007	
10x NuPAGE Sample Reducing Agent	Invitrogen, Waltham, MA	NP0009	

Reagent Name	Manufacturer	Catalog Number	Dilution Used (if applicable)
Protease Inhibitor Cocktail Set III, EDTA-Free	Millipore, Burlington, MA	539134	
Intercept (PBS) Protein-Free Blocking Buffer	Li-Cor Biosciences, Lincoln, NE	927-90001	
Antioxidant	Invitrogen, Waltham, MA	NP0005	
Zoledronic Acid	Toronto Research Chemicals, Toronto, ON, Canada	TRC-Z623500	
1mL Syringe	BD, Franklin Lakes, NJ	309659	
30G Needle	BD, Franklin Lakes, NJ	305106	
ZOL647	Biovinc, Pasadena, CA	BV501001	
HBSS	Corning, Corning, NY	21-023-CV	
HEPES	ThermoFisher, Waltham, MA	15630080	
EDTA	SigmaAldrich, St. Louis, MO	MT25053CI	
Fetal Bovine Serum (heat inactivated)	American Type Culture Collection, Manassas, VA	30-2020	
AlexaFluor antibodies - various	ThermoFisher, Waltham, MA		1:500
VectaShield Vibrance	Vector Labs, Newark, CA	H-1700	
Iba1	Fujifilm Wako, Richmond, VA	019-19741	1:200
DMEM	Corning, Corning, NY	10-013-CV	
0.25% Trypsin	Corning, Corning, NY	25-053-CI	
2.5% Trypsin	Corning, Corning, NY	17-160E	
Penicillin-Streptomycin	Corning, Corning, NY	30-002-CI	
Non-essential amino acids	Corning, Corning, NY	25-025-CI	
Ciprofloxacin	Sigma-Aldrich, St. Louis, MO	17850-5G-F	
Acti-stain 488 phalloidin	Cytoskeleton, Denver, CO	PHDG1	1:200

Reagent Name	Manufacturer	Catalog Number	Dilution Used (if applicable)
DC protein assay reagents	Bio-Rad, Hercules, CA	5000116	
129S1/SvlmJ Mice	Jackson Labs, Sacramento, CA	RRID:IMSR_JAX:002448; Strain: 002448	
Abca4$^{-/-}$ Mice	Jackson Labs, Sacramento, CA	RRID: IMSR_JAX:023725; Strain: 023725	
GraphPad Prism	GraphPad Prism, La Jolla, CA		
Adobe Illustrator	Adobe, San Jose, CA		
Photoshop	Adobe, San Jose, CA		
Imaris	Bitplane, Concord, MA		
Microsoft Excel	Microsoft Corporation, Albuquerque, NM		
NIS Elements	Nikon, Melville, NY		
T25 Culture Flasks	Corning, Corning, NY	353108	
Primary porcine RPE	Lampire Biologicals		
Transwell Filters	Corning, Corning, NY	7200161	
Ceramide	Enzo Farmingdale, NY	86153-838	1:10
Connexin 43	Abcam, Waltham, MA	Ab11370-50ul	1:200
Hrs	Novus, Centennial, CO	NB1002839	1:500
Alix	Abcam, Waltham, MA	Ab50249	1:500
Calnexin	Abcam, Waltham, MA	Ab75801	1:2000
RPE65	Novus, Centennial, CO	NB100355	1:5000
Li-Cor Infrared Secondaries	Li-Cor Biosciences, Lincoln, NE		1:5000
Embed-812 Kit	Electron Microscopy, Sciences, Hatfield, PA	14121	

Reagent Name	Manufacturer	Catalog Number	Dilution Used (if applicable)
Integra Biopsy Punches	Miltex, Mansfield, MA	33-31	
Type B Freezing Hats	Pelco Redding, CA	50-193-1254	
2mm Copper Slot Grids	Pelco Redding, CA	4514	
200 Mesh Copper Grids	Pelco Redding, CA	01800-F	
TissueTek OCT	Sakura Finetek, Torrance, CA	25608-930	
Application Kit: EV Profiler	ONI San Diego, CA		
Mix-n-Stain Antibody Labeling Kit 561	Biotium, Fremont, CA	89171-586 (EA)	
Mix-n-Stain 647 CF	Biotium, Fremont, CA	89171-594 (EA)	
CD63-pHlourin Plasmid	A gracious gift from Dr. Pegtel's lab	Verweij 2018	
Desipramine	Enzo, Farmingdale, NY	BML-AR119-0100	
Glutaraldehyde (25%)	Electron Microscopy, Sciences, Hatfield, PA	16220	
1-Hexadecene	TCI, Tokyo, Japan	H0323	
Methylcellulose	SigmaAldrich, St. Louis, MO	M6385-100G	
Uranyl Acetate	Electron Microscopy, Sciences, Hatfield, PA	22400	
Lead Citrate Trihydrate Air-Free	Electron Microscopy, Sciences, Hatfield, PA	22410	
Sodium Cacodylate Trihydrate	Electron Microscopy, Sciences, Hatfield, PA	12300	
Osmium Tetroxide	Electron Microscopy, Sciences, Hatfield, PA	19132	
Pure Acetone	Electron Microscopy, Sciences, Hatfield, PA	10000	
200 Proof Ethanol	Koptec King of Prussia, PA	V1001	
H3K9Me	Cell Signaling Technology, Danvers, MA	13969S	
Piezo1	ProteinTech, Rosemont, IL	15939-1-AP	
CellMask Green	ThermoFisher, Waltham, MA	C37608	

Reagent Name	Manufacturer	Catalog Number	Dilution Used (if applicable)
Yoda1	Sigma-Aldrich, St. Louis, MO	SML 1558-MG	
GsMtX4	R&D Systems, Minneapolis, MN	4912100U	
Cospheric Beads	Cospheric, Somis, CA	SiO2MS-2.0 0.166um	
C57BL/6 RPE65 Cre Mice	Jackson Labs, Sacramento, CA	RRID: IMSR_JAX:035973 Strain: 035973	
Piezo1-Flox Mice	A Generous Gift from Dr. David Krizaj		
Tamoxifen	SigmaAldrich, St. Louis, MO	T2859-1G	
647-ZOL	Biovinc, Pasadena, CA	BV501001	
TOM20	ProteinTech	11802-1-AP	1:200
OPA1	Novus	NB11055290	1:200
MFN2	Abcam	Ab56889	1:200
S637 DRP1	Cell Signaling	4867S	1:200
DRP1	ProteinTech	12957-1-AP	1:200
MitoTracker Deep Red	ThermoFisher, Waltham, MA	M22426	
20nm Glass Filter	GE Healthcare, Chicago, IL	6809-1002 GE	
Fluo4NW	ThermoFisher, Waltham, MA	F36206	

CHAPTER 5: CONCLUSIONS, FUTURE DIRECTIONS, AND PERSPECTIVES

In this thesis I have described two mechanisms through which RPE dysfunction can occur in models of disease along with evaluating a promising therapeutic intervention. The first is ceramide inducing the release of pro-inflammatory containing EVs into the retina. This causes retinal dysfunction and drives the migration of microglia into the subretinal space. By treating mouse models of inherited MD with drugs that decrease ceramide, these defects can be ameliorated. More research is needed to understand the precise role of these microglia within the subretinal space. Ongoing work in the lab shows that there is a phenotypic difference in how the microglia interact with the RPE in various models of retinal degeneration. For example, in the progranulin knockout mouse, a model of frontotemporal dementia, subretinal microglia have high levels of CD68, a marker for phagocytically active microglia. These microglia phagocytose microvilli of the RPE, which indicates destruction of the RPE monolayer. In the P23H mutant mouse, a model of autosomal dominant retinitis pigmentosa, subretinal microglia tend to be ramified in appearance, an indicator of quiescent microglia. We have observed that P23H subretinal microglia do not phagocytose photoreceptor outer segments as readily as subretinal microglia in *Abca4*$^{-/-}$ mice. There is much debate in the field as to whether the microglia are detrimental or protective in various models of retinal degenerations and more work needs to be done in elucidating how they function in each disease. As the RPE recruits microglia into the subretinal space, it may be possible to modulate the behavior of microglia via the RPE. This has exciting implications not only for diseases that have the primary site of dysfunction at the RPE but also for disease that may affect the retina as a whole, such as diabetic retinopathies and glaucoma!

The second mechanism is through altering the mechanical environment surrounding the RPE, either through the deposition of drusen or the increase of ceramide in the RPE. Both of these activate the calcium permeable cation channel Piezo1 which then induces mitochondrial fragmentation. ASM inhibitors pose a likely treatment for ceramide-induced activation of Piezo1 in the RPE. However, more research is needed to identify drugs that prevent drusen mediated activation of Piezo1. It is unlikely that GsMTx4 could be safely administered in the eye, as specifically targeting the RPE without harming the rest of the retina will be difficult. And systemic administration could have off-target effects as Piezo1 is ubiquitously expressed throughout the body. A better course of action would be to identify the causes of drusen formation and Bruch's membrane stiffening and hopefully develop therapeutics that target and prevent these. Further study into the roles Piezo1 plays within the RPE and retina are also necessary as even hemizygous knockout of Piezo1 from the RPE is enough to induce a reduction in functional vision, at least in photoreceptors.

The therapeutic intervention comes in the form of the bisphosphonate ZA. As a potent inhibitor of both cholesterol synthesis and ASM, ZA can greatly reduce ceramide levels in the RPE. This restores RPE homeostasis and can preserve vision in models of MD. To translate ZA to the clinic for MD, it would be exciting to analyze electronic medical records in suitably-sized databases to determine if there is a reduction in the incidence of AMD progression in patients taking ZA. Ideally, clinical trials to enroll both early and intermediate AMD patients along with early-stage Stargardt disease patients evaluate whether low-dose zoledronic acid can stave off vision loss.

REFERENCES

1. Frick, K.D., Gower, E.W., Kempen, J.H., and Wolff, J.L. (2007). Economic impact of visual impairment and blindness in the United States. Arch. Ophthalmol. *125*, 544–550. 10.1001/archopht.125.4.544.

2. Ben-Shabat, S., Parish, C.A., Vollmer, H.R., Itagaki, Y., Fishkin, N., Nakanishi, K., and Sparrow, J.R. (2002). Biosynthetic studies of A2E, a major fluorophore of retinal pigment epithelial lipofuscin. J. Biol. Chem. *277*, 7183–7190. 10.1074/jbc.M108981200.

3. Sparrow, J.R., Fishkin, N., Zhou, J., Cai, B., Jang, Y.P., Krane, S., Itagaki, Y., and Nakanishi, K. (2003). A2E, a byproduct of the visual cycle. Vision Res. *43*, 2983–2990. 10.1016/s0042-6989(03)00475-9.

4. Kim, S.R., He, J., Yanase, E., Jang, Y.P., Berova, N., Sparrow, J.R., and Nakanishi, K. (2007). Characterization of dihydro-A2PE: an intermediate in the A2E biosynthetic pathway. Biochemistry *46*, 10122–10129. 10.1021/bi7009635.

5. Tanna, P., Strauss, R.W., Fujinami, K., and Michaelides, M. (2017). Stargardt disease: clinical features, molecular genetics, animal models and therapeutic options. Br. J. Ophthalmol. *101*, 25–30. 10.1136/bjophthalmol-2016-308823.

6. Tsang, S.H., and Sharma, T. (2018). Stargardt Disease. Adv. Exp. Med. Biol. *1085*, 139–151. 10.1007/978-3-319-95046-4_27.

7. Mitchell, P., Liew, G., Gopinath, B., and Wong, T.Y. (2018). Age-related macular degeneration. Lancet *392*, 1147–1159. 10.1016/S0140-6736(18)31550-2.

8. Wong, W.L., Su, X., Li, X., Cheung, C.M.G., Klein, R., Cheng, C.-Y., and Wong, T.Y. (2014). Global prevalence of age-related macular degeneration and disease burden projection for 2020 and 2040: a systematic review and meta-analysis. Lancet Glob. Health *2*, e106-16. 10.1016/S2214-109X(13)70145-1.

9. Fritsche, L.G., Igl, W., Bailey, J.N.C., Grassmann, F., Sengupta, S., Bragg-Gresham, J.L., Burdon, K.P., Hebbring, S.J., Wen, C., Gorski, M., et al. (2016). A large genome-wide association study of age-related macular degeneration highlights contributions of rare and common variants. Nat. Genet. *48*, 134–143. 10.1038/ng.3448.

10. Ferris, F.L., Wilkinson, C.P., Bird, A., Chakravarthy, U., Chew, E., Csaky, K., Sadda, S.R., and Beckman Initiative for Macular Research Classification Committee (2013). Clinical classification of age-related macular degeneration. Ophthalmology *120*, 844–851. 10.1016/j.ophtha.2012.10.036.

11. Heesterbeek, T.J., Lorés-Motta, L., Hoyng, C.B., Lechanteur, Y.T.E., and den Hollander, A.I. (2020). Risk factors for progression of age-related macular degeneration. Ophthalmic Physiol. Opt. *40*, 140–170. 10.1111/opo.12675.

12. Fleckenstein, M., Schmitz-Valckenberg, S., and Chakravarthy, U. (2024). Age-Related Macular Degeneration: A Review. JAMA *331*, 147–157. 10.1001/jama.2023.26074.

13. Bakri, S.J., Bektas, M., Sharp, D., Luo, R., Sarda, S.P., and Khan, S. (2023). Geographic atrophy: Mechanism of disease, pathophysiology, and role of the complement system. J. Manag. Care Spec. Pharm. *29*, S2–S11. 10.18553/jmcp.2023.29.5-a.s2.

14. Shughoury, A., Sevgi, D.D., and Ciulla, T.A. (2023). The complement system: a novel therapeutic target for age-related macular degeneration. Expert Opin. Pharmacother. *24*, 1887–1899. 10.1080/14656566.2023.2257604.

15. Schachar, I.H. (2024). Concerning syfovre approval for geographic atrophy. JAMA Ophthalmol. *142*, 85–86. 10.1001/jamaophthalmol.2023.5584.

16. Bergen, A.A., Arya, S., Koster, C., Pilgrim, M.G., Wiatrek-Moumoulidis, D., van der Spek, P.J., Hauck, S.M., Boon, C.J.F., Emri, E., Stewart, A.J., et al. (2019). On the origin of proteins in human drusen: The meet, greet and stick hypothesis. Prog. Retin. Eye Res. *70*, 55–84. 10.1016/j.preteyeres.2018.12.003.

17. Murdaugh, L.S., Avalle, L.B., Mandal, S., Dill, A.E., Dillon, J., Simon, J.D., and Gaillard, E.R. (2010). Compositional studies of human RPE lipofuscin. J. Mass Spectrom. *45*, 1139–1147. 10.1002/jms.1795.

18. Mullins, R.F., Russell, S.R., Anderson, D.H., and Hageman, G.S. (2000). Drusen associated with aging and age-related macular degeneration contain proteins common to extracellular deposits associated with atherosclerosis, elastosis, amyloidosis, and dense deposit disease. FASEB J. *14*, 835–846. 10.1096/fasebj.14.7.835.

19. Russell, S.R., Mullins, R.F., Schneider, B.L., and Hageman, G.S. (2000). Location, substructure, and composition of basal laminar drusen compared with drusen associated with aging and age-related macular degeneration. Am. J. Ophthalmol. *129*, 205–214. 10.1016/s0002-9394(99)00345-1.

20. Wang, L., Clark, M.E., Crossman, D.K., Kojima, K., Messinger, J.D., Mobley, J.A., and Curcio, C.A. (2010). Abundant lipid and protein components of drusen. PLoS ONE *5*, e10329. 10.1371/journal.pone.0010329.

21. Johnson, L.V., Leitner, W.P., Staples, M.K., and Anderson, D.H. (2001). Complement activation and inflammatory processes in Drusen formation and age related macular degeneration. Exp. Eye Res. *73*, 887–896. 10.1006/exer.2001.1094.

22. Khan, K.N., Mahroo, O.A., Khan, R.S., Mohamed, M.D., McKibbin, M., Bird, A., Michaelides, M., Tufail, A., and Moore, A.T. (2016). Differentiating drusen: Drusen and drusen-like appearances associated with ageing, age-related macular degeneration, inherited eye disease and other pathological processes. Prog. Retin. Eye Res. *53*, 70–106. 10.1016/j.preteyeres.2016.04.008.

23. Sparrow, J.R., Dowling, J.E., and Bok, D. (2013). Understanding RPE lipofuscin. Invest. Ophthalmol. Vis. Sci. *54*, 8325–8326. 10.1167/iovs.13-13214.

24. Hazim, R.A., Paniagua, A.E., Tang, L., Yang, K., Kim, K.K.O., Stiles, L., Divakaruni, A.S., and Williams, D.S. (2022). Vitamin B3, nicotinamide, enhances mitochondrial metabolism to promote differentiation of the retinal pigment epithelium. J. Biol. Chem. *298*, 102286. 10.1016/j.jbc.2022.102286.

25. Hazim, R.A., Volland, S., Yen, A., Burgess, B.L., and Williams, D.S. (2019). Rapid differentiation of the human RPE cell line, ARPE-19, induced by nicotinamide. Exp. Eye Res. *179*, 18–24. 10.1016/j.exer.2018.10.009.

26. Hazim, R.A., Karumbayaram, S., Jiang, M., Dimashkie, A., Lopes, V.S., Li, D., Burgess, B.L., Vijayaraj, P., Alva-Ornelas, J.A., Zack, J.A., et al. (2017). Differentiation of RPE cells from integration-free iPS cells and their cell biological characterization. Stem Cell Res. Ther. *8*, 217. 10.1186/s13287-017-0652-9.

27. Smith, E.N., D'Antonio-Chronowska, A., Greenwald, W.W., Borja, V., Aguiar, L.R., Pogue, R., Matsui, H., Benaglio, P., Borooah, S., D'Antonio, M., et al. (2019). Human iPSC-Derived Retinal Pigment Epithelium: A Model System for Prioritizing and Functionally Characterizing Causal Variants at AMD Risk Loci. Stem Cell Reports *12*, 1342–1353. 10.1016/j.stemcr.2019.04.012.

28. Foltz, L.P., and Clegg, D.O. (2017). Rapid, Directed Differentiation of Retinal Pigment Epithelial Cells from Human Embryonic or Induced Pluripotent Stem Cells. J. Vis. Exp. 10.3791/56274.

29. Bharti, K., den Hollander, A.I., Lakkaraju, A., Sinha, D., Williams, D.S., Finnemann, S.C., Bowes-Rickman, C., Malek, G., and D'Amore, P.A. (2022). Cell culture models to study retinal pigment epithelium-related pathogenesis in age-related macular degeneration. Exp. Eye Res. *222*, 109170. 10.1016/j.exer.2022.109170.

30. Nakai-Futatsugi, Y., Jin, J., Ogawa, T., Sakai, N., Maeda, A., Hironaka, K.-I., Fukuda, M., Danno, H., Tanaka, Y., Hori, S., et al. (2024). Pigmentation level of human iPSC-derived RPE does not indicate a specific gene expression profile. eLife *12*. 10.7554/eLife.92510.

31. Toops, K.A., Tan, L.X., and Lakkaraju, A. (2014). A detailed three-step protocol for live imaging of intracellular traffic in polarized primary porcine RPE monolayers. Exp. Eye Res. *124*, 74–85. 10.1016/j.exer.2014.05.003.

32. Lakkaraju, A., Finnemann, S.C., and Rodriguez-Boulan, E. (2007). The lipofuscin fluorophore A2E perturbs cholesterol metabolism in retinal pigment epithelial cells. Proc Natl Acad Sci USA *104*, 11026–11031. 10.1073/pnas.0702504104.

33. Toops, K.A., Tan, L.X., Jiang, Z., Radu, R.A., and Lakkaraju, A. (2015). Cholesterol-mediated activation of acid sphingomyelinase disrupts autophagy in the retinal pigment epithelium. Mol. Biol. Cell *26*, 1–14. 10.1091/mbc.E14-05-1028.

34. Kaur, G., Tan, L.X., Rathnasamy, G., La Cunza, N., Germer, C.J., Toops, K.A., Fernandes, M., Blenkinsop, T.A., and Lakkaraju, A. (2018). Aberrant early endosome biogenesis mediates complement activation in the retinal pigment epithelium in models of macular degeneration. Proc Natl Acad Sci USA *115*, 9014–9019. 10.1073/pnas.1805039115.

35. Tan, L.X., Toops, K.A., and Lakkaraju, A. (2016). Protective responses to sublytic complement in the retinal pigment epithelium. Proc Natl Acad Sci USA *113*, 8789–8794. 10.1073/pnas.1523061113.

36. Shi, J., Hyman, A.J., De Vecchis, D., Chong, J., Lichtenstein, L., Futers, S.T., Rouahi, M., Negre-Salvayre, A., Auge, N., Kalli, A.C., et al. (2019). Sphingomyelinase disables Piezo1 channel inactivation to enable sustained response to mechanical force. BioRxiv. 10.1101/792564.

37. Qi, Y., Andolfi, L., Frattini, F., Mayer, F., Lazzarino, M., and Hu, J. (2015). Membrane stiffening by STOML3 facilitates mechanosensation in sensory neurons. Nat. Commun. *6*, 8512. 10.1038/ncomms9512.

38. Raposo, G., and Stoorvogel, W. (2013). Extracellular vesicles: exosomes, microvesicles, and friends. J. Cell Biol. *200*, 373–383. 10.1083/jcb.201211138.

39. Kalluri, R., and LeBleu, V.S. (2020). The biology, function, and biomedical applications of exosomes. Science *367*, eaau6977. 10.1126/science.aau6977.

40. Guo, H., Chitiprolu, M., Roncevic, L., Javalet, C., Hemming, F.J., Trung, M.T., Meng, L., Latreille, E., Tanese de Souza, C., McCulloch, D., et al. (2017). Atg5 Disassociates the V1V0-ATPase to Promote Exosome Production and Tumor Metastasis Independent of Canonical Macroautophagy. Dev. Cell *43*, 716-730.e7. 10.1016/j.devcel.2017.11.018.

41. Elsherbini, A., and Bieberich, E. (2018). Ceramide and exosomes: A novel target in cancer biology and therapy. Adv. Cancer Res. *140*, 121–154. 10.1016/bs.acr.2018.05.004.

42. Isaac, R., Reis, F.C.G., Ying, W., and Olefsky, J.M. (2021). Exosomes as mediators of intercellular crosstalk in metabolism. Cell Metab. *33*, 1744–1762. 10.1016/j.cmet.2021.08.006.

43. Sharma, P., Mesci, P., Carromeu, C., McClatchy, D.R., Schiapparelli, L., Yates, J.R., Muotri, A.R., and Cline, H.T. (2019). Exosomes regulate neurogenesis and circuit assembly. Proc Natl Acad Sci USA *116*, 16086–16094. 10.1073/pnas.1902513116.

44. Haney, M.J., Klyachko, N.L., Zhao, Y., Gupta, R., Plotnikova, E.G., He, Z., Patel, T., Piroyan, A., Sokolsky, M., Kabanov, A.V., et al. (2015). Exosomes as drug delivery vehicles for Parkinson's disease therapy. J. Control. Release *207*, 18–30. 10.1016/j.jconrel.2015.03.033.

45. Phinney, D.G., and Pittenger, M.F. (2017). Concise Review: MSC-Derived Exosomes for Cell-Free Therapy. Stem Cells *35*, 851–858. 10.1002/stem.2575.

46. Atienzar-Aroca, S., Flores-Bellver, M., Serrano-Heras, G., Martinez-Gil, N., Barcia, J.M., Aparicio, S., Perez-Cremades, D., Garcia-Verdugo, J.M., Diaz-Llopis, M., Romero, F.J., et al. (2016). Oxidative stress in retinal pigment epithelium cells increases exosome secretion and promotes angiogenesis in endothelial cells. J. Cell. Mol. Med. *20*, 1457–1466. 10.1111/jcmm.12834.

47. Zhao, Y., Weber, S.R., Lease, J., Russo, M., Siedlecki, C.A., Xu, L.-C., Chen, H., Wang, W., Ford, M., Simó, R., et al. (2018). Liquid biopsy of vitreous reveals an abundant vesicle population consistent with the size and morphology of exosomes. Transl. Vis. Sci. Technol. *7*, 6. 10.1167/tvst.7.3.6.

48. Zhang, W., Wang, Y., and Kong, Y. (2019). Exosomes Derived From Mesenchymal Stem Cells Modulate miR-126 to Ameliorate Hyperglycemia-Induced Retinal Inflammation Via Targeting HMGB1. Invest. Ophthalmol. Vis. Sci. *60*, 294–303. 10.1167/iovs.18-25617.

49. Purushothaman, A. (2019). Exosomes from Cell Culture-Conditioned Medium: Isolation by Ultracentrifugation and Characterization. Methods Mol. Biol. *1952*, 233–244. 10.1007/978-1-4939-9133-4_19.

50. Liu, W.-Z., Ma, Z.-J., and Kang, X.-W. (2022). Current status and outlook of advances in exosome isolation. Anal. Bioanal. Chem. *414*, 7123–7141. 10.1007/s00216-022-04253-7.

51. Tiwari, S., Kumar, V., Randhawa, S., and Verma, S.K. (2021). Preparation and characterization of extracellular vesicles. Am. J. Reprod. Immunol. *85*, e13367. 10.1111/aji.13367.

52. Jung, M.K., and Mun, J.Y. (2018). Sample preparation and imaging of exosomes by transmission electron microscopy. J. Vis. Exp. *131*, 56482. 10.3791/56482.

53. Dragovic, R.A., Gardiner, C., Brooks, A.S., Tannetta, D.S., Ferguson, D.J.P., Hole, P., Carr, B., Redman, C.W.G., Harris, A.L., Dobson, P.J., et al. (2011). Sizing and phenotyping of cellular vesicles using Nanoparticle Tracking Analysis. Nanomedicine *7*, 780–788. 10.1016/j.nano.2011.04.003.

54. Welsh, J.A., Goberdhan, D.C.I., O'Driscoll, L., Buzas, E.I., Blenkiron, C., Bussolati, B., Cai, H., Di Vizio, D., Driedonks, T.A.P., Erdbrügger, U., et al. (2024). Minimal information for studies of extracellular vesicles (MISEV2023): From basic to advanced approaches. J. Extracell. Vesicles *13*, e12404. 10.1002/jev2.12404.

55. Quinney, K.B., Frankel, E.B., Shankar, R., Kasberg, W., Luong, P., and Audhya, A. (2019). Growth factor stimulation promotes multivesicular endosome biogenesis by prolonging recruitment of the late-acting ESCRT machinery. Proc Natl Acad Sci USA *116*, 6858–6867. 10.1073/pnas.1817898116.

56. Vietri, M., Radulovic, M., and Stenmark, H. (2020). The many functions of ESCRTs. Nat. Rev. Mol. Cell Biol. *21*, 25–42. 10.1038/s41580-019-0177-4.

57. Baietti, M.F., Zhang, Z., Mortier, E., Melchior, A., Degeest, G., Geeraerts, A., Ivarsson, Y., Depoortere, F., Coomans, C., Vermeiren, E., et al. (2012). Syndecan-syntenin-ALIX regulates the biogenesis of exosomes. Nat. Cell Biol. *14*, 677–685. 10.1038/ncb2502.

58. Trajkovic, K., Hsu, C., Chiantia, S., Rajendran, L., Wenzel, D., Wieland, F., Schwille, P., Brügger, B., and Simons, M. (2008). Ceramide triggers budding of exosome vesicles into multivesicular endosomes. Science *319*, 1244–1247. 10.1126/science.1153124.

59. Arya, S.B., Chen, S., Jordan-Javed, F., and Parent, C.A. (2022). Ceramide-rich microdomains facilitate nuclear envelope budding for non-conventional exosome formation. Nat. Cell Biol. *24*, 1019–1028. 10.1038/s41556-022-00934-8.

60. Fadjukov, J., Wienbar, S., Hakanen, S., Aho, V., Vihinen-Ranta, M., Ihalainen, T.O., Schwartz, G.W., and Nymark, S. (2022). Gap junctions and connexin hemichannels both contribute to the electrical properties of retinal pigment epithelium. J. Gen. Physiol. *154*. 10.1085/jgp.202112916.

61. Iwai-Takekoshi, L., Ramos, A., Schaler, A., Weinreb, S., Blazeski, R., and Mason, C. (2016). Retinal pigment epithelial integrity is compromised in the developing albino mouse retina. J. Comp. Neurol. *524*, 3696–3716. 10.1002/cne.24025.

62. Danesh-Meyer, H.V., Zhang, J., Acosta, M.L., Rupenthal, I.D., and Green, C.R. (2016). Connexin43 in retinal injury and disease. Prog. Retin. Eye Res. *51*, 41–68. 10.1016/j.preteyeres.2015.09.004.

63. Charbel Issa, P., Barnard, A.R., Singh, M.S., Carter, E., Jiang, Z., Radu, R.A., Schraermeyer, U., and MacLaren, R.E. (2013). Fundus autofluorescence in the Abca4(-/-) mouse model of Stargardt disease--correlation with accumulation of A2E, retinal function, and histology. Invest. Ophthalmol. Vis. Sci. *54*, 5602–5612. 10.1167/iovs.13-11688.

64. Anderson, D.M.G., Ablonczy, Z., Koutalos, Y., Hanneken, A.M., Spraggins, J.M., Calcutt, M.W., Crouch, R.K., Caprioli, R.M., and Schey, K.L. (2017). Bis(monoacylglycero)phosphate lipids in the retinal pigment epithelium implicate lysosomal/endosomal dysfunction in a model of Stargardt disease and human retinas. Sci. Rep. *7*, 17352. 10.1038/s41598-017-17402-1.

65. Radu, R.A., Hu, J., Yuan, Q., Welch, D.L., Makshanoff, J., Lloyd, M., McMullen, S., Travis, G.H., and Bok, D. (2011). Complement system dysregulation and inflammation in the retinal pigment epithelium of a mouse model for Stargardt macular degeneration. J. Biol. Chem. *286*, 18593–18601. 10.1074/jbc.M110.191866.

66. Tabel, M., Wolf, A., Szczepan, M., Xu, H., Jägle, H., Moehle, C., Chen, M., and Langmann, T. (2022). Genetic targeting or pharmacological inhibition of galectin-3 dampens microglia reactivity and delays retinal degeneration. J. Neuroinflammation *19*, 229. 10.1186/s12974-022-02589-6.

67. Zhang, Y., Zhao, L., Wang, X., Ma, W., Lazere, A., Qian, H.-H., Zhang, J., Abu-Asab, M., Fariss, R.N., Roger, J.E., et al. (2018). Repopulating retinal microglia restore endogenous organization and function under CX3CL1-CX3CR1 regulation. Sci. Adv. *4*, eaap8492. 10.1126/sciadv.aap8492.

68. O'Koren, E.G., Yu, C., Klingeborn, M., Wong, A.Y.W., Prigge, C.L., Mathew, R., Kalnitsky, J., Msallam, R.A., Silvin, A., Kay, J.N., et al. (2019). Microglial Function Is Distinct in Different Anatomical Locations during Retinal Homeostasis and Degeneration. Immunity *50*, 723-737.e7. 10.1016/j.immuni.2019.02.007.

69. Flores-Bellver, M., Mighty, J., Aparicio-Domingo, S., Li, K.V., Shi, C., Zhou, J., Cobb, H., McGrath, P., Michelis, G., Lenhart, P., et al. (2021). Extracellular vesicles released by human retinal pigment epithelium mediate increased polarised secretion of drusen proteins in response to AMD stressors. J. Extracell. Vesicles *10*, e12165. 10.1002/jev2.12165.

70. Biasutto, L., Chiechi, A., Couch, R., Liotta, L.A., and Espina, V. (2013). Retinal pigment epithelium (RPE) exosomes contain signaling phosphoproteins affected by oxidative stress. Exp. Cell Res. *319*, 2113–2123. 10.1016/j.yexcr.2013.05.005.

71. Théry, C., Amigorena, S., Raposo, G., and Clayton, A. (2006). Isolation and characterization of exosomes from cell culture supernatants and biological fluids. Curr. Protoc. Cell Biol. *Chapter 3*, Unit 3.22. 10.1002/0471143030.cb0322s30.

72. Livshits, M.A., Khomyakova, E., Evtushenko, E.G., Lazarev, V.N., Kulemin, N.A., Semina, S.E., Generozov, E.V., and Govorun, V.M. (2015). Isolation of exosomes by

differential centrifugation: Theoretical analysis of a commonly used protocol. Sci. Rep. *5*, 17319. 10.1038/srep17319.

73. Verweij, F.J., Bebelman, M.P., Jimenez, C.R., Garcia-Vallejo, J.J., Janssen, H., Neefjes, J., Knol, J.C., de Goeij-de Haas, R., Piersma, S.R., Baglio, S.R., et al. (2018). Quantifying exosome secretion from single cells reveals a modulatory role for GPCR signaling. J. Cell Biol. *217*, 1129–1142. 10.1083/jcb.201703206.

74. Cunza, N.L., Tan, L.X., Thamban, T., Germer, C.J., Rathnasamy, G., Toops, K.A., and Lakkaraju, A. (2021). Mitochondria-dependent phase separation of disease-relevant proteins drives pathological features of age-related macular degeneration. JCI Insight.

75. Ranade, S.S., Syeda, R., and Patapoutian, A. (2015). Mechanically activated ion channels. Neuron *87*, 1162–1179. 10.1016/j.neuron.2015.08.032.

76. Miles, L., Powell, J., Kozak, C., and Song, Y. (2023). Mechanosensitive ion channels, axonal growth, and regeneration. Neuroscientist *29*, 421–444. 10.1177/10738584221088575.

77. Koser, D.E., Thompson, A.J., Foster, S.K., Dwivedy, A., Pillai, E.K., Sheridan, G.K., Svoboda, H., Viana, M., Costa, L. da F., Guck, J., et al. (2016). Mechanosensing is critical for axon growth in the developing brain. Nat. Neurosci. *19*, 1592–1598. 10.1038/nn.4394.

78. Kentish, S.J., Frisby, C.L., Kritas, S., Li, H., Hatzinikolas, G., O'Donnell, T.A., Wittert, G.A., and Page, A.J. (2015). TRPV1 channels and gastric vagal afferent signalling in lean

and high fat diet induced obese mice. PLoS ONE *10*, e0135892. 10.1371/journal.pone.0135892.

79. Qin, L., Liu, W., Cao, H., and Xiao, G. (2020). Molecular mechanosensors in osteocytes. Bone Res. *8*, 23. 10.1038/s41413-020-0099-y.

80. Masterton, S., and Ahearne, M. (2018). Mechanobiology of the corneal epithelium. Exp. Eye Res. *177*, 122–129. 10.1016/j.exer.2018.08.001.

81. Downs, J.C. (2015). Optic nerve head biomechanics in aging and disease. Exp. Eye Res. *133*, 19–29. 10.1016/j.exer.2015.02.011.

82. Coste, B., Mathur, J., Schmidt, M., Earley, T.J., Ranade, S., Petrus, M.J., Dubin, A.E., and Patapoutian, A. (2010). Piezo1 and Piezo2 are essential components of distinct mechanically activated cation channels. Science *330*, 55–60. 10.1126/science.1193270.

83. Ma, S., Dubin, A.E., Zhang, Y., Mousavi, S.A.R., Wang, Y., Coombs, A.M., Loud, M., Andolfo, I., and Patapoutian, A. (2021). A role of PIEZO1 in iron metabolism in mice and humans. Cell *184*, 969-982.e13. 10.1016/j.cell.2021.01.024.

84. Fang, X.-Z., Zhou, T., Xu, J.-Q., Wang, Y.-X., Sun, M.-M., He, Y.-J., Pan, S.-W., Xiong, W., Peng, Z.-K., Gao, X.-H., et al. (2021). Structure, kinetic properties and biological function of mechanosensitive Piezo channels. Cell Biosci. *11*, 13. 10.1186/s13578-020-00522-z.

85. Chen, X., Wanggou, S., Bodalia, A., Zhu, M., Dong, W., Fan, J.J., Yin, W.C., Min, H.-K., Hu, M., Draghici, D., et al. (2018). A feedforward mechanism mediated by

mechanosensitive ion channel PIEZO1 and tissue mechanics promotes glioma aggression. Neuron *100*, 799-815.e7. 10.1016/j.neuron.2018.09.046.

86. Morozumi, W., Inagaki, S., Iwata, Y., Nakamura, S., Hara, H., and Shimazawa, M. (2020). Piezo channel plays a part in retinal ganglion cell damage. Exp. Eye Res. *191*, 107900. 10.1016/j.exer.2019.107900.

87. Gudipaty, S.A., Lindblom, J., Loftus, P.D., Redd, M.J., Edes, K., Davey, C.F., Krishnegowda, V., and Rosenblatt, J. (2017). Mechanical stretch triggers rapid epithelial cell division through Piezo1. Nature *543*, 118–121. 10.1038/nature21407.

88. Stewart, T.A., and Davis, F.M. (2019). Formation and function of mammalian epithelia: roles for mechanosensitive PIEZO1 ion channels. Front. Cell Dev. Biol. *7*, 260. 10.3389/fcell.2019.00260.

89. Ranade, S.S., Qiu, Z., Woo, S.-H., Hur, S.S., Murthy, S.E., Cahalan, S.M., Xu, J., Mathur, J., Bandell, M., Coste, B., et al. (2014). Piezo1, a mechanically activated ion channel, is required for vascular development in mice. Proc Natl Acad Sci USA *111*, 10347–10352. 10.1073/pnas.1409233111.

90. Liu, T.-T., Du, X.-F., Zhang, B.-B., Zi, H.-X., Yan, Y., Yin, J.-A., Hou, H., Gu, S.-Y., Chen, Q., and Du, J.-L. (2020). Piezo1-Mediated Ca2+ Activities Regulate Brain Vascular Pathfinding during Development. Neuron *108*, 180-192.e5. 10.1016/j.neuron.2020.07.025.

91. Romac, J.M.-J., Shahid, R.A., Swain, S.M., Vigna, S.R., and Liddle, R.A. (2018). Piezo1 is a mechanically activated ion channel and mediates pressure induced pancreatitis. Nat. Commun. *9*, 1715. 10.1038/s41467-018-04194-9.

92. Kefauver, J.M., Ward, A.B., and Patapoutian, A. (2020). Discoveries in structure and physiology of mechanically activated ion channels. Nature *587*, 567–576. 10.1038/s41586-020-2933-1.

93. Nourse, J.L., and Pathak, M.M. (2017). How cells channel their stress: Interplay between Piezo1 and the cytoskeleton. Semin. Cell Dev. Biol. *71*, 3–12. 10.1016/j.semcdb.2017.06.018.

94. Shi, J., Hyman, A.J., De Vecchis, D., Chong, J., Lichtenstein, L., Futers, T.S., Rouahi, M., Salvayre, A.N., Auge, N., Kalli, A.C., et al. (2020). Sphingomyelinase disables inactivation in endogenous PIEZO1 channels. Cell Rep. *33*, 108225. 10.1016/j.celrep.2020.108225.

95. Saotome, K., Murthy, S.E., Kefauver, J.M., Whitwam, T., Patapoutian, A., and Ward, A.B. (2018). Structure of the mechanically activated ion channel Piezo1. Nature *554*, 481–486. 10.1038/nature25453.

96. De Vecchis, D., Beech, D.J., and Kalli, A.C. (2021). Molecular dynamics simulations of Piezo1 channel opening by increases in membrane tension. Biophys. J. *120*, 1510–1521. 10.1016/j.bpj.2021.02.006.

97. Bae, C., Sachs, F., and Gottlieb, P.A. (2011). The mechanosensitive ion channel Piezo1 is inhibited by the peptide GsMTx4. Biochemistry *50*, 6295–6300. 10.1021/bi200770q.

98. Gnanasambandam, R., Ghatak, C., Yasmann, A., Nishizawa, K., Sachs, F., Ladokhin, A.S., Sukharev, S.I., and Suchyna, T.M. (2017). Gsmtx4: mechanism of inhibiting mechanosensitive ion channels. Biophys. J. *112*, 31–45. 10.1016/j.bpj.2016.11.013.

99. Velasco-Estevez, M., Mampay, M., Boutin, H., Chaney, A., Warn, P., Sharp, A., Burgess, E., Moeendarbary, E., Dev, K.K., and Sheridan, G.K. (2018). Infection Augments Expression of Mechanosensing Piezo1 Channels in Amyloid Plaque-Reactive Astrocytes. Front. Aging Neurosci. *10*, 332. 10.3389/fnagi.2018.00332.

100. Curcio, C.A., and Johnson, M. (2013). Structure, function, and pathology of bruch's membrane. In Retina (Elsevier), pp. 465–481. 10.1016/B978-1-4557-0737-9.00020-5.

101. Hussain, A.A., Starita, C., Hodgetts, A., and Marshall, J. (2010). Macromolecular diffusion characteristics of ageing human Bruch's membrane: implications for age-related macular degeneration (AMD). Exp. Eye Res. *90*, 703–710. 10.1016/j.exer.2010.02.013.

102. Booij, J.C., Baas, D.C., Beisekeeva, J., Gorgels, T.G.M.F., and Bergen, A.A.B. (2010). The dynamic nature of Bruch's membrane. Prog. Retin. Eye Res. *29*, 1–18. 10.1016/j.preteyeres.2009.08.003.

103. Ridone, P., Pandzic, E., Vassalli, M., Cox, C.D., Macmillan, A., Gottlieb, P.A., and Martinac, B. (2020). Disruption of membrane cholesterol organization impairs the activity of PIEZO1 channel clusters. J. Gen. Physiol. *152*. 10.1085/jgp.201912515.

104. Etem, E.Ö., Ceylan, G.G., Özaydın, S., Ceylan, C., Özercan, I., and Kuloğlu, T. (2018). The increased expression of Piezo1 and Piezo2 ion channels in human and mouse bladder carcinoma. Adv. Clin. Exp. Med. *27*, 1025–1031. 10.17219/acem/71080.

105. Nava, M.M., Miroshnikova, Y.A., Biggs, L.C., Whitefield, D.B., Metge, F., Boucas, J., Vihinen, H., Jokitalo, E., Li, X., García Arcos, J.M., et al. (2020). Heterochromatin-Driven Nuclear Softening Protects the Genome against Mechanical Stress-Induced Damage. Cell *181*, 800-817.e22. 10.1016/j.cell.2020.03.052.

106. Becker, J.S., Nicetto, D., and Zaret, K.S. (2016). H3K9me3-Dependent Heterochromatin: Barrier to Cell Fate Changes. Trends Genet. *32*, 29–41. 10.1016/j.tig.2015.11.001.

107. Pilgrim, M.G., Lengyel, I., Lanzirotti, A., Newville, M., Fearn, S., Emri, E., Knowles, J.C., Messinger, J.D., Read, R.W., Guidry, C., et al. (2017). Subretinal pigment epithelial deposition of drusen components including hydroxyapatite in a primary cell culture model. Invest. Ophthalmol. Vis. Sci. *58*, 708–719. 10.1167/iovs.16-21060.

108. Tan, L.X., Germer, C.J., La Cunza, N., and Lakkaraju, A. (2020). Complement activation, lipid metabolism, and mitochondrial injury: Converging pathways in age-related macular degeneration. Redox Biol. *37*, 101781. 10.1016/j.redox.2020.101781.

109. Choi, E.H., Suh, S., Einstein, D.E., Leinonen, H., Dong, Z., Rao, S.R., Fliesler, S.J., Blackshaw, S., Yu, M., Peachey, N.S., et al. (2021). An inducible Cre mouse for studying roles of the RPE in retinal physiology and disease. JCI Insight.

110. Kim, L.A., Amarnani, D., Gnanaguru, G., Tseng, W.A., Vavvas, D.G., and D'Amore, P.A. (2014). Tamoxifen toxicity in cultured retinal pigment epithelial cells is mediated by concurrent regulated cell death mechanisms. Invest. Ophthalmol. Vis. Sci. *55*, 4747–4758. 10.1167/iovs.13-13662.

111. Cho, K.S., Yoon, Y.H., Choi, J.A., Lee, S.-J., and Koh, J.-Y. (2012). Induction of autophagy and cell death by tamoxifen in cultured retinal pigment epithelial and photoreceptor cells. Invest. Ophthalmol. Vis. Sci. *53*, 5344–5353. 10.1167/iovs.12-9827.

112. Ralston, S.H., Corral-Gudino, L., Cooper, C., Francis, R.M., Fraser, W.D., Gennari, L., Guañabens, N., Javaid, M.K., Layfield, R., O'Neill, T.W., et al. (2019). Diagnosis and management of paget's disease of bone in adults: A clinical guideline. J. Bone Miner. Res. *34*, 579–604. 10.1002/jbmr.3657.

113. Gozzetti, A., Gennari, L., Merlotti, D., Salvadori, S., De Paola, V., Avanzati, A., Franci, B., Marchini, E., Tozzi, M., Campagna, M.S., et al. (2008). The effects of zoledronic acid on serum lipids in multiple myeloma patients. Calcif. Tissue Int. *82*, 258–262. 10.1007/s00223-008-9123-8.

114. Qaseem, A., Hicks, L.A., Etxeandia-Ikobaltzeta, I., Shamliyan, T., Cooney, T.G., Clinical Guidelines Committee of the American College of Physicians, Cross, J.T., Fitterman, N., Lin, J.S., Maroto, M., et al. (2023). Pharmacologic treatment of primary osteoporosis or low bone mass to prevent fractures in adults: A living clinical guideline from the american college of physicians. Ann. Intern. Med. *176*, 224–238. 10.7326/M22-1034.

115. Russell, R.G.G., Watts, N.B., Ebetino, F.H., and Rogers, M.J. (2008). Mechanisms of action of bisphosphonates: similarities and differences and their potential influence on clinical efficacy. Osteoporos. Int. *19*, 733–759. 10.1007/s00198-007-0540-8.

116. Mirrakhimov, A.E. (2015). Hypercalcemia of malignancy: an update on pathogenesis and management. N. Am. J. Med. Sci. *7*, 483–493. 10.4103/1947-2714.170600.

117. Kornhuber, J., Tripal, P., Gulbins, E., and Muehlbacher, M. (2013). Functional inhibitors of acid sphingomyelinase (FIASMAs). Handb. Exp. Pharmacol., 169–186. 10.1007/978-3-7091-1368-4_9.

118. Adami, S., Braga, V., Guidi, G., Gatti, D., Gerardi, D., and Fracassi, E. (2000). Chronic intravenous aminobisphosphonate therapy increases high-density lipoprotein cholesterol and decreases low-density lipoprotein cholesterol. J. Bone Miner. Res. *15*, 599–604. 10.1359/jbmr.2000.15.3.599.

119. Munoz, M.A., Fletcher, E.K., Skinner, O.P., Jurczyluk, J., Kristianto, E., Hodson, M.P., Sun, S., Ebetino, F.H., Croucher, D.R., Hansbro, P.M., et al. (2021). Bisphosphonate drugs have actions in the lung and inhibit the mevalonate pathway in alveolar macrophages. eLife *10*. 10.7554/eLife.72430.

120. Burns, M.P., and Rebeck, G.W. (2010). Intracellular cholesterol homeostasis and amyloid precursor protein processing. Biochim. Biophys. Acta *1801*, 853–859. 10.1016/j.bbalip.2010.03.004.

121. Jahnke, W., Rondeau, J.-M., Cotesta, S., Marzinzik, A., Pellé, X., Geiser, M., Strauss, A., Götte, M., Bitsch, F., Hemmig, R., et al. (2010). Allosteric non-bisphosphonate FPPS inhibitors identified by fragment-based discovery. Nat. Chem. Biol. *6*, 660–666. 10.1038/nchembio.421.

122. ElSheikh, R.H., Chauhan, M.Z., and Sallam, A.B. (2022). Current and Novel Therapeutic Approaches for Treatment of Neovascular Age-Related Macular Degeneration. Biomolecules *12*. 10.3390/biom12111629.

123. Beckmann, N., Sharma, D., Gulbins, E., Becker, K.A., and Edelmann, B. (2014). Inhibition of acid sphingomyelinase by tricyclic antidepressants and analogons. Front. Physiol. *5*, 331. 10.3389/fphys.2014.00331.

124. Mir, I.H., and Thirunavukkarasu, C. (2023). The relevance of acid sphingomyelinase as a potential target for therapeutic intervention in hepatic disorders: current scenario and anticipated trends. Arch. Toxicol. *97*, 2069–2087. 10.1007/s00204-023-03529-w.

125. Kornhuber, J., Muehlbacher, M., Trapp, S., Pechmann, S., Friedl, A., Reichel, M., Mühle, C., Terfloth, L., Groemer, T.W., Spitzer, G.M., et al. (2011). Identification of novel functional inhibitors of acid sphingomyelinase. PLoS ONE *6*, e23852. 10.1371/journal.pone.0023852.

126. Roth, A.G., Drescher, D., Yang, Y., Redmer, S., Uhlig, S., and Arenz, C. (2009). Potent and selective inhibition of acid sphingomyelinase by bisphosphonates. Angew. Chem. Int. Ed *48*, 7560–7563. 10.1002/anie.200903288.

127. Luo, W., Zhang, J., Xu, L., Zhou, Y., Xu, D., Lv, Q., Xiao, Y., and Yang, Q. (2022). Use of zoledronic acid in antiosteoporosis treatment is associated with a decreased blood lipid level in postmenopausal women with osteoporosis: a cohort study in China. Postgrad. Med. *134*, 406–412. 10.1080/00325481.2022.2051983.

128. Goffinet, M., Thoulouzan, M., Pradines, A., Lajoie-Mazenc, I., Weinbaum, C., Faye, J.C., and Séronie-Vivien, S. (2006). Zoledronic acid treatment impairs protein geranyl-geranylation for biological effects in prostatic cells. BMC Cancer *6*, 60. 10.1186/1471-2407-6-60.

Publishing Agreement

It is the policy of the University to encourage open access and broad distribution of all theses, dissertations, and manuscripts. The Graduate Division will facilitate the distribution of UCSF theses, dissertations, and manuscripts to the UCSF Library for open access and distribution. UCSF will make such theses, dissertations, and manuscripts accessible to the public and will take reasonable steps to preserve these works in perpetuity.

I hereby grant the non-exclusive, perpetual right to The Regents of the University of California to reproduce, publicly display, distribute, preserve, and publish copies of my thesis, dissertation, or manuscript in any form or media, now existing or later derived, including access online for teaching, research, and public service purposes.

DocuSigned by:
Colin Germer
A62EF96EB69E432...
Author Signature

8/19/2024
Date